DEVELOPMENT OF SELECTED ELECTRO-ACTIVE POLYMER-CERAMIC NANOCOMPOSITES AS PYROELECTRIC THERMAL/INFRARED DETECTOR MATERIALS

Thesis submitted to
Cochin University of Science and Technology
in partial fulfilment of the requirements for the award of the degree of
Doctor of Philosophy

By

Jayalakshmy M. S.

Department of Instrumentation
Cochin University of Science and Technology
Cochin – 682 022, Kerala, India

May 2015

Development of selected electro-active polymer-ceramic nanocomposites as pyroelectric thermal/infrared detector materials

Ph. D. Thesis in the field of Applied Physics

Author

Jayalakshmy M. S.
Department of Instrumentation
Cochin University of Science and Technology
Cochin – 682 022, Kerala, India
email: jayalakshmy.ms@gmail.com

Supervising Guide

Dr. Jacob Philip
Professor (Emeritus)
Department of Instrumentation
Cochin University of Science and Technology
Cochin – 682 022, Kerala, India
email: jp@cusat.ac.in

May 2015

Cover page: Industry's one and only truly digital pyroelectric infrared detector family 'DigiPyro®' developed by *Excelitas*, pyroelectric infrared sensors developed by *Nippon Ceramic Co., Ltd.* and world's smallest and thinnest surface mount pyroelectric infrared sensor developed by *Murata Manufacturing Co., Ltd.*

Dr. Jacob Philip
Professor (Emeritus)
Department of Instrumentation
Cochin University of Science and Technology
Cochin – 682 022

Certificate

This is to certify that the thesis entitled '**Development of Selected Electro-active Polymer-Ceramic Nanocomposites as Pyroelectric Thermal/Infrared Detector Materials**' is an authentic record of research work carried out by **Ms. Jayalakshmy M. S.** under my supervision at the Department of Instrumentation in partial fulfilment of the requirements for the award of the degree of Doctor of Philosophy of Cochin University of Science and Technology, and further that no part of thereof has hitherto been submitted for any degree in any University.

Cochin – 22
18-05-2015

Prof. (Dr.) Jacob Philip
Supervising Guide

E-mail: jp@cusat.ac.in Mob: 09447762471

Dr. Jacob Philip
Professor (Emeritus)
Department of Instrumentation
Cochin University of Science and Technology
Cochin – 682 022

Certificate

This is to certify that all the relevant corrections and modifications suggested by the audience during the pre-synopsis seminar presented by **Ms. Jayalakshmy M. S.** and recommended by the doctoral committee of the candidate have been incorporated in her thesis entitled '**Development of Selected Electro-active Polymer-Ceramic Nanocomposites as Pyroelectric Thermal/Infrared Detector Materials**' submitted to Cochin University of Science and Technology in partial fulfilment of the requirements for the award of the degree of Doctor of Philosophy.

Cochin – 22
18-05-2015

Prof. (Dr.) Jacob Philip
Supervising Guide

E-mail: jp@cusat.ac.in Mob: 09447762471

Declaration

I hereby declare that the work presented in the thesis entitled '**Development of Selected Electro-active Polymer-Ceramic Nanocomposites as Pyroelectric Thermal/Infrared Detector Materials**' is the outcome of the original work done by me independently under the supervision of Dr. Jacob Philip, Professor (Emeritus), Department of Instrumentation, Cochin University of Science and Technology and the work did not form part of any dissertation submitted for the award of any degree, diploma, associateship, or any other title or recognition from any University/Institution.

Cochin – 22 **Jayalakshmy M. S.**
18-05-2015

Dedication.....

With tears in my eyes I dedicate my thesis to the loving memory of my father **(Late) M. R. Sudhakaran** *who was eagerly waiting for the completion of my Ph. D. degree*

&

To my mother **Vanaja Sudhakaran** *who was always doing more than I needed and expecting nothing in return. She was stable in all the toughest circumstances and took care of me with her silent prayers for my academic and personal life*

Contents

Acknowledgements.....

My captivation with nanotechnology and sensors started during the last four and half years of stay in the laboratory of Prof. (Dr.) Jacob Philip. I am extremely thankful to Prof. Philip who offered me the chance to do research in the field of nanotechnology and thermal/infrared sensing under his supervision. Unparalleled logic, perpetual inspiration and motivation were always a part of his supervision; and I am sure, I was so lucky to be there in his team. There were times that were overwhelmingly difficult with a lot of problems and mental agony during the last couple of months of my course of study, especially after my father's demise. He got things moving again when I got bogged down. He prompted me to look forward to a bright future with his insightful comments. Also he did a very thorough job of proofreading this thesis, and I must take full responsibility for the remaining errors. Prof. Philip, in the truest sense, played the ideal role of a philosopher, father and guide to me.

Prof. (Dr.) A. V. Alex, who was my professor and M Sc. Project co-ordinator during my post graduation, also deserves a great deal of credit. He was always inspiring me to get into the research field and directed me to here. I greatly appreciate his continuous encouragements and support. At this moment I remember Prof. K, M. Chandrahasan Nampoothiri and Prof. T. V. Shankarankutty Warrier, from whom I learned and sharpened hands-on working attitude, creative thinking and effective communication.

I extent my sincere thanks to the Head of the Department, Dr. K, Rajeev Kumar and former HODs Dr. Stephen Rodriguez and Dr. K. N. Madhusoodanan for allowing me to use the department facilities. My greatful thanks are also extended to Dr. Johney Isaac for his help and support during my research.

I would like to thank Dr. Seema Ansari and Dr. Raghu, Scientists, CMET, Thrissur, Prof. (Dr.) Rani Joseph, Dept. of Polymer Science and Rubber Technology and Prof. (Dr.) M. K. Jayaraj, Dept. of Physics, CUSAT for their advices, helps and supports.

SAIF, STIC, CUSAT is gratefully acknowledged for the help in sample characterization. Mr. Melbin Baby (Research scholar in the Dept. of Instrumentation) and Mr. Shyam Kumar, who are from STIC, and Mr. Murali, Mr. Prakash, Mr. Babu and Mr. Shaji who are from the Dept. of Instrumentation, CUSAT deserve special mention for their timely help. Also, my sincere thanks go to Mr. Rohith, Mrs. Sona and Mss. Teena who are from the Dept. of Polymer Science and Rubber Technology, Mss. Bhavya from the Dept. of Applied Chemistry and Mrs. Shajira and Dr. Sanal from the Dept. of Physics for their help and support.

I am taking this opportunity to acknowledge Dept. of Science and Technology, Govt. of India and Cochin University of Science and Technology for providing fellowships and contingency grants to pursue my research. Cochin University of Science and Technology was an unbelievably great experience for me. The academic life here was phenomenal. For me, this university was exhilarating, fascinating and sometimes even discouraging but always challenging.

I have a lot of friends in CUSAT, still best friends are rare to find, but I was fortunate enough to get somebody like Mrs. Asha and Mss. Greeshmam, my hostel mates.

Our research group has been a dynamic team. New members come in, old ones move on and now it's my turn. I enjoyed working together with Dr. M. V. Manjusha, Dr. M. R. Nisha, Dr. S. Uma, Mrs. Rakhikrishna, Mss. Soumya, Mrs. Nighila, Mrs. Sheeja P. George, Mr. Jiss Paul and Mr. Nissamuddeen, my seniors and lab mates. I also cherish and appreciate the help and support from other research scholars of the department.

Last but not the least I thank my parents, brother and sister-in-low for their everlasting love and support. I now understand why most books and theses are dedicated to the author's family. I take pride of myself being a member of such an ideal family for their unceasing sacrifice, affectionate blessings and help, without which it would be impossible for me to complete my investigation. Even though my father is not with me physically, I am pretty sure that his soul is with me and will always be there. I am very grateful that mine is such a brave and multitasking mother. She showed a difference and courage in my painful days and was always stable in the toughest times. Special thanks to my Amma, who stood firm with me during those

days. Definitely she tried to understand me and was a great solace for me during the last couple of months of my Ph.D. life.

Above all I bow before the supreme power of GOD for giving me the mental power, health and strength to complete my investigation and to prepare this thesis.

Jayalakshmy

Preface

This thesis embodies the work carried out on the preparation and characterization of selected polymer-ceramic nanocomposites as well as polymer-microcrystalline composites with potential application as thermal and/or infrared detectors. It has been shown by earlier workers that pyroelectric and piezoelectric properties of electro-active polymers can be enhanced by the addition of ceramic components that exhibit these properties much higher than the polymer matrices. Even though the pyroelectric/piezoelectric coefficients of the composites are lower than that of pure ceramic materials, the figures of merit often show high values because of the low dielectric permittivity of the composites compared to the pure ceramic phase. Composites made of ferroelectric ceramics dispersed in polymer matrices have been widely studied as promising candidates for the development of pyroelectric and piezoelectric sensors and actuators.

Requirements for Pyroelectric thermal/IR detectors are on the increase in various fields such as military applications like missile guidance, target acquisition, military night vision, etc. and non-military applications like medical diagnostics, thermal imaging, contactless temperature measurement, human proximity sensors, etc. Polymer/ceramic composites (including nanocomposites) have a significant role in pyroelectric thermal/infrared detection due to the fact that they can be made flexible and mouldable. They can be very strong and stiff, still very light in weight. They will not corrode like metals but their toughness is often greater. Recently a good number of polymer/ceramic composites have been proposed for pyroelectric thermal/IR detection applications.

Electro-active polymers are those exhibiting a change in size or shape when aroused by an external electric field. They are characterized by internal polarization and consequent ferroelectricity possessed by them. Good examples for electro-active polymers are PVDF (Poly(vinylidene fluoride)), PU (Polyurethane), P(VDF-TrFE) (Poly(vinylidene fluoride-

Trifluoroethylene, a co-polymer of PVDF), etc. The β form of PVDF is inherently electro-active and is widely used in the film form as wide area infrared as well as acoustic detectors. Technical data relating to these materials are available in literature.

Ceramic materials that possess ferroelectric properties have attracted the attention of material scientists for a very long time. Some of them possess very attractive piezoelectric and pyroelectric properties and are widely used for sensor and actuator applications. A classical example is PZT (Lead Zirconate Titanate), which is widely used as pizodrives in a variety of devices and systems such as Atomic Force Microscopes. Some other popular electro-active ceramics are PLZT (Lanthanum modified Lead Zirconate Titanate), $BaTiO_3$ (Barium Titanate), SBN (Strontium Barium Niobate) etc. The technical data related to such materials are available in literature. Of late there has been a great deal of interest in developing lead free ceramics as lead is a toxic material. SBN is a good example for a lead free piezoelectric and pyroelectric ceramic.

There is a great deal of interest in developing smart materials and structures with tuneable properties for various applications. Many applications require transducers, with high transduction coefficients, that are flexible and mouldable. Conventional pyro/piezoceramics like PZT, with high pyroelectric/piezoelectric coefficients, are highly brittle; so are not flexible or mouldable. Attempts have been made to overcome this drawback with the use of electro-active polymers, but these have comparatively low transduction coefficients. A recent approach has been to develop smart composites by dispersing pyroelectric/piezoelectric ceramics in electro-active polymer matrices. Good amount of work in these lines has appeared in literature during the past few years. In most of the reported work micron size particles of ceramics have been dispersed in polymer matrices to synthesize composites. In the work presented in this thesis, we have gone further ahead by dispersing nanoparticles of the ceramics in polymer matrices. This has the advantage that the composites will have greater uniformity in its properties. Moreover, it becomes possible to attain the desired properties at lower volume fractions of the ceramic.

The present work emphasises on the synthesis and characterization of electro-active polymer-ceramic nanocomposites which can be used for pyroelectric thermal/infrared detection applications. Two sets of samples belong to polymer-microcrystalline composites have also been investigated in the work. The polymers used in the work have been commercially available ones, but the nanoceramics have been synthesized following simple chemical routes and aqueous organic gel routes. After characterizing the nanoceramics for their structure by powder XRD, they have been dispersed in liquid polymer and sonicated for uniform dispersion. The viscous mixture so formed was cast in the form of films for experimentation. Samples with volume fraction of the ceramic phase varied from 0 to 0.25 have been prepared. Solution growth was followed to prepare microcrystalline samples for the polymer-microcrystalline composites.

The physical properties that determine the pyroelectric sensitivity of a material are dielectric constant, dielectric loss, pyroelectric coefficient, thermal conductivity and specific heat capacity. These parameters have been determined for all the samples and compositions reported in this work. The pyroelectric figures of merit for all the samples were determined from the above data. The pyroelectric figures of merit that determine the pyroelectric sensitivity of a material are current sensitivity, voltage responsivity and detectivity. All these have been determined for each set of samples and reported in the thesis. In order to assess the flexibility and mouldability of the composites we have measured the Shore hardness of each of the composites by indentation technique and compared with the pyroelectric figures of merit.

The specific works presented in each of the chapters of the thesis are outlined in the following paragraphs.

In the first chapter we present an over view of composite materials, including electro-active polymer-ceramic composites. The importance of electro-active polymer-ceramic composites in the application of pyroelectric thermal/infrared detection is put in proper perspective. This

chapter gives an idea about the theory, equivalent circuit and configuration of pyroelectric thermal/IR detectors. Present scenario of polymer/ceramic nanocomposites as pyroelectric IR detectors is included. This chapter also includes a literature review on the pyroelectric figures of merit of polymer/ceramic composite materials to act as pyroelectric thermal/infrared detectors.

Chapter 2 is devoted to a description of the experimental methods employed for the complete study. This chapter covers the sample preparation methods and characterization techniques. Simple chemical routs are adopted for the preparation of $LiTaO_3$ (Lithium Tantalate) and $LiNbO_3$ (Lithium Niobate) nanocrystalline ceramics. SBN nanocrystalline samples were prepared by an aqueous organic gel route. TGS (Triglycine Sulfate) and DTGS (partially deuterated Triglycine Sulfate) polycrystalline samples were synthesised by a conventional slow evaporation of solution method. Solvent cast method was used for the preparation of polymer composite films. Structural characterizations were carried out using powder XRD, morphology by electron microscopy (SEM and TEM) and thermal characterizations by DSC. The dielectric constant following capacitance measurement technique and dielectric loss were measured with an impedance analyzer. The pyroelectric measurements of all the samples were carried out by a direct method developed by Byer and Roundy, subjecting the samples to a controlled heating/cooling program. Both dielectric and pyroelectric studies have been done in a home built measurement cell. Hardness measurements for all the samples were carried by indentation technique with a durometer. The thermal conductivity and specific heat capacity of the samples were measured with a home-built photopyroelectric spectrometer. A brief description of the instruments, principle of the techniques and measurement methods employed for the complete work are also included in this chapter.

Chapter 3 focuses on the investigations on the pyroelectric properties of free standing films of $LiTaO_3$/PVDF nanocomposites, systematically prepared by varying the ceramic volume fraction. All the samples prepared were characterized using standard techniques such as

powder XRD, DSC, FTIR, SEM and TEM. Pyroelectric IR detection figures of merit were calculated for each sample and found out the exact proportion of the polymer and ceramic parts for which the composite shows high values for current sensitivity, voltage responsivity and detectivity with maximum flexibility. In order to assess the flexibility or mouldability of the samples, mechanical hardness measurements are carried out for all compositions, using a durometer. All properties have been reported as a function of volume fraction of the ceramic. It is found that enhancement in pyroelectric figures of merit are at the expense of the flexibility of the composite.

Chapter 4 discusses the pyroelectric properties of $LiNbO_3$/PVDF nanocomposites. Here also we prepared free standing films of LN/PVDF composite with different volume fractions of nano $LiNbO_3$, by adopting the solvent cast method. Pyroelectric, thermal, dielectric and hardness studies are carried out and found that these composites are suitable for thermal/IR detection. All the measurements and analysis done on $LiTaO_3$/PVDF nanocomposites have been carried out on these composites as well.

A complete study of the pyroelectric and associated properties of SBN30/PU nanocomposites and the relevance of these composites in pyroelectric thermal/IR detection are presented in chapter 5. For this we prepared SBN30 nanoparticles following an aqueous organic gel route and dispersed them in polymer matrix of Polyurethane (PU) in various concentrations and investigated their pyroelectric, thermal, dielectric, and hardness properties systematically. From these measured parameters we calculated the pyroelectric figures of merit for each of these composites to act as pyroelectric thermal/IR detectors and observed that these composites form good candidates for thermal/IR sensing applications.

In chapter 6 we present a comparison of the pyroelectric properties of microcrystalline composites of TGS and DTGS in PU matrix. The motivation for doing such a study was that, even though TGS and DTGS crystals possess very high pyroelectric coefficients and figures of merit, their applications as detectors are limited to controlled environments due to

their property of being highly susceptible to humidity. We prepared microcrystalline powders of TGS and DTGS from the corresponding crystallites grown from solution. These were dispersed in PU matrix to form composites, thereby making these samples immune to humidity. By measuring the pyroelectric, thermal, dielectric and hardness parameters of these polymer-polycrystalline composites and calculating the figures of merit values, it was inferred that these flexible composites also are good materials for thermal detection. All relevant properties of these composites with variations in volume fractions of TGS/DTGS have been measured and reported. A comparison of the properties of TGS/PU and DTGS/PU composites with other comparable composites have been made and presented in this chapter. This will provide guidelines for the selection of composites for pyroelectric detector applications.

An overall summary of the research work done is presented in chapter 7. Prospectus to carry out further research and development work in this area is also outlined in this last chapter.

Chapter 1

Introduction: Polymer-Ceramic Nanocomposites

This opening chapter provides a detailed overview of the history of composite materials and a review on about different kinds of composite materials including nanocomposites. The mechanism of pyroelectric thermal/infrared detection is presented. A review of literature on the pyroelectric and associated properties of polymer-ceramic composites that can be used as materials for pyroelectric detection is given. This chapter also discusses applications of polymer-ceramic nanocomposites other than pyroelectric thermal/IR detection applications. The chapter concludes with a short discussion of the overall work presented in the thesis.

1.1 Composite materials – An overview

Mankind has been aware composite materials since several hundred years before Christ and applied innovation to improve the quality of life. The concept of composites is not a human invention. A well known example for a natural composite material is wood, which consists of one

species of polymer-cellulose fibres with good strength and stiffness. Recent review articles and books consider the technology of composite materials as one of the ancient materials technologies [1-8]. Early civilizations, which used laminated bows for extra strength [9] and mixtures of straw (as reinforcing fibre) and mud (matrix) for building bricks [10], are cited as some of the first users of composite materials. Although these ancient materials can be broadly classed as a type of composite material, modern science of composite materials began only relatively recently.

Composite is a material system composed of two or more physically distinct phases whose combination produces aggregate properties that are different from those of its constituents. In the broadest sense, practically every material used today is a composite, since it is rare to find a material used in its purest form. For example, fillers, lubricants, ultraviolet absorbers, etc. are added to plastics for commercial reasons such as economy and ease of processing, it is also rare to find metals without impurities, alloying elements, and unwanted second phases. Furthermore, if we consider them on the atomic or molecular scales, most materials are merely composites of various atoms or molecules. Recently, most composite materials have been created to improve mechanical properties such as stiffness, toughness, and high-temperature strength [11-14]. As the evolution of new technologies progresses, the traditional distinction made between the five classes of materials (i.e., metals, ceramics, polymers, elastomers, and glasses) tends to fade and many new possibilities arise to intelligently process these classes together to produce new, smarter composite materials and engineering structures that respond to stimuli [15-

18]. A brief overview of different generations of composite materials as a function of time is given below.

The modern era of composites began when scientists developed plastics. Until then, natural resins derived from plants and animals were the only source of glues and binders. In the early 1900s, plastics such as vinyl, polystyrenes, phenols and polyesters were developed. These new synthetic materials outperformed resins which were derived from nature. However, plastics alone could not provide enough strength for structural applications. Reinforcement was needed to provide the strength and rigidity. In 1935, Owens-Corning introduced the first glass fibre, i.e., fibreglass. Fibreglass, when combined with a plastic polymer created an incredibly strong structure that was also lightweight. Thus the first commercial composites were called glass fibre reinforced plastics (GFRP) [19, 20]. These were the *first generation of composites*. Also it was the beginning of the Fibre Reinforced Polymers (FRP) industry as we know it today. Remarkably, they still dominate the market today, comprising about 90% of the composites market.

GFRP technology spread rapidly in the 1950s. However new demands emerged for the military, space programs and new fibres which prompted the search for new high modulus fibres. The conjunction of the world geopolitical situation and materials research prompted the emergence of a general notion of composites. The major world event was the launch of the Soviet Sputnik satellite in 1957 and the space race that it prompted. Space craft that would have to break the Earth's gravitational grip required even lighter, stronger components than GFRPs. Also, the heat generated

during re-entry of a space craft into the Earth's atmosphere could exceed 1500^{o}C, which was beyond the temperature limits of any monolithic or composite material then known. In 1956 laboratories developed asbestos fibre-phenolic resin composite for use as a possible re-entry nosecone material [21]. At that time scientists also began looking at metal matrix composites (MMC) for a solution. The space race thus provided an impetus for the development of the carbon and boron fibres that had been discovered more recently. Thus with the use of a variety of fibres and the use of a variety of matrices, a general notion of composites emerged in the 1960s. These high performance composites in the post Sputnik era were the *second generation of composites*. A schematic diagram showing the relative importance of the four classes of materials (ceramics, composites, polymers and metals) in mechanical and civil engineering as a function of time is shown in Fig. 1.1.

In the 1970s the composite industry began to mature. This was the beginning of *third generation of composites* (1970s and 1980s). Better plastic resins and improved reinforcing fibres were developed during this time. Fibres known as Kevlar, carbon fibres, etc. were also developed [22, 23]. Whereas space and aircraft demands had prompted the quest for new high modulus fibres in the 1960s, composites made with such expensive fibres had to find civil applications in the 1970s. At that time sports and automobile industries became major markets. A new approach of materials design made possible by the use of computers favoured the quest for a synergy of properties. Carbon fibres were used extensively in sporting goods in the beginning of 1970s. After the race to the moon was over, aerospace engineers began designing reusable spacecrafts such as space

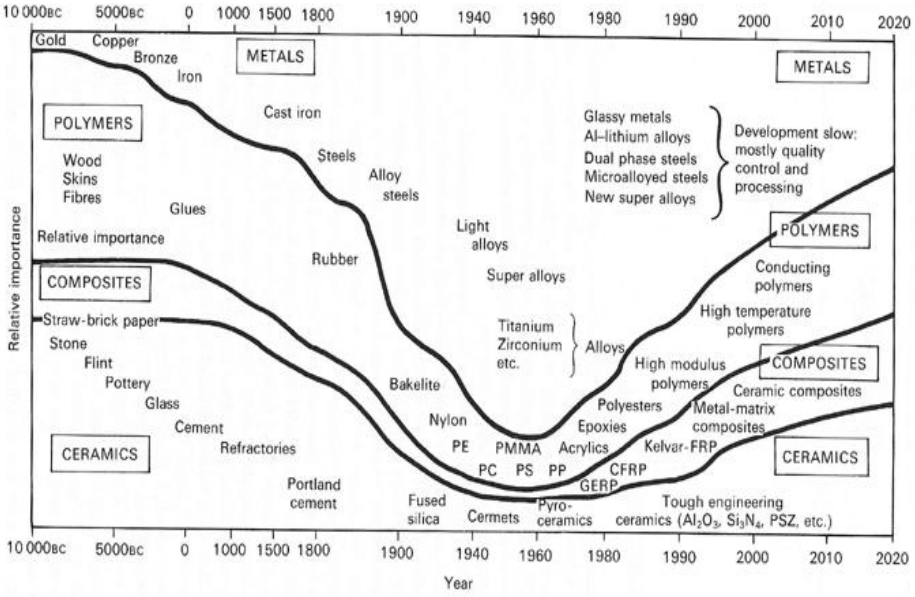

Fig. 1.1 Schematic diagram showing the relative importance of the four classes of materials (ceramics, composites, polymers and metals) in mechanical and civil engineering as a function of time (The time scale is nonlinear)

station, space shuttle, etc. and all these were subjected to extreme and repeated temperature swings. This required the optimization of the metal-matrix composites (MMCs) that had first been investigated at the beginning of the space race. By the mid-1990s, a variety of MMCs had found uses in spacecraft applications. For example, the antenna boom on the Hubble Space Telescope is made of a graphite-aluminum composite [24-27]. The ceramic matrix composites (CMCs) were also developed during this period. Graphite fibres in a carbon matrix produce another important class of CMCs: carbon-carbon composites. Whereas in the 1970s, composites had been defined by the association of a matrix, and reinforcing fibres in the 1980s; the synergy effect became part of their standard definition.

In the 1990s, both academic and industrial researchers started to extend the composite paradigm to smaller and smaller scales. Since microsynthesis has been successful in making computer components, material scientists have aimed to go beyond the microscale and to build up materials atom by atom, i.e. at nanoscales, in order to make complex materials that can function as devices or micromachines [28-30]. This was the beginning of the *fourth generation* of composites. This generation includes hybrids and *nanocomposites*. Hybrid materials have sizes from macroscopic scales to molecular scales, while nanocomposites have inclusion particle sizes in nanoscales. Hybrid materials mix organic and inorganic components at the molecular scale. Hystorically it was the study of biomineralization that focused the attention of materials scientists to the possibilities of such hybrid structures. Thus a new design strategy emerged and that is known as biomimetism [31, 32]. In the design of hybrid materials the main target is to mimic nature's processes, i.e. to get a spontaneous association of molecules into stable structures. When we explore life around us, it can be found that organization of nanomaterials is central to biology. Architectures made by organisms are all based on nano-assemblies. The thrills, effects and influences of nanotechnology are still on the move.

1.1.1 Classification of composites

Composite materials are commonly classified as two distinct entities. The first level of classification is usually made with respect to the matrix constituent. In composite materials, the matrix is the continuous phase of the system and in most cases the phase with the greater volume fraction. Based on the matrix constituent the major composite classes

include Metal Matrix Composites (MMCs), Organic Matrix Composites (OMCs) and Ceramic Matrix Composites (CMCs). The term organic matrix composite is generally assumed to include two classes of composites, namely Polymer Matrix Composites (PMCs) and Carbon Matrix Composites (CMCs), commonly referred to as carbon – carbon composites. Fig. 1.2 demonstrates classification of matrices.

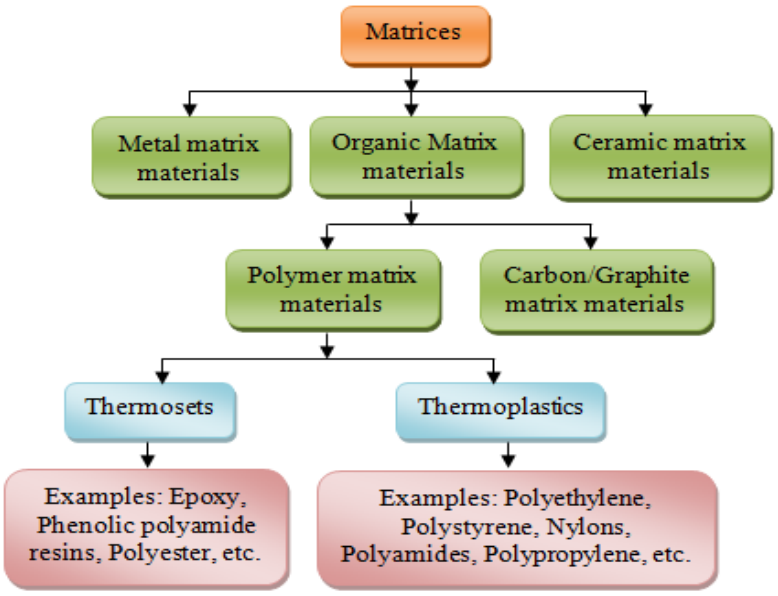

Fig. 1.2 Classification of matrix materials (including different kinds of thermoplastics and thermosets)

The second level of classification refers to the reinforcement form such as fibre reinforced composites, laminar composites and particulate composites. Fibre reinforced composites are composed of fibres embedded in matrix materials. Such a composite is considered to be a discontinuous fibre or short fibre composite if its properties vary with fibre length. On the other hand, when the length of the fibre is such that any further increase in length does not further increase the elastic modulus of the composite, the

composite is considered to be continuous fibre reinforced. Fibres are small in diameter and when pushed axially, they bend easily although they have very good tensile properties. These fibres must be supported to keep individual fibres from bending and buckling. Laminar composites are composed of layers of materials held together by matrix. Sandwich structures fall under this category. Particulate composites are composed of particles distributed or embedded in a matrix body. The particles may be flakes or in powder form. Concrete and wood particle boards are examples of this category. The classification of reinforcements is given in Fig. 1.3.

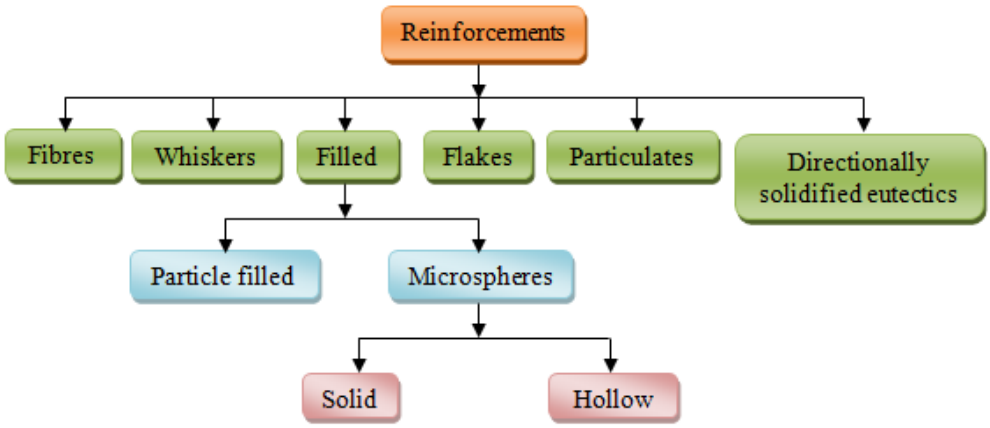

Fig. 1.3 Classification of reinforcements

Composites that form heterogeneous structures which meet the requirements of specific design and function, imbued with desired properties which limit the scope for classification. However, this lapse is made up for by the fact that new types of composites are being innovated all the time, each with their own specific purpose like the filled, flake, particulate and laminar composites. Table 1.1 gives a general classification of composite materials including examples for each.

Table 1.1 Classification of composite materials

Secondary phase (Reinforcement)	Primary phase (Matrix)			
		Metal	Ceramic	Polymer
	Metal	Infiltrated powder metallurgy parts	Cermets	Some molding compounds, Brake linings
	Ceramic	Cermets, Cemented carbides, fibre reinforced metals	Concrete	Plastic molding compounds, Fibre glass reinforced plastic
	Polymer	NA	NA	Kevlar reinforced epoxy
	Elements (E.g., C, B)	Fibre reinforced metals	NA	Rubber with carbon black, B or C reinforced plastics

(NA: not applicable currently)

In the following section the polymer composites are discussed in more detail, including the electro-active polymer composites.

1.2 Polymer composites

Polymers are long chain molecules made up of repeating smaller chemical units called monomers. Two general types of polymers are thermoplastics (can be molded and remolded many times by heating) and thermosets (once set, cannot be remolded). Thermoplastic polymer chains are not connected to each other. They are only semi-crystalline or

amorphous. Thermoset polymer chains have numerous cross-links that bond them into rigid networks. Their structure is much more crystalline.

Polymer composites have been considered scientifically and technologically important engineering materials mostly because of their thermo-mechanical performance. The investigation of the electrical, thermal and mechanical responses of this new class of materials started after a period of time, during which substantial work on manufacturing techniques and thermo-mechanical behaviour have been carried out. The two starting points of these investigations were, studying the effect of micro/nanoscaled filler on molecular mobility, polarization mechanisms and interfacial effects, and the significant enhancement of material properties in composites. In polymer composites the nature of the filler could be metallic, ceramic or any allotropic form of carbon. The properties of such composites depend on properties of their constituents, volume fraction of each constituent, polarizability of particles and nature of interconnection of these particles. An interesting group of ceramic inclusions includes the active or functional dielectrics, such as piezoelectric, ferroelectric and pyroelectric elements. The presence of such fillers can lend functionality to the system's performance.

The synthesis of polymer composites is an integral aspect of polymer technology. By inserting organic or inorganic particles, the properties of polymers improve and have a lot of applications depending upon the inclusions present in the polymers. So polymer composites are important structural materials due to their high tensile strength, high tensile modulus, and low density. They are used for lightweight structures such as satellites, aircraft, automobiles, bicycles, ships, submarines, sporting goods,

wheel chairs, armour, and rotating machinery (such as turbine blades and helicopter rotors) [33-35].

1.2.1 Electro-active polymer (EAP) composites

An important class of polymer composite materials are electro-active polymer (EAP) composite materials. They exhibit a change in size or shape when stimulated by an electric field. Their large electrically induced strains, low density, mechanical flexibility, and ease of processing offer advantages over traditional ceramic electro-active materials [36-38]. In the late 1990s, it has been demonstrated that some EAPs can exhibit up to a 380% strain, which is much more than any ceramic actuator. The most common applications of this type of materials are in the fields of actuators and sensors, robotics [39-41], in the development of artificial muscles [42, 43] etc. Electroactive polymers are promising alternatives for energy harvesting devices [44]. Two different families of EAPs can be identified as electronic EAPs such as electro-strictive polymers and ionic EAPs such as conductive polymers and ionic polymer-metal composites (IPMCs).

Electronic polymers (‘*dry’ polymers*) are characterized by a high dielectric breakdown strength and in operation they require a high activation field (> 150 V/mm), which is applied directly to the polymer [45]. They usually exhibit high and fast response within the applied high electric field with high voltages, along with relatively large induced actuation forces. Also, the strain achieved by the electric field is nominally proportional to the square of the applied electric field. The efficiency of electro-mechanical coupling is strongly influenced by the mechanical properties of the polymers themselves. They can maintain an induced

displacement under activation of a DC electric potential and they can be operated in air, which is compatible with robotic applications. Examples of such polymers are: dielectric elastomers, ferroelectric polymers such as Poly(vinylidene fluoride-Trifluoroethylene (PVDF-TFE) and some electrostrictive polymers.

In contrast, ionic polymers rely on the mobility of ions and electro-chemo-mechanical coupling. They generally require a wet environment. Hence they are referred to as *'wet' polymers.* The applied electric potential acts on an electrolyte, involving motion of both anions or cations and solvent in the actuation process. This effect is exploited to create structural and volume changes. The electrically generated strain of such polymer actuators is mainly controlled by the charge transferred between anode and cathode; depend on the applied voltage and not the applied electric field. Ionic polymers can be operated at relatively low driving voltages (1-10 V/mm). Large displacements and large forces are possible and whilst, they are more versatile, such systems tend to be much more complicated than electronic polymers, mainly due to the wet environment and the complexity of the compounds used to provide electro-chemo-mechanical coupling. Ionic polymers encompass a large variety of materials such as: polyelectrolyte gels, ionomeric polymers and conducting polymers (CP), featuring conjugated structures such as polyacetylene, polyaniline, polypyrrole, and polythiophene (and its derivatives).

A composite form of ion-exchange polymer films with metal electrodes, called Ionic Polymer Metal Composites (IPMCs), are receiving attention for applications such as artificial muscles [46]. The IPMC actuators are made of an ion conducting membrane material incorporated

with lithium or sodium, which is plated with metal electrodes, such as platinum. While the actuation mechanism of IPMCs is similar to conductive polymers, here the ion movement causes a dimensional change in the material and so the IPMC actuators require only much lower voltage for their operation.

The ionic EAPs, in general, provide a slow response and need to be moist continuously, since the performance degrades as the material becomes dry. A polysilicon coating technique was thus developed to maintain the moisture content of ionic EAPs, extending their operation in air from a few minutes to about four months [47, 48].

1.3 Nanocomposites

The word '*nano*' came from a Greek word meaning '*dwarf*'. One nanometer means one billionth of a meter (i.e., $l0^{-9}$ m) or is approximately the length equivalent to 10 hydrogen or 5 silicon atoms aligned in a line. As the size of the particles reduces from macro or micrometer scale to the nanometer regime, they exhibit new and different physical and chemical properties such as mechanical [49], thermal [50], electrical [51], magnetic [52], optical [53], and catalytic [54] features, for example copper which is an opaque substance in bulk becomes transparent at nanoscales. Silicon insulators become conductors. Gold which is solid, inert and yellow at room temperature at micro scale becomes liquid and red in colour at nano scale at room temperature. It also gets unusual catalytic properties not seen at macro scales. In recent years, nanocrystalline materials and nanotechnology have considerably attracted the interest of materials research community [55-57]. Table 1.2 provides an idea about the history

of scientific revolutions including a technology forecast.

Table 1.2 History of scientific revolutions (Wilson *et al*., Nanotechnology: Basic Science and Emerging technologies, Chapman & Hall, CRC Press, New York (2002.))

Discovery type	Name	Age	Start date
Industrial	Tools	Stone	2,200,000 BC
Industrial	Metallurgy	Bronze	3500 BC
Industrial	Steam power	Industrial	1764
Automation	Mass production	Consumer	1906
Automation	Computing	Information	1946
Health	Genetic Engineering	Genetic	1953
Industrial	*Nanotechnology*	*Nano age*	*1991*
Automation	Molecular assemblers	(Assembler age)	2020
Health, industrial, automation	Life assemblers	(Life age)	2050

The synthesis, characterization and processing of *nanostructured materials* is an emerging and rapidly growing field. Nanostructured materials may be grouped under *nanoparticles* (the building blocks including nanocrystalline materials such as ceramic, metal and metal oxide nanoparticles; fullerenes, nanotubes and related structures; nanofibers and wires, and precise organic as well as hybrid organic-inorganic nanoarchitechtures such as dendrimers and polyhedral silsesquioxanes), *nano-intermediates* (such as nanostructured films, dispersions, high surface

area materials, and supramolecular assemblies), and *nanocomposites.* In the following paragraphs only the subdivision *'nanocomposites'* will be discussed in detail.

Roy and colleagues first used the term nanocomposites in the early 1980s [58]. The most general definition of a nanocomposite is a multi-phase compound in which one of the phases has a length scale in the nanometer range. In 1992 a more practical definition, was given by Komarneni as '*composites of more than one Gibbsian solid phase where at least one-dimension is in the nanometer range and typically all solid phases are in the 1-20 nanometer range'*. The solid phases can be crystalline or amorphous, or a combination of both. Generally, nanocomposites are materials with a nanoscale structure that improve the macroscopic properties of products. Typically, nanocomposites are clay, polymer or carbon, or a combination of these materials with nanoparticle building blocks. Nanocomposites can generally be divided into two types: multilayer structures and inorganic/organic composites. Multilayer structures are typically formed by gas phase deposition or from self-assembly of monolayers. Inorganic/organic composites can be formed by sol-gel techniques, bridging between clusters or by coating nanoparticles (e.g. in polymer layers).

The class of nanoparticle-nanoparticle composites covers a very wide range of materials, as the criterion is simply that the two phases are on nanoscale. A common variety is the case of composites of metals (or alloys) with an inorganic oxide. There is a range of potential applications for such systems including catalysts, sensors, magnetic devices and

coatings. Nanocrystalline metal oxides such as MgO, SnO_2 and ZrO_2 are being investigated for a range of potential applications, such as gas-sensing, fuel cells and catalysis [59-61]. Nanocomposites also lend themselves to applications that are generally referred to as '*smart materials'* [62]. Perhaps the most active area, however, is that of increasing the energy density of capacitors [63]. The real possibility of increasing the relative permittivity while maintaining the electric strength could herald a breakthrough in capacitor industry and in the area of Helmholtz capacitor devices to be used as battery substitutes.

1.3.1 Pyroelectric and piezoelectric nanocomposites

Crystals are commonly classified into seven systems according to their geometric structure, such as triclinic, monoclinic, orthorhombic, tetragonal, trigonal, hexagonal and cubic. These seven systems can be subdivided into 32 crystal point groups according to their symmetry with respect to a point. Out of these 32 crystal point groups, 11 are centrosymmetric and are not electrically polarized when subjected to a uniform stress. The remaining 21 crystal classes are non-centrosymmetric and 20 of these become electrically polarized when subjected to an applied stress. This property is called the piezoelectric effect. Pyroelectric materials form a subgroup (containing 10 crystal classes) of the piezoelectrics. They possess a spontaneous electrical polarization. This polarization is usually masked by stray charges from the atmosphere which collect on the surface and tend to neutralize it. However, when the temperature of such a crystal is altered, the polarization changes; this change can be observed, hence the name pyroelectric. Pyroelectricity, like piezoelectricity, is solely a property of crystal symmetry. Hence, any crystal belonging to one of the 10

pyroelectric crystal classes will have the pyroelectric property as well. A diagram depicting the relationships between acentric crystal class and corresponding physical property is shown in Fig. 1.4.

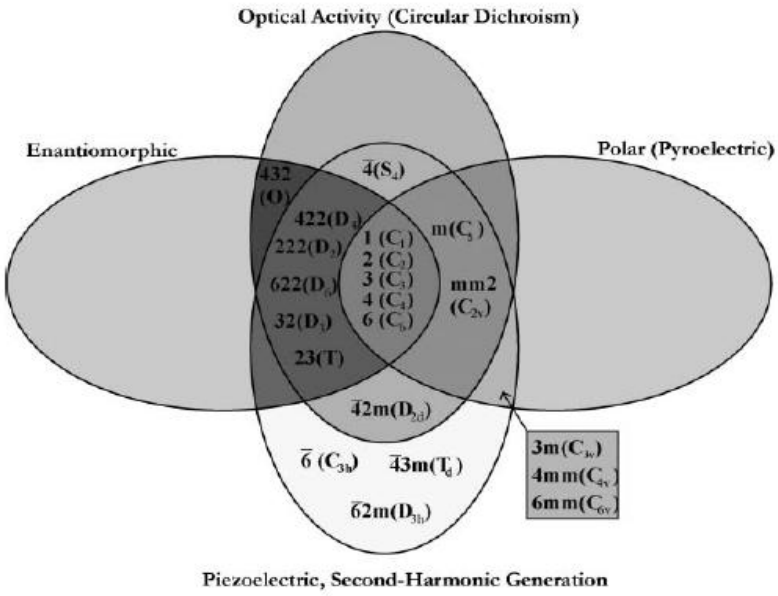

Fig. 1.4 Physical property inter-relationships in non-centrosymmetric crystal classes [64]

It has been found that most of the pyroelectrics which possess the largest pyroelectric coefficients also belong to the relatively small class of materials called ferroelectrics. These materials typically have a pyroelectric coefficient 10 to 100 times greater than nonferroelectric pyroelectrics. They possess spontaneous electrical polarization, like the pyroelectrics, but have the additional property that their polarization can be reversed by an applied electric field.

Fig. 1.5 is a colour scheme illustration showing that ferroelectrics form a subclass of pyroelectrics and pyroelectrics are a subclass of piezoelectrics, and they are a subclass of dielectrics [64]. In recent years, the synthesis and fabrication of pyroelectric and piezoelectric nanomaterials have attracted considerable attention.

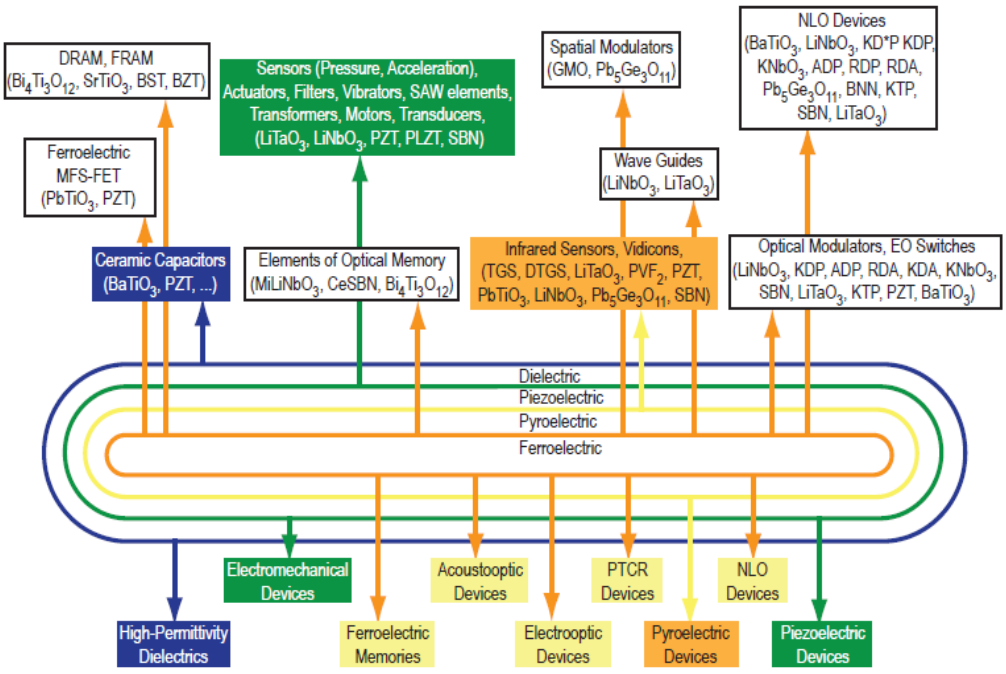

Fig. 1.5 Important pyroelectric, piezoelectric and ferroelectric materials and selected applications

The pyroelectric/piezoelectric nanoparticles and their composites can be synthesised from liquid, vapour or solid state processing routes. The liquid processing route is particularly attractive due to its simplicity and versatility. This route includes sol-gel, wet chemical and colloidal processing.

1.4 Polymer-ceramic nanocomposites

Polymer-ceramic nanocomposites are materials in which nanoscopic ceramic particles, typically 10-100 nm in at least one dimension, are dispersed in an organic polymer matrix in order to dramatically improve the properties of the polymer. Polymer-ceramic nanocomposites represent an alternative to conventionally filled polymers. The large industrial demand for polymers and the progress in nano-science and technology have lead to an equally large interest in polymer-ceramic nanocomposites to enhance their properties. Because of their nanometer size filler dispersion, nanocomposites exhibit markedly improved properties when compared to pure polymers or their traditional composites. Particle-reinforced polymer composites or compounds have been used for decades to increase the stiffness and strength of polymers and to reduce thermal expansion. The applications also make use of increased modulus and strength, outstanding barrier properties, improved solvent and heat resistance and decreased flammability.

Compared to polymer composites containing larger dispersed particles, polymer nanocomposites have the advantage of achieving the optimal properties at relatively low filler content, resulting in a lower density and better surface smoothness and transparency. Polymer-ceramic nanocomposites have shown significant improvement in mechanical, thermal and electrical properties also.

Recently, electro-active polymers (EAP) have taken the place of normal polymers as the matrix for nanocomposites in order to enhance electro-activity properties further. A 0-3 connectivity electro-active

polymer-ceramic nanocomposite is easy to fabricate, which allows for commercial production of the composites in a cost-effective manner. Tremendous possibilities and applications exist for different combinations in nanocomposites between ceramics and electro-active polymer species allow achievement of properties that cannot be obtained with normal polymer-ceramic nanocomposite materials. In recent decades a good number of electro-active polymer-ceramic nanocomposites have been introduced for various medical, telecommunication and microelectronics applications, including devices ranging from micromechanical systems through sensors and actuators.

1.5 Pyroelectric detector materials

Pyroelectric detector materials are famous for detecting even a very small change in the incident thermal/IR radiation. There are two kinds of infrared detectors viz. photon detectors (also called quantum detectors), in which radiation absorption process directly produces a measurable effect (which is not pyroelectric) and thermal detectors, in which absorbed radiation is converted first into heat, which subsequently produces a measurable effect (pyroelectric) [65]. Photon detectors are, in general, more sensitive than thermal detectors. The advantage of thermal detectors over photon detectors is that they can be operated at room temperature without requiring cooling and have very wide spectral response [66]. Recently, more research using many materials and different fabrication techniques have been directed towards room temperature operated infrared sensors [67, 68]. Thermal detectors are widely accepted because of their low cost, light weight, low power consumption, sensitivity over a large spectral bandwidth, sensitivity in a very wide temperature range and fast response.

The most critical component of a pyroelectric thermal/IR detector is the pyroelectric material which is used as the sensing element (i.e., the real sensor). The main focus of present day investigation is on those pyroelectric thermal/ IR sensors, which are very important for military, industrial and space applications. The material developments in the area continue to be primarily for military applications such as thermal/IR sensing.

Some well known pyroelectric infrared detecting materials are single crystals such as TGS (Triglycine Sulphate) and DTGS (deuterated Triglycine Sulphate), ceramics such as PZT (Lead Zirconate Titanate), $LiTaO_3$ (Lithium Tantalite), SBN (Strontium Barium Niobate), and polymer matrix hosts like PVDF (Poly(vinylidene fluoride)) and its co-polymers [65, 69-71].

Presently in the market there are new kinds of pyroelectric IR detectors as well as laser components. They have a wide spectral sensitivity ranging from UV to Terahertz wavelengths, limited by the detector window used. These detectors are based on deuterated and L-alanine-doped Triglycine Sulfate (DLaTGS), whose detectivity is typically 2.5 to 5 times higher than $LiTaO_3$ detectors, even at high frequencies [72]. All detectors possess thinned-out elements and optionally feature an absorbing black coating with a low thermal mass that offers a wide spectral response and high speed.

1.5.1 Theory and equivalent circuits

A pyroelectric thermal/IR detector is based on the conversion of photons to phonons and then to electrons. Theoretically it is like a capacitor

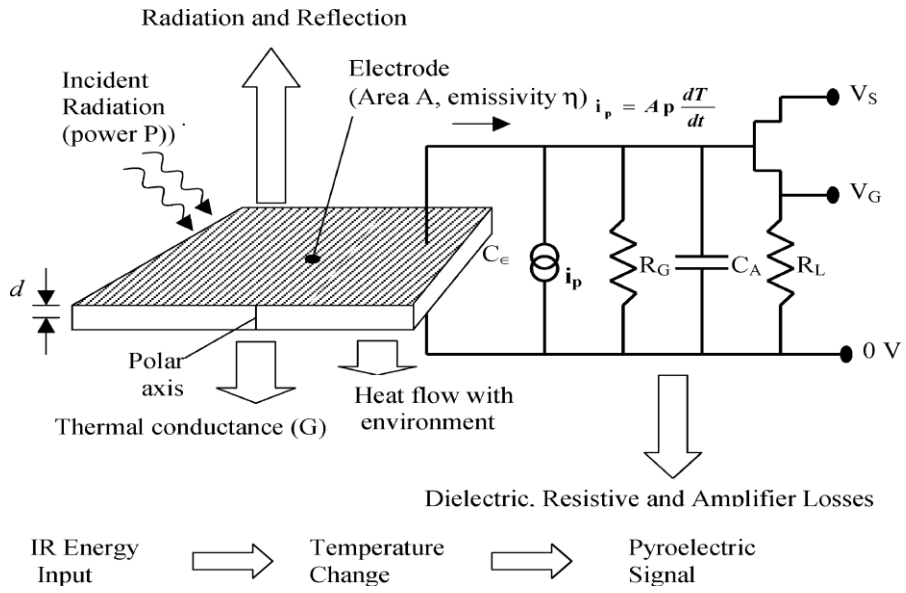

Fig. 1.6 Equivalent circuit of a pyroelectric IR detector and detection process

whose spontaneous polarization vector is oriented normal to the plane of the electrodes. In a pyroelectric IR material, the absorbed incident infrared radiation is converted into heat by photothermal effect. This causes a temperature change (*dT*) within the material and correspondingly a change in the spontaneous polarization of the sensing element. Change in this polarization alters the surface charge on the electrodes coated on either side of the pyroelectric detector material, and to keep neutrality the charges are expelled from the surface which results in a pyroelectric current in an external circuit, which is proportional to the rate of temperature change (*dT/dt*). This pyroelectric current can be measured using an appropriate measurement circuit. The pyroelectric current produced (I_P) is also proportional to the electrode area (*A*) of the sensing element. Thus the expression can be written as,

$$I_p = p(T)A\frac{dT}{dt} \qquad (1.1)$$

where *p(T)* is the pyroelectric coefficient of the sensor. An equivalent circuit of a pyroelectric detector and the detection process is illustrated in Fig. 1.6 [73].

1.5.2 Configuration

The most important and necessary part of a pyroelectric thermal/IR detector is its sensor element for detecting infrared radiation impinging thereon. For producing signals representing the detected radiation, there will be electronic circuit for readout of the signals from the detector array. In some applications, an integrating device for integrating the signals produced by the detector array would also be included. If it is a digital detector, an analogue to digital converter will be there for conversion. In order to isolate the sensor thermally from its surroundings, the detector element will usually be coated with a blackened thin film to increase the light/radiation absorption. Low noise and high input impedance amplifiers are necessary to detect the small amount of charge produced by heating. Typical circuit incorporates a field effect transistor with an appropriate load resister or an operational amplifier with a feedback resister to boost the signal. Doping the detector with various elements can control the detector's resistance and thereby eliminate the load resistor [74]. The pyroelectric detector element can also be configured to attenuate noise from ambient temperature changes and from vibrations. A general configuration is shown in Fig. 1.7.

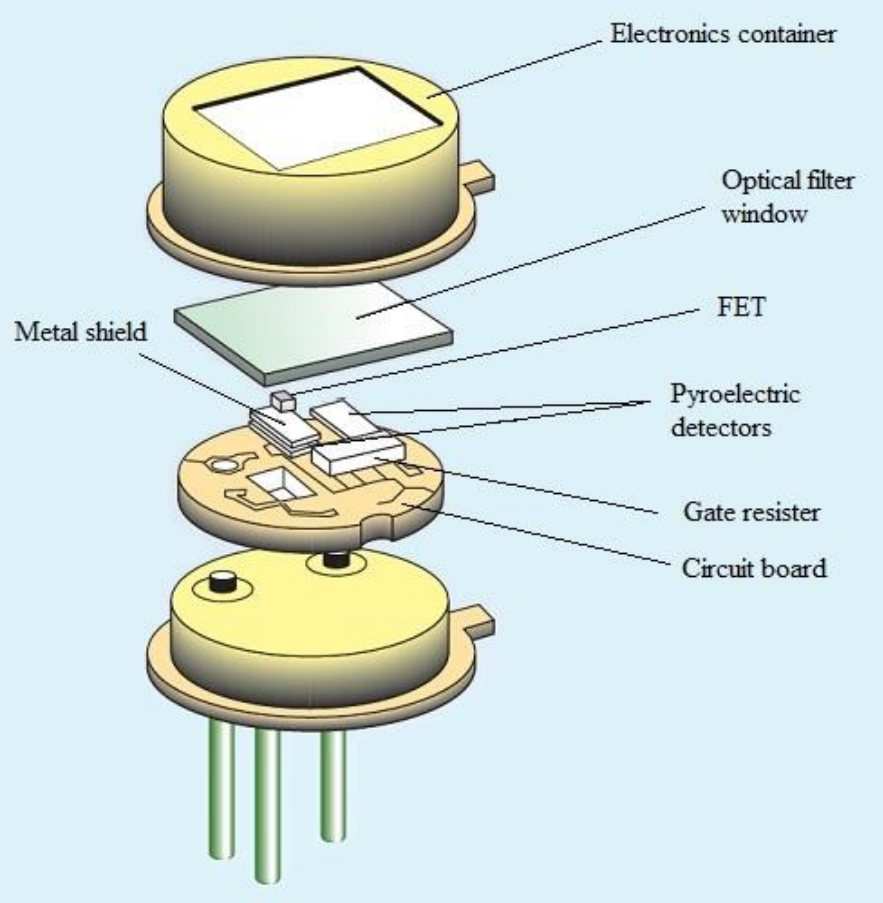

Fig. 1.7 Configuration of a pyroelectric IR detector [75]

One requirement for pyroelectric infrared detection systems is that the pyroelectric material must be subjected to a temperature change or changes between readouts of the electrical charge patterns produced in the material since the displacement current in the material is produced by changes in temperature. That is, the infrared radiation falling on the pyroelectric material must in some manner be time modulated and this can be done by provision of an infrared optical chopper between the material and the source producing the infrared radiation. The slower the chopping

rate, the longer is the time the heat from the infrared radiation can integrate on the pyroelectric material to produce larger temperature changes and thus larger displacement currents. The result is better sensitivity, i.e., good ability to detect even low level infrared radiation. However, in some pyroelectric detection systems, the slow chopping results in poor spatial resolution due to lateral thermal diffusion in the pyroelectric material. Thermal diffusion is simply the flow of heat from hot to cold areas giving rise to a smearing of the image. Slow chopping rates give the heat more time to flow from the hot to the cold areas before the signals are read from the pyroelectric material.

In solid state pyroelectric infrared image detectors (those in which the pyroelectric material is mated with solid state readout electronics), slow chopping gives rise to another problem. The heat produced in the pyroelectric material tends to flow through the mechanical electrode connections to solid state electronics and thereby reduce the detected temperature changes in the material. The displacement current and the signals produced by the pyroelectric material are thus reduced. This problem can be solved in low density pyroelectric arrays by mounting the pyroelectric material over an air gap and providing connection electrodes remote from the active detector area. This is feasible, however, only when the detector element spacing is 0.5 mm or more. With higher density arrays, it is possible with integrated circuit readout electronics, remote electrodes become impractical to use, especially with two-dimensional arrays. Chopping the incident infrared radiation at a faster rate would also serve to obviate this problem since the heat would have less time, between sampling the signals from the pyroelectric material, to flow from the material into the

solid state electronics. This would appear to be more economical and feasible than the previously mentioned spacing of connection electrodes; or of other techniques which have been tried, such as making very low thermal conductivity electrodes.

1.5.3 Figures of merit for pyroelectric IR detection

It is important to develop some criteria that can be used to assess the performance of a material for a particular application based solely on material properties. In such situations material figures of merit will allow the material assessment outside of geometric and/or engineering constraints for the purpose of material selection. Some material figures of merit (FOMs) have been developed as criteria for selecting optimum materials for IR detector applications. The FOMs are directly related to the material pyroelectric coefficient, which in large part determines the amount of signal generated by the material in response to a temperature change. Therefore, quantifiable determination of the pyroelectric coefficient is essential in order to optimize processing strategies for material development. Anyway, in the assessment of pyroelectric materials, there is not one global FOM that can be applied to all situations. The correct FOM must conform to the intended application of the material. Since the pyroelectric materials are essentially thermal transducers, both the electrical and thermal properties must be taken into account. Necessary analysis has been reviewed by esearchers to derive the current and voltage response and subsequent FOMs for pyroelectric detector materials [74].

In the case of a pyroelectric thermal/IR sensor the required FOMs are,

$$F_I = \frac{p(T)}{C} \qquad (1.2)$$

$$F_V = \frac{p(T)}{C\varepsilon} \qquad (1.3)$$

$$F_D = \frac{p(T)}{C\sqrt{\varepsilon'}} \qquad (1.4)$$

where F_I, F_V, F_D are the figures of merit for high current sensitivity, high voltage responsivity and high detectivity respectively; C is the specific heat capacity, ε is the dielectric constant and ε' is the dielectric loss of the sensor material [76-79].

The current sensitivity is defined as the amount of pyroelectric current generated per watt of incident radiation power on the pyroelectric element. Likewise, the voltage responsivity is the amount of pyroelectric voltage generated per watt of incident power. The FOM, F_I, is generally a sufficient choice for materials used at high frequency, such as in fast-pulse detectors, and F_V may be used as criteria for large area detectors with large element capacitance [80]. The quality of a pyroelectric sensor is not judged solely by the pyroelectric response, but by the signal-to-noise ratio of the sensor, where the noise may be intrinsic or extrinsic in origin [71]. The signal-to-noise performance is given by the specific detectivity. The detection limit of a pyroelectric sensor is typically limited by the Johnson noise (resistive noise) generated in the capacitor element. In such case, a useful FOM that weighs the material properties for optimal signal-to-noise ratio is F_D.

1.5.4 Material properties

Crucial material properties for pyroelectric IR sensors are high pyroelectric coefficient, low dielectric constant, low dielectric loss, better physical and chemical stability, low piezoelectric response, high quality,

low cost, ease of processing and stability against depoling.

Single crystal materials possess high FOM values due to their high pyroelectric coefficients. However their dielectric constants also are too high. Of course, these materials are usually available in bulk form [81-86]. So, it is very difficult to make devices using single crystal materials. Ceramic materials also have high figures of merit because they also possess high pyroelectric coefficient and low dielectric loss. But they have high dielectric constants and it is very difficult to prepare thin films having optimum thickness. But in the case of polymers, they can be prepared into the form of thin films exhibiting low dielectric properties over a wide frequency range and they can be produced with exact optimum thickness.

Composites based on ferroelectric ceramic particles embedded in ferroelectric polymers possess hybrid properties derived from individual components. These hybrid properties include large pyroelectric coefficients of ceramic material and the excellent mechanical strength, formability, flexibility and robustness of the polymer, eventually useful for infrared detector applications. Numerous kinds of 0-3 ceramic-polymer composites have been investigated in order to enhance their pyroelectric performance and other physical properties for use in various devices [87-89].

1.5.5 Applications

Pyroelectric IR sensors have a wide range of potential applications in many areas. They are a class of room temperature thermal detectors that produce a current output which is directly proportional to the rate of change of temperature when exposed to a source of radiation.

Pyroelectric IR detectors find their applications extensively in broad areas. They are in military, industrial, medical, space fields, etc. Their pertinence in such areas attracts scientists to continue studies on the pyroelectric materials. Pyroelectric thermal/IR detector materials are used to develop temperature sensing devices due to their efficiency in the conversion of thermal energy into electrical energy [90, 91]. This property allows them to be used in variety of applications such as thermometry, pyrometry, radiometry, spectrometry, direction sensing, remote temperature measurement, solar energy conversion, laser diagnostics, infrared imaging, pollution monitoring, etc. [74, 92-99]. Intruder/burglar and fire alarm security systems also benefit from pyroelectric thermal/IR detectors [100]. The pyroelectric vidicon tube and the detector array are good examples of thermal imaging devices [101-109]. Another application of pyroelectric detector materials is radiometry [110, 111]. They are highly sensitive to even very small temperature changes. This property is exploited in radiometers. Pyroelectric detectors are very familiar in medical field, since they can sense cells which are warmer than usual that can show the disease of rheumatoid arthritis or malignant tumours [112]. Their application in medical field includes monitoring patients' burns also [113]. The detection and protection of wild life is also reported in the literature [114]. Infrared detection has also been used for military night vision, target acquisition, missile guidance, etc. [115-118].

1.6 Present scenario of pyroelectric thermal/IR detectors

According to the '*IR detector market – global forecast to 2013-2020*' the long wave infrared (LWIR) detector market is the largest and the fastest growing market for IR detectors, mainly, due to its low price and

wide application range. Thermopile, Pyroelectric, and Microbolometers technologies are the most popular for this spectral range. MCT (Mackay Communication Technologies) and InGaAs are the expensive technologies, which are more popular in military applications. With the new product developments and advancement of these technologies, they are finding applications in a wider range of products such as biomedical imaging and spectroscopy. The major challenges faced by the IR detector market are government regulations and the high cost of technologies like MCT and InGaAs.

The geographical areas covered in the report on the IR detector market are the Americas, Europe, APAC (Asia-Pacific) region and ROW (Rest of World). APAC region has the largest market share in the overall IR detector market, followed by the Americas. Japan and the U.S. are the leading countries in this market as some of the largest manufacturers of IR detectors are located there. Major players in the IR detector market are Excelitas (U.S), Nicera (Japan), Murata Manufacturing (Japan), Hamamatsu (Japan), Flir (U.S.), Ulis (France), Raython (U.S.), Melexis (Belgium), Texas Instruments (U.S.), and Omron (Japan).

Also, according to the *TechNavio*'s analysts forecast report, the '*Global Infrared Detection Equipment Market 2015-2019*', the global infrared detection equipment market to grow at a compound annual grow rate (CAGR) of 11.86 percent over the period 2014-2019. The *TechNavio*'s report has been prepared based on an in-depth market analysis with inputs from industry experts. The report covers the Americas, the APAC region and the EMEA (Europe, the Middle East and Africa) region. It also covers the market landscape and its growth prospects in the coming years.

Yole Développement announced its "*Infrared Detectors Technology & Market Trends*" report on 9th July 2013, which provides a complete analysis, market segmentation and forecast by application, IR detectors technology analysis and evolution. It also focuses on the latest industry news and analysis of the new market entrants and exits. According to them, the total IR detector market generated revenue of more than $153 million (USD) in 2012, mostly due to the mature motion detection market, which relies on high-volume sales of automatic lighting and intrusion detection systems. However, in a scenario that includes spot thermometer function in mobile devices, these revenues are expected to reach $381 million in 2018, growing at a 16% compound annual grow rate.

Yole Developpement's report includes market insights in units and revenue by market segment and also by detector resolution. IR detector market forecasts are realized for 2013-2018. The report includes an overview of small-size IR arrays for imaging purposes. Fig. 1.8 gives the market forecast of IR detectors.

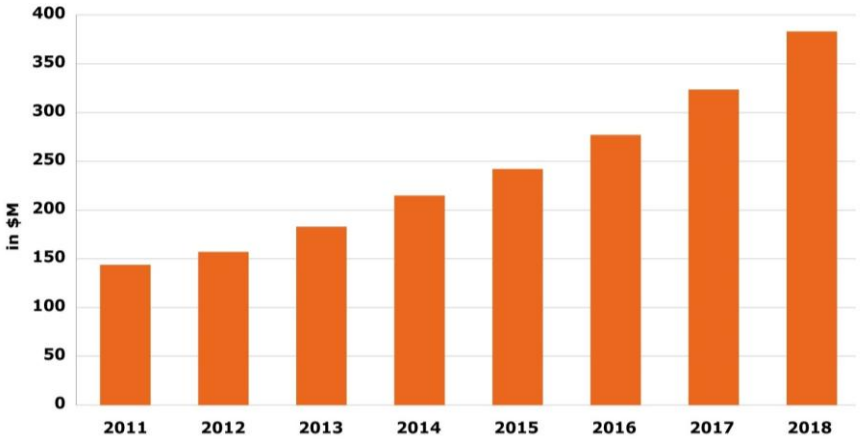

Fig. 1.8 Market forecast of IR detectors

Low-cost and easy-to-manufacture, IR detectors have been used in diverse markets, such as construction, security, appliances and industrial, and for a wide variety of functions (e.g., motion detection, counting and fire and gas detection). Initially limited to single-pixel pyroelectric detectors with a basic motion-detection function, IR detectors have progressively been used in more complex systems. This has diversified the market into higher-end applications (e.g., temperature-sensing, gas and fire detection and spectroscopy).

At the end of 2000, the diversification had been pushed further into the high end of the market by the introduction of array detectors. Multiple companies, led by *Heimann Sensors*, adopted a technology-push strategy to introduce IR detector arrays based on either pyroelectric technology or thermopile technology. Coming from the micro-electro-mechanical systems (MEMS) industry, several companies, such as *Omron* and *Panasonic*, have ensured the domination of thermopile technology on the array detector market by capitalizing on their knowhow in complex MEMS structure manufacturing. However, in 2013 the domination of thermopiles has been challenged by a new entrant based on a technology coming from the IR imaging market, *ULIS*.

The IR detector competitive landscape is complex due to the diversity of players in that market. Having a clear understanding of each player's technological background and positioning clarifies what the total available market is and the challenges that it has to face. While the small-size IR detector market is a commodity market driven by price, medium-size and large-size array detectors are cost and performance driven and offer room for differentiation for new entrants. However, strong barriers lie

between each IR detector technology (i.e., pyroelectric, thermopiles and microbolometers) because these technologies are based on different manufacturing processes, making the move from one technology to another difficult without a merger or acquisition.

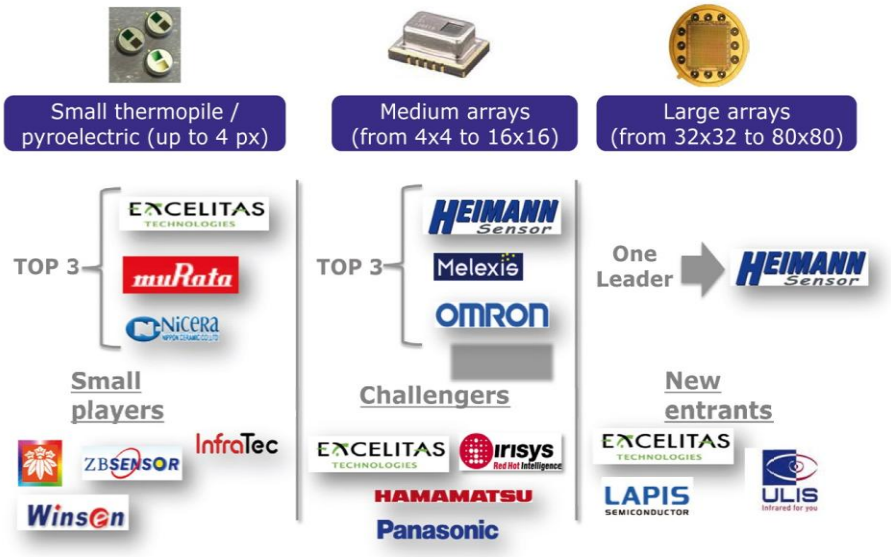

Fig. 1.9 Worldwide leading companies in the IR detector market

The U. S. base company *Excelitas* offers a wide range of Pyroelectric Infrared Detectors in both digital and analogue models. DigiPyro® is the industry's one and only truly digital pyroelectric infrared detector family (Fig. 1.10.). The DigiPyro® Family is setting the standard in digital motion and presence detection. *Excelitas* offers a complete range of DigiPyro® pyroelectric infrared detectors in TO metal housings including dual-element models - PYD 1788 and 1798, four-element - PYQ 2898 and PYQ 5848 as well as "Smart" DigiPyro® models - PYD 1096 and PYQ 1098, with total motion electronics integration.

Fig. 1.10 DigiPyro® infrared detector family developed by *Excelitas* (U. S.)

Excelitas has also introduced new pyroelectric SMD (Surface Mount Detector) to facilitate high-volume, SMT-compatible production in key motion and presence detection applications, including intrusion alarm systems and energy-saving motion-activated automatic light switches. *Excelitas*' new PYD 5790 is a dual-element pyro in a ceramic-type SMD package that is the smallest of its kind on the market.

Fig. 1.11 IRS-B series detectors manufactured by *Murata Manufacturing Co., Ltd.* (Japan)

The world famous Japan based company *Murata Manufacturing Co., Ltd.*, a world-leading innovator in electronics and the largest global supplier of ceramic passive components, has developed the world's

smallest and thinnest surface mount pyroelectric infrared sensor, 'IRS-B series' (Fig. 1.11). The new sensor (global part number IRS-B210ST01-R1) measures 5.0mm x 4.7mm x 2.4mm, making it ideal for use in compact, low profile electronic equipment and, in particular, energy saving devices. As the only surface mount pyroelectric IR sensor available on the market today, it provides numerous features including high sensitivity and signal to noise ratio, excellent stability against temperature changes and white light and enhanced radio frequency interference immunity.

1.6.1 Polymer-ceramic composites as pyroelectric thermal /IR detectors

During the literature survey it could be notice that most of the studies show that the ceramic materials have a larger pyroelectric coefficient than the polymer materials. Also they are highly brittle. But the advantages of polymer materials over ceramics are low dielectric constant and low dielectric loss. So by combining the ceramics and polymers we can achieve high figures of merit for IR detection, including high flexibility and robustness. Also one important advantage is that they are mouldable, so that the polymer/ceramic composites are applicable for curved surfaces too.

1.6.1.1 Importance of composite materials for IR detection

It was proposed by theoretical physicists that pyroelectric materials with figure of merit for high detectivity, significantly higher than presently available ferroelectric materials, whether it is a ceramic, polymer or single crystal in its pure form, is unlikely to be found. They have proved it based on the relationship,

$$P_0 = \frac{k\varepsilon_0 C_c}{V} \qquad (1.5)$$

where P_0 is the polarization at temperature 0K, k is the Boltzmann constant, ε_0 is the permittivity of free space, C_c is the Curie constant and V is the volume per unit dipole, which has been derived by using Devonshire's two-level dipolar effective field model and the Aizu-Lines lattice dynamic effective field model [119]. In order to maximize the polarization one has to maximize C_c and/or minimize the dipole volume V, which are the only material properties in the expression. Normally, the C_c value of ferroelectric materials is in the range 2×10^5 to 5×10^5 K and the polarizable volume seems to have a minimum of approximately 50 $A^{\circ 3}$. This proves that finding materials with higher polarization seems unlikely because it is not possible to increase the polarization beyond a certain limit. So, an increase in performance may be possible by preparing polymer-ceramic 0-3 composites. The figure of merit for high voltage responsivity is proportional to the pyroelectric coefficient and inversely proportional to the dielectric constant of the material. In order to decrease the dielectric constant, efforts have been made by forming a matrix-void composite. In the forming process only particles are introduced into the matrix so as to decrease the dielectric constants and hence obtain an increase in the figure of merit. By this way, 0-3 connectivity polymer-ceramic composite gives attractive results for IR detection applications.

Table 1.3 shown below gives a literature survey of the studies undertaken so far regarding the pyroelectric/dielectric properties and figures of merit for infrared detection, in the case of polymer-ceramic composites (including nanocomposites).

Table 1.3 Literature review on pyroelectric properties of polymer/ ceramic composites

Polymer matrix	Particle inclusion	Volume fraction	Pyroelectric co-efficient, $p(T)$ ($\mu C/m^2K$)	Dielectric constant, ε (at 1 kHz)	Dielectric loss, ε' (at 1 kHz)	Pyroelectric figure of merit, F_D ($\mu C/m^2K$)	Refer-ence
-	TGS crystal		550	55	0.025	469	120
PVDF	-		27	12 @10Hz	0.015 @10Hz	63.6	120
-	$LiTaO_3$ crystal		180	47	0.235	371	78
-	TGS crystal		280	38	0.38	454	78
-	PLZT ceramic		450	700	7.0	170	78
PVDF	PZT	0.50	140	95			121
PVDF	PZT	0.32	0.18	~ 45	~ 0.76	0.2	122
P(VDF-TrFe)	PZT	0.24	0.50	~ 38	~ 1.52	0.4	122
VDF-TrFE	PZT	0.50	140	85			121
PVDF-HFP	PZT	0.50	24	83	4	12	121
P(VDF-TrFE)	PZT	0.60	49.9	121			123
P(VDF-TrFE)	PZT	0.20	92	29	0.034	499	124
PVDF	$LiTaO_3$	0.17	147	48			125
PU	PZT	0.30	90	23	0.7	107.57	126
P(VDF-TrFE)	PTCa	0.65	130	67	0.013	139.29	127
PVDF	PT	0.62	130	54			128
P(VDF-TrFE)	PLZT	26 wt%	16.7	25	0.026	20.5	129

P(VDF-TrFE)	PLZT	33 wt%	9	14.12			129
P(VDF-TrFE)	PLZT	10.57 wt%	11.07	33.15			129
PVDF	PZT	0.50	90	10			128
P(VDF-TrFE)	PZT	0.50	39	118			130
PVDF	TGS		30	10			131
PVC	BT		0.08	3.7			128
P(VDF-TrFE)	PTCam	0.60	60	66			76
P(VDF-TrFE)	PZT	0.50	39	118			76
PVDF	TGS	0.80	90	12			76, 132
P(VDF-TrFE)	PLZT	0.24	130	44	0.037	102	122
P(VDF-TrFE)	PCaT	0.10	40	18	0.29	74	133
P(VDF-TrFE)	PCLT	0.11	58	13.2	.019	115.81	134
$P(VDF\text{-}TrFE)_{70/30}$	PT	0.54	68.2	55	0.034	49.4	135
PVDF-HFP	PZT	0.50	450 @ 70 ^{o}C	85			121
$P(VDF\text{-}TrFE)_{70/30}$	65PMN-35PT	0.40	30	42			136
PVA	Cement+steel fibers		0.06	2500			137
PEKK	PSTM-1	0.50	5.0	45			138
PEKK	PSTM-3	0.50	1.1	18			138
PEKK	PTCa	0.50	17	26	0.011	31.5	138
PS	TGS (400 µm)	0.60	1.14	6.6			139

PVDF	TGS	0.50	15	7.25			140
PVDF	DTGS	40 wt%	499 @ 36 °C	14.9	1.49	409	141
PVDF	ATGS	0.50	35	10.2			142
P(VDF-TrFE)	TGS	0.43	102	12.27	0.098	325	143
P(VDF-TrFE)	PT	0.27	45	40 @5MHz	0.010 @5MHz	450	130
P(VDF-TrFE)	PLZT	0.15	139.2	19.88	0.015	109.5	144
P(VDF-TrFE)	PZT	0.30	79	45	0.032	442	145
P(VDF-TrFE)	PT		68	48			146
P(VDF-TrFE)	PTCa		41	67			146
PEEK	PTCa	0.70	91	48.8			146
P(VDF-TrFE)	PLT	0.44	33	75			147
P(VDF-TrFE)	PMNZT + KTN	0.32+0.8	40.6	72.11	3.33	22.25	148
PVDF	MWCNT		639 @ 35 °C	26.17	12.33	182.1	149
P(VDF-TrFE)	LT	10 wt%	90 @ 65 °C	28	4.22	44	150
PVDF	SBN70	0.10	38	10.85	0.24	77.3	151
VDF-TrFE	PT	0.41	50 @ 25 °C	30	0.45		152
P(VDF-TrFE)	LT	0.08	137.5	20.7	4.2	67	153
P(VDF-TrFE) + Silver nanopart-icles	LT	0.02	449 @ 60 °C	40.99	29	83.4	154
P(VDF-TrFE)	PZT (50 wt%) + Mn (2 mol%)		113	21.5	0.024		155

PVDF	TiO_2	20 wt%	24.5	16	4		156
PU	PZT	0.50	5.6	50	0.75		157
PU	$PZT_{(0.49)}$ + Graphile $_{(0.01)}$		10.7	48	2	7.56	157
PU	PZT	0.32	58 @ 70 ^oC	24			158
P(VDF-TrFE)	PCLT		56.5	15.1	0.016	113.20	159
PVDF	LT	0.25	327	17.16	0.30	597	160*
PVDF	LN	0.25	134	15.53	0.32	237	161*
PU	SBN30	0.25	395	13.51	0.13	1095	162*
PU	TGS	0.25	325	10.46	0.23	678	163*
PU	DTGS	0.25	374	9.53	0.23	780	163*
P(VDF-TrFE)	$BaTiO_3$		70	15	0.02	130	164
Epoxy SPURRS	PZT	0.40	40	110			165

*****Present work. (Here division by specific heat capacity is not considered for direct comparison with literature values). Mearement details can be found in later chapters of the thesis.

1.7 Other applications of polymer-ceramic nanocomposites

The wide variety of nanocomposite materials leads, in turn, to a very wide range of applications other than IR detection. These range from biomedical applications such as dental materials [166] and bone grafting [167] to use in solar cells [168] photocatalysis [169] and frame retardancy [170]. Areas such as the use of nanocomposites in coatings have been

widely investigated with applications ranging from abrasion resistance [171], corrosion resistance [172], hard coatings to paints [173]. Polymer based nanocomposites are also being studied for use in batteries [174], fuel cells [175] and other energy storage devices [176]. Polymer-ceramic nanocomposite catalysts based on oxides are of great interest [177]. Equally, a variety of novel nanocomposites are of interest in the field of sensors. Examples include carbon nanotube based nanocomposites such as Prussian blue nanoparticles/ carbon nanotubes/ chitosan for glucose sensing [178] and carbon nanotube-polypyrrole nanocomposites for gas sensing [179]. Other applications of polymer-ceramic nanocomposites being investigated include hydrogen storage [180], electrical [181], and nanolithography [177].

Polymer-ceramic nanocomposite materials are aimed at being a substitute for more expensive technical parts such as gear systems in wood drilling machines, wear resistance materials, etc. and in the production of barrier plastic film for food industry [182-184]. Besides structural applications, polymer nanoparticle compounds have very interesting functional applications. For e.g., γ-Fe_2O_3/polymer nanocomposites are used as advanced toner materials for high quality colour copiers and printers and as contrast agents in NMR analysis, memory devices [184].

The composites industry is still evolving with higher growth rates every year. Today, composites are utilizing even better fibres and resins, many of which will incorporate nanomaterials. Composites are on the path towards being more environmentally friendly. They will continue to make the world lighter, stronger, more durable and a far advanced place to live.

1.8 Work presented in the thesis

In the present modern world, there are countless devices fabricated using ceramics, polymers, polymer-ceramic composites, etc. for radiation detection. Further progress in this field demands a better understanding of the fundamental properties of materials used in sensor industry. A detailed investigation of the pyroelectric, dielectric, thermal properties of selected electroactive polymer-ceramic composites (including nanocomposites) and hence the evaluation of pyroelectric figures of merit have been attempted in the present work.

- The main objective of the present investigation was to prepare highly sensitive, at the same time inexpensive, pyroelectric thermal/IR detector materials.

- Another objective of the investigation to prepare flexible pyroelectric thermal/IR detection materials which are more convenient to use, in which the strength may be improved without significantly reducing the sensitivity thereof. Experimental work toward this objective was done by choosing composites of polymers and ceramics.

- A further objective of the present study was to prepare polycrystalline samples of TGS and DTGS, the currently using IR detector materials which are highly susceptible to humidity, and convert them capable for use in humid atmosphere as well. This is explored by preparing polymer/polycrystalline composites of TGS/PU and DTGS/PU. Their properties for using them as pyroelectric thermal/IR detection applications have been measured and compared with other

polymer/ceramic composites (including nanocomposites) prepared for the same purpose.

- It was still another objective of the present research, in accordance with one aspect thereof, to provide such a type of pyroelectric infrared detection material which can cover even a large surface so that most of the incident radiation can be captured by the detection material. This goal was achieved by preparing free standing films of polymer/ceramic composites.

The above and other objectives of the investigation are realized in the study. In a nutshell, the thesis personifies the work carried out on the preparation, characterization and investigation of selected polymer-ceramic nanocrystalline and polymer-polycrystalline composites for pyroelectric thermal/IR detection applications. Since the applications of pyroelectric thermal/IR detectors continue to grow in a wide range of areas, the pyroelectric property and the materials possessing that property are still active topics of research.

References:

1. R. M. Jones, "Mechanics of composite materials", Second edition, Taylor & Francis, Inc., CRC Press, USA (1998)

2. K. K. Chawla, "Composite materials - Science and Engineering", Third edition, Springer, Ney York (2012)

3. S. K. Mazumdar, "Composites manufacturing – materials, product, and process engineering", CRC Press (2001)

4. L. Tong, A. P. Mourits, M. K. Bannister, "3D fibre reinforced polymer composites", Elsevier (2002)

5. A. K. Kulshreshtha and C. Vasile, "handbook of polymer blends and composites", volume 1, Rapra Technology Limited (2002)

6. T. Pradeep, "Nano : The essentials, Understnding nanoscience and nanotechnology", Tata Mc Graw-Hill (2007)

7. J. Liu, A. Y. Kim, L. Q. Wang, *et al.*, *Advances in Colloid and Interface Science* **69**, 131 (1996)

8. S. Y. Zhang, E. Godfrey, W. Kockelmann, *et al.*, *Materials Today* 78 (2009)

9. B. L. J. Bowden, "The origin and the role of the composite bow in the ancient near east", *http://www.academia.edu/1561842/The_Origin_ of_the_Composite_Bow_in_ Ancient_Mesopotamia*

10. A. R. Bunsell, "Fibre reinforcements for composite materials", Composite Materials Series, Volume 2, Elsevier, Amsterdam (1988)

11. S. Ansari and E. P. Giannelis, *J. Polym. Sci.: Part B: Polym. Phys.* **47**, 888 (2009)

12. I. Y. Jeon and J. B. Baek, *Materials* **3**, 3654 (2010)

13. P. H. C. Camargo, K. G. satyanarayana and F. Wypych, *Materials Research* **12**, 1 (2009)

14. S. Chen, X. Li, K. Yao, F. E. H. Tay, A. Kumar and K. Zeng, *Polymer* **53**, 1404 (2012)

15. E. Ogut, O. S. Yordem, Y. Z. Menceloglu and M. Papila, *Proc. of SPIE* **6526**, 65260Q (2007)

16. D. Li, Y. Wang and Y. Xia, *Nano Lett.* **3**, 1167 (2003)

17. J. Goniakowski, F. Finocchi and C. Noguera, *Rep. Prog. Phys.* **71**, 016501 (2008)

18. H. C. Zeng "Synthetic architecture of inorganic nanomaterials" in S. C. Tjong's "Nanocrystalline materials: their synthesis-structure-property relationships and applications", Elsevier, New York (2006)

19. R. M. Mayer, "Design with reinforced plastics", Springer, Netherlands (1993)

20. E. G. Nawy, "Fundamentals of high performance concrete", Second Edition, John Wiley and Sons, (2000)

21. I. S. Bhardwaj, "Polymer science recent advances", Editors TECHNIP, Paris (1994)

22. W. Watt, *Proc. Roy. Soc. Lond.* **A319**, 5 (1970)

23. H. H. Yang, "Kevlar Aramid Fibre", John Wiley, Chichester (1993)

24. S. M. Lee, "Handbook of composite reinforcements", John Wiley and Sons, California (1992)

25. R. K. Everett and R. J. Arsenault, "Metal matrix composites: processing and interfaces", Academic Press, Inc., San Diego (1991)

26. C. M. Gilmore, "Materials science and engineering properties", Timothy Anderson, Canada (2013)

27. S. Ochiai, "Mechanical properties of metallic composites", Marcel Dekker, Inc., Ney York (1994)

28. H. S. Khoo, C. Lin, S. H. Huang and F. G. Tseng, *Micromachines* **2**, 17 (2011)

29. P. Saravanan, N. Satyanarayana and S. K. Sinha, Tribol. Lett. **49**, 169 (2013)

30. K. R. Choudhury, Y. Sahoo, T. Y. Ohulchanskyy and P. N. Prasad, Appl. Phys. Lett. **87**, 073110 (2005)

31. G. Siebke, P. Holik, S. Schmitz, H. Schmitz, M. Lacher and S. Steltenkamp, *Bioinspir. Miomim.* **9**, 036012 (2014)

32. J. M. Taboas, R. D. Maddox, P. H. Krebsbach and S. J. Hollister, *Biomaterials* **24**, 181 (2003)

33. G. Oprisan, N. Taranu, V. Munteanu and I. Entuc, *Bul. Inst. Polit. Iasi.* **3**, 121 (2010)

34. T. Hanemann and D. V. Szabo, *Materials* **3**, 3468 (2010)

35. E. W. Gacitua, A. A. Ballerini and J. Zhang, *Maderas. Ciencia. Tecnologia.* **7**, 159 (2005)

36. T. B. Xu and J Su, *J. Microelectromechanical Systems* **14**, 539 (2005)

37. V. K. Varadan, X. N. Jiang and V. V. Varadan, "Microstereolithography and Other Fabrication Techniques for 3D MEMS", Wiley, Ney York (2001)

38. K. J. Pawlowski, H. L. Belvin, D. L. Raney, J. Su, J. S. Harrison and E. J. Siochi, *Polymer* **44**, 1309 (2003)

39. Y. Bar-Cohen, "Electroactive polymer (EAP) actuators as artificial muscles: Reality, potential and challenges", WA:SPIE Press, Bellingham (2001)

40. J-F. Capsal, J. Galineau, M. Lallart, P-J. Cottinet and D. Guyomar, *Sens. Actuators A: Phys.* **207**, 25 (2014)

41. K. S. Ramadan, D. Sameoto and S. Evoy, *Smart. Mater. Struct.* **23**, 033001 (2014)

42. C. Huang, Q. M. Zhang, J. Y. Li and M. Rabeony, *Appl. Phys. Lett.* **87**, 182901 (2005)

43. S. Priya, *J. Electroceram* **19**, 165 (2007)

44. Y. Wang, J. Wang, F. Wang, S. Li and J. Xiao, *Polymer Bulletin* **60**, 647 (2008)

45. J. Wang, C. Wu, R. Liu and S. Li, *Polym. Bull.* **71**, 1263 (2014)

46. M. Yamakita, N. Kamamichi, Y. Kaneda, K. Asaka and Z. Luo, *Advanced Robotics* **18**, 383 (2004)

47. Y. Bar-Cohen, S. Leary, M. Shahinpoor, J. O. Harrison and J. Smith, *SPIE* **3669**, 57 (1997)

48. Y. Bar-Cohen, T. Xue, M. Shahinpoor, J. O. Simpson and J. Smith, *SPIE* **3324**, 218 (1998)

49. X. Liang, D. M. King, P. Li and A. W. Weimer, *J. Am. Ceram. Soc.* **92**, 649 (2009)

50. Y. W. C. Yang, H. C. Yang, G. J. Li and Y. K. Li, *J. Polym. Res.* **11**, 275 (2004)

51. M. T. N. Pham, B. A. Boukamp, H. J. M. Bouwmeester and D. H. A. Blank, *Ceramics International* **30**, 1499 (2004)

52. B. Hallouet, B. Wetzel and R. Pelster, *Journal of Nanomaterials* **2007**, 34527 (2007)

53. O. A. Plaksin and N. Kishimoto, *Physics of the Solid State* **48**, 1933 (2006)

54. M. Sethi, D. B. Pacardo and M. R. Knecht, *Langmuir* **26**, 15121 (2010)

55. R. Abraham, S. P. Thomas, S. Kuryan, J. Isac, K. T. Varughese and S. Thomas, *eXPRESS Polymer Letters* **3**, 177 (2009)

56. Z. C. Tan, L. Wang and Q. Shi, *Pure Appl. Chem.* **81**, 1871 (2009)

57. B. A. H. Sanchez, T. J. Boyle, C. M. Baros, L. N. Brewer, T. J. Headley, D. R. Tallant, M. A. Rodriguez and B. A. Tuttle, *Chem. Mater.* **19**, 1459 (2007)

58. R. Roy, R. A. Roy and D. M. Roy, *Mater. Lett.* **4**, 323 (1986)

59. J. Hu, K. Zhu, L. Chen, C. Kubel and R. Richards, *J. Phys. Chem. C.* **111**, 12038 (2007)

60. D. Deng and J. Y. Lee, *Chem. Mater.* **20**, 1841 (2008)

61. M. Haruta, *Catalysis Surveys of Japan* **1**, 61 (1997)

62. I. Kang, Y. Y. Heung, J. H. Kim, J. W. Lee, R. Gollapudi, S. Subramaniam, S. Narasimhadevara, D. Hurd, G. R. Kirikera, V. Shanov, M. J. Schulz, D. Shi, J. Boerio, S. Mall, M. R. Wren, *Composites: Part B* **37**, 382 (2006)

63. L. Cao, F. Xu, Y. Y. Liang and H. L. Li, *Adv. Mater.* **16**, 1853 (2004)

64. K. M. Ok, E. O. Chi and P. S. Halasyamani, *Chem. Soc. Rev.* **35**, 710 (2006)

65. R. Capan, BAU FBE Dergisi **12**, 75 (2010)

66. P. W. Kruse, "Uncooled Thermal Imaging Arrays, Systems, and Applications", SIE Press, USA (2001)

67. M. Beck, D. Hofstetter, T. Aellen, J. Faist, U. Oesterle, M. Ilegems, E. Gini and H. Melchior, *Science* **295**, 301 (2002)

68. P. Werle, R. Mucke, F. D. Amato and T. Lancia, *Appl. Phys. B* **67**, 307 (1998)

69. S. N. Kumar and P. Kumar, *Int. J. Appl. Ceram. Technol.* **10**, E11 (2013)

70. X. Li, S. G. Lu, X. Z. Chen, H. Gu, X. S. Qian and Q. M. Zhang, *J. Mater. Chem. C* **1**, 23 (2013)

71. P. Muralt, *Rep. Prog. Phys.* **64**, 1339 (2001)

72. M. R. Srinivasan, *Bull. Mater. Sci.* **6**, 317 (1984)

73. P. Guggilla and A. K. Batra, "Novel electroceramic: polymer composites – preparation, properties and applications" in "Nanocomposites and polymers with analytical methods", J. Cuppoletti *(Ed)*, In Tech, 2011, (ISBN: 9789533073521)

74. R. W. Whatmore, *Rep. Prog. Phys.* **49**, 1335 (1986)

75. S. B. Lang, *Physics Today* **58**, 31 (2005)

76. B. L. Sidney and D. K. Das-Gupta, *Ferroelectrics Review* **2**, 217 (2000)

77. R. W. Whatmore and R. Watton, "'Pyroelectric Materials and Devices' in 'Infrared Detectors and Emitters: Materials and Devices'", Kluwer Academic Publishers, The Netherlands (2001)

78. P. Guggilla, A. K. Batra, J. R. Currie, M. D. Aggarwal, M. A. Alim and R. B. Lal, *Mater. Lett.* **60**, 1937 (2006)

79. A. Rogalski, Prog. Quantum Electron. **27**, 59 (2003)

80. M. H. Lee, R. Guo and A. S. Bhalla, *J. Electroceramics* **2**, 229 (1998)

81. R. Blinc, M. Burgar and A. Levstik, *Solid State Communications* **8**, 317 (1970)

82. Y. W. Song and B. A. Strukov, *Journal of the Korean Physical*

Society **35**, 362 (1999)

83. G. M. Loiacono and G. Kostecky, *Thermchimica Acta* **45**, 133 (1981)

84. A. Gerwens, M. Simon, K. Buse and E. Kratzig, *Optics Communications* **135**, 347 (1997)

85. M. Kovar, L. Dvorak and S. Cerny, *Applied Surface Science* **74**, 51 (1994)

86. M. N. Palatnikov, N. V. Sidorov, V. I. Skiba, D. V. Makarov, I. V. Biryukova, Y. A. Serebryakov, O. E. Kravchenko, Y. I. Balabanov and V. T. Kalinnikov, *Inorganic Materials* **36**, 489 (2000)

87. W. Nhuapeng, J. Tontrakoon and T. Tunkasiri, *CMU Journal* **1**, 61 (2002)

88. C. K. Wong and F. G. Shin, *J. Mater. Sci.* **41**, 229 (2006)

89. N. Wei, D-m. Zhang, F-x. Yang, X-y. Han, Z-c. Zhong and K-y. Zheng, *J. Phys. D: Appl. Phys.* **40**, 2716 (2007)

90. E. H. Putley, *Optics and Laser Technology* **3**, 150 (1971)

91. S. B. Zhang, X. Y. Guo and J. T. Xu, *Ferroelectrics* **232**, 1064 (1999)

92. A. J. Hadni, *Phy. E: Sci. Instrum.* **14**, 1233 (1981)

93. W. H. A. Majid, "Pyroelectric Activity in Cyclic and Linear Polysiloxane Langmuir-Blodgett Films", University of Sheffield, UK (1994)

94. P. D. Fairley and H. N. Rutt, *Sens. Actuators B: Chem.* **75**, 192 (2001)

95. V. K. Novik and N. D. Gavrilova, *Physics of the Solid State* **42**, 991 (2000)

96. F. Cascetta, *Measurements* **16**, 239 (1995)

97. E. Ph. Pevtsov, M. I. Maleto, V. I. Petrovsky, A. S. Sigov and V. V. Chernokozhin, *Microelectronic Engineering* **29**, 97 (1995)

98. B. Willing, M. Kohli, P. Muralt and O. Oehler, *Infrared Physics & Technology* **39**, 443 (1998)

99. R. Kohler, P. Padmini, G. Gerlach, G. Hofmann and R. Bruchhaus, *Integrated Ferroelectrics* **22**, 903 (1998)

100. D. Tar, *Infrared Physics* **25**, 349 (1985)

101. J. P. Nicholson and H. Ahmed, *Optics Communications* **49**, 55 (1984)

102. R. Watton, D. Burgess and P. Nelson, *Infrared Physics* **19**, 683 (1979)

103. B. Turner and H. A. H. Boot, *Infrared Physics* **16**, 367 (1976)

104. R. M. Logan, *Infrared Physics* **15**, 51 (1975)

105. R. M. Logan and R. Watton, *Infrared Physics* **12**, 17 (1972)

106. A. Lozinski, F. Wang, A. Uusimaki and S. Leppavuori, *Sens. Actuators A: Phys.* **68**, 290 (1998)

107. L. L. Sun, O. K. Tan, W. G. Liu, W. G. Zhu and X. Yao, *Infrared Physics & Technology* **44**, 177 (2003)

108. T. Sokoll, V. Norkus and G. Gerlach, *Surface & Coatings Technology* **97**, 469 (1997)

109. R. W. Whatmore and R. Watton, *Ferroelectrics* **236**, 258 (2000)

110. R. J. Clark and D. C. W. Sanderson, *Radiation Measurements* **23**, 641 (1994)

111. T. Yokoo, K. Shibata and Y. Kuwano, *Japanise Journal of Applied Physics* **24**, 149 (1986)

112. M. C. McCartney, "Electrical and Structural Properties of Calixarene Langmuir-Blodgett Films", Ph.D. Thesis, University of Sheffield, UK (1998)

113. S. N. Kumar, "Synthesis and characterization of $Sr_{0.53}Ba_{0.47}Nb_2O_6$ based ferroelectric composites for pyroelectric applications", Ph. D. Dissertation, NIT Rourkela, Orissa (2012)

114. P. Haschberger, M. Bundschuh and V. Tank, *Optical Engineering* **35**, 882 (1996)

115. R. G. Driggers, E. L. Jacobs, R. H. Vollmerhausen, B. O'. Kane, M. Self, S. Moyer, J. G. Hixson, G. Page, K. Krapels, D. Dixon, R. Kistner and J. Mazz, *Proc. SPIE* **6207**, (2006)

116. B. Bhanu and T. L. Jones, *IEEE AES Systems Magazine* **8**, 15 (1993)

117. R. C. Harney, *Proc. SPIE* **0300**, (1982)

118. R. D. Hudson (Jr.) and J. W. Hudson, *Proc. IEEE* **63**, 104 (1975)

119. J. D. Zook and S. T. Liu, *Ferroelectrics* **11**, 371 (1976)

120. M. Petty, J. Tsibouklis, M. C. Petty and W. J. Feast, *Thin Solid Films* **210**, 320 (1992)

121. L. F. Malmonge, J.A. Malmonge and W.K. Sakamoto, *Mat. Res.* **6**, 469 (2003) (and references therein)

122. B. Hilczer, J. Kulek, E. Markiewicz and M. Kosec, *Ferroelectrics* **267**, 277 (2002)

123. W. Y. Ng, B. Ploss, H. L. W. Chan, F. G. Shin and C. L. Choy, *IEEE* **0-7803-5940-2/01**, 767 (2001)

124. M. Dietze, J. Krause, C. –H. Solterbeck and M. Es-Souni, *J. Appl. Phys.* **101**, 154113 (2007)

125. S. Satapathi, P. K. Gupta and K. B. R. Varma, *J. Phys. D: Appl. Phys.* **42**, 055402 (2009)

126. K. S. Lam, Y. W. Wong, L. S. Tai, Y. M. Poon and F. G. Shin, *J. Appl. Phys.* **96**, 3896 (2004)

127. C. J. Dias and D. K. Das-Gupta, *Proceedings of the 4th international conference on properties and applications of dielectric materials* 175 (1994)

128. C. J. Dias and D. K. Das-Gupta, *IEEE Trans. Diel. Elect. Ins.* **3**, 706 (1996) (and references therein)

129. P. Guggilla, "Studies on pyroelectric materials for infrared sensor application", Ph. D. Dissertation, Alabama A & M University, Normal, Alabama, U.S.A. (2007)

130. B. Ploss, B. Ploss, F. G. Shin, H. L. W. Chan and C. L. Choy, *IEEE transactions on dielectrics and electrical insulation* **7**, 517 (2000)

131. M. Kobune, A. Mineshige, S. Fujii and Y. Maeda, *Japn. J. Appl. Phys.* **36**, 5976 (1997)

132. M. Wang, C. S. Fang and H. S. Zhuo, *Ferroelectrics* **118**, 191 (1991)

133. Q. Q. Zhang, H. L. W. Chan, B. Ploss, Q. F. Zhou and C. L. Choy, *J. Non. Cryst. Solids* **254**, 118 (1999)

134. Q. Q. Zhang, H. L. W. Chan and C. L. Choy, *Composites Part A: Applied Science and Manufacturing* **30**, 163 (1999)

135. H. L. W. Chan, W. K. Chan, Y. Zhang and C. L. Choy, *IEEE Trans. Dielec. and Elec. Ins.* **5**, 505 (1998)

136. K. H. Lam and H. L. W. Chan, *Comp. Sci. Technol.* **65**, 1107 (2005)

137. S. Wen and D. D. L. Chung, *Cement and Concrete Research* **33**, 1675 (2003)

138. A. Pelaiz-Barranco, O. P. Martinez and D. K. Das-Gupta, *J. Appl.Phys.* **92**, 1494 (2002)

139. A. Pelaiz-Barranco and P. Marin-Franch, *J. Appl. Phys.* **97**, 4104 (2005)

140. K. Sreenivas, T. S. Rao, A. Dhar and A. Mansingh, *Bull. Mater. Sci.* **6**, 105 (1984)

141. A. K. Batra, M. Simmons, P. Guggilla, M. D. Aggarwal and R. B. Lal, *Integrated Ferroelectrics* **63**, 161 (2004)

142. F. Changshui, W. Qingwu and Z. Hongsheng, *Ferroelectrics* **197**, 151 (1997)

143. Y. Wang, W. Zhong and P. Zhang, *J. Appl. Phys.* **74**, 512 (1993)

144. M. Olszowy, E. Markiewicz, C. Pawlaczyk, J. Kulek and E. Nogas-Cwikiel, *J. Electroceram.* **23**, 94 (2009)

145. M. Dietze and M. Es-Souni, *Sens. Actuators A: Phys.* **143**, 329 (2008)

146. C. J. Dias, R. Igreja, R. Marat-Mendes, P. Inacio, J. N. Marat-Mendes and D. K. Das-Gupta, *IEEE transactions on dielectrics and electrical insulation* **11**, 35 (2004)

147. Q. Zhang, H. L. W. Chan, Q. Zhou and C. L. Choy, *Chinese Science Bulletin* **43**, 111 (1998)

148. Y. F-. Xia, Z. D-. Ming, D. Z-. Wei, C. Z-. Yuan and J. S-. Lin, *J. Phys. D: Appl. Phys.* **41**, 055408 (2008)

149. M. E. Edwards, A. K. Batra, A. K. Chilvery, P. Guggilla, M. Curley and M. D. Aggarwal, *Mater. Sci. Appl.* **3**, 851 (2012)

150. P. Guggilla, A. K. Batra and M. E. Edwards, *J. Mater. Sci.* **44**, 5469 (2009)

151. M. Olszowy, E. N-. Cwikiel and K. Cwikiel, *Journal of Physics: Conference Series* **289**, 012017 (2011)

152. Y. Chen, H. L. W. Chan and C. L. Choy, *Journal of the Korean Physical Society* **32**, S1072 (1998)

153. A. K. Batra, J. Corda, P. Guggilla, M. D. Aggarwal and M. E. Edwards, *Proc. of SPIE* **7213**, 721313 (2009)

154. A. K. Batra, J. Corda, P. Guggilla, M. D. Aggarwal and M. E. Edwards, *Proc. of SPIE* **7419**, 741904 (2009)

155. C. Wu, G. Cai, W. Luo, Q. Peng, X Sun and W. Zhang, *Sens. Acturs. A: Phys.* **199**, 24 (2013)

156. W. C. Gan and W. H. A. Majid, *Smart Mater. Struct.* **23**, 045026 (2014)

157. W. K. Sakamoto, P. M-. Franch and D. K. Das-Gupta, *Sens. Actuators A: Phys.* **100**, 165 (2002)

158. W. K. Sakamoto, S. Kagesawa, D. H. Kanda and D. K. Das-Gupta, *J. Mater. Sci.* **33**, 3325 (1998)

159. L. Jinhua, Y. Ningyi and H. L. W. Chan, *Sens. Actuators A: Phys.* **100**, 231 (2002)

160. M. S. Jayalakshmy and J. Philip, *Sens. Actuators A: Phys.* **206**, 121 (2014)

161. M. S. Jayalakshmy and J. Philip, *J. Polym. Res.* **22**, 42 (2015)

162. M. S. Jayalakshmy and J. Philip, *Comp. Sci. Tech.* **109**, 6 (2015)

163. M. S. Jayalakshmy and J. Philip, *J. Appl. Polym. Sci.*, DOI: 10.1002/APP.42250 (2015)

164. C. E. Murphy and P. J. Dobson, *Ferroelectrics* **152**, 127 (1994)

165. S. B. Lang and D. K. Das-Gupta, Ferroelectrics Review **2**, 217 (2000)

166. H. Liu and T. J. Webster, *Int. J. Nanomedicine* **5**, 299 (2010)

167. K. Rezwan, Q. Z. Chen, J. J. Blaker and A. R. Boccaccini, *Biomaterials* **27**, 3413 (2006)

168. S. Ramasundaram, S. Yoon, K. J. Kim, J. S. Lee and C. Park, *Macromol. Chem. Phys.* **210**, 951 (2009)

169. A. J. Nathanael, D. Mangalaraj, P. C. Chen and N. Ponpandian, *Comp. Sci. Technol.* **70**, 419 (2010)

170. P. Kiliaris and C. D. Papaspyrides, *Prog. Polym. Sci.* **35**, 902 (2010)

171. I. V. Khudyakov, R. D. Zopf and N. J. Turro, *Designed Monomers and Polymers* **12**, 279 (2009)

172. V. Panwar, J. O. Par, S. H. Park, S. Kumar and R. M. Mehra, *J. Appl. Polym. Sci.* **115**, 1306 (2010)

173. A. S. Khanna, *Asian J. Exp. Sci.* **21**, 25 (2008)

174. A. M. Stephan, K. S. Nahm, M. A. Kulandainathan, G. Ravi and J. Wilson, *European Polymer Journal* **42**, 1728 (2006)

175. B. P. Tripathi and V. K. Shahi, *Prog. Polym. Sci.* **36**, 945 (2011)

176. D-H. Kuo, C-C. Chang, T-Y. Su, W-K. Wang and B-Y. Lin, *Journal of the European Ceramic Society* **21**, 1171 (2001)

177. B. A. Rozenberg and R. Tenne, *Prog. Polym. Sci.* **33**, 40 (2008)

178. X. Zhai, W. Wei, J, Zeng, X. Liu and S. Gong, *Analytical Letters* **39**, 913 (2006)

179. K. H. An, S. Y. Jeong, H. R. Hwang and Y. H. Lee, *Advanced Materials* **16**, 1005 (2004)

180. K. S. Triantafyllidis, P. C. LeBaron, I. Park and T. J. Pinnavaia, *Chem. Mater.* **18**, 4393 (2006)

181. Q. Wang and L. Zhu, *J. Polym. Sci. Part B: Polym. Phys.* **49**, 1421 (2011)

182. M. Aliofkhazraei, "Nanocoatings: size effect in nanostructured films", Springer, Ney York (2011)

183. A. G. Ingale, "Nanocomposites for surface coating" in "Handbook of research on diverse applications of nanotechnology in Biomedicine, Chemistry and Engineering" (Edited by, S. Soni, A. Salhotra and M. Suar), ACME Book Series, Engineering Science Reference, USA (2014)

184. A. Lagashetty and A. Venkataraman, *Resonance* **10**, 49 (2005)

Chapter

2

Experimental Methods

This chapter of the thesis provides a detailed overview of the experimental and sample preparation techniques used for the study. In this chapter, the first few sections give an idea of the sample preparation methods and the basics of the standard characterization techniques chosen in the entire study, including the theoretical and experimental background for conducting data analyses. Details of the major experimental techniques used to investigate the relevant properties of the prepared samples, in order to use them as pyroelectric thermal/IR detectors are described in the last few sections of this chapter.

2.1 Introduction

This chapter covers the experimental techniques adopted for the complete investigation revealed in the thesis. The various experimental techniques include standard characterization techniques such as powder X-ray Diffraction (XRD), Scanning Electron Microscopy (SEM), Electron Diffraction Spectroscopy (EDS), Transmission Electron Microscopy (TEM), Differential Scanning Calorimetry (DSC) and Fourier Transform Infrared Spectroscopy (FTIR). Material characterization involves determination of the characteristic physical and chemical properties following these established analysis techniques carried out under known conditions. Besides these, the dielectric properties of all the samples are measured by a capacitance method. The pyroelectric coefficients are measured using the Byer-Roundy method and the measurements of thermal properties are carried out by employing Photopyroelectric (PPE) technique. This chapter gives a description of the sample poling technique used in the work, which is necessary for the enhancement of the pyroelectric properties of the prepared polymer composite samples. The chapter also describes the Shore hardness test which is used to analyse the flexibility of polymer composites.

2.2 Sample preparation

In an effort to maximise the figures of merit for thermal/IR detection mentioned in section 1.5.3 of Chapter 1, and to attain the goals of the investigation as mentioned in section 1.8 of Chapter 1, all the samples are prepared as composites in the form of flexible free standing films. For studies presented in the thesis, nanocrystalline ceramic powders and microcrystalline powders are synthesized as the inclusion materials.

Conventional slow evaporation technique is used to prepare microcrystalline samples. The nanocrystalline powders are prepared by known aqueous organic gel routes and known chemical routes. Solvent cast method is adopted to prepare polymer-ceramic composites in the form of films. All the nanocrystalline, microcrystalline and polymer composite samples are prepared with utmost care in order to avoid impurities. The preparation techniques are given in detail in respective chapters.

2.2.1 Polymer matrix

The polymer matrices selected for the present investigations are commercially available in the market in the forms of powders or granules. In order to prepare them as films, they are liquefied first and cast into films. More details about the selected polymers and the synthesis methods are explained in the respective chapters.

2.2.2 Nanocrystal or microcrystal inclusions

The preparation of nanoparticles can be accomplished through many different approaches such as milling or attrition, repeated quenching, lithography, electrochemical deposition, sol-gel process, hydrothermal method, auto combustion method, etc. [1-4]. The ceramic nanoparticles mentioned in this thesis are prepared by simple direct chemical routes and aqueous organic gel routes.

In the direct chemical routes stoichiometric ratio of the required oxides or hydroxides which are synthesized by hydrothermal or some other chemical methods are mixed well using an agate mortar and the mixture is then heat treated at higher temperatures to produce nanoparticles.

In the aqueous organic gel route, first, the major components of the material which we want to synthesize are dissolved in deionised water and then mixed with suitable aqueous solutions to prepare complexes separately. Then stoichiometric amounts of these prepared complex solutions are mixed together to form the precursor solution. This solution is then heated to produce a gelatinous precursor, which after calcination produces nanopowders.

For growing crystals there are different methods including growth from solution, growth from flux, hydrothermal growth, high pressure growth, gel growth, etc [5]. We have adopted the conventional slow evaporation from solution technique. For this we prepared crystals from supersaturated solutions. Once getting the seed crystals, they are re-crystallised four to five times for further purification. After these processes we get pure small crystals. These small crystals can be ground into powders. Such prepared microcrystalline powders are also used for this study.

The synthesis procedures of each micro and nanocrystalline samples are explained in detail in the respective chapters.

2.2.3 Composites

In order to prepare composite films there are also many different ways like hot rolling, solvent casting, tape casting, etc. Here the composite film samples were prepared using a solvent cast technique. This method is one of the easiest and less time consuming methods for the synthesis of polymer composite films. In solvent casting, first of all the solid polymer in the form of granules, flakes or powder is dissolved in a suitable solvent.

Then, a required quantity of the ceramic inclusion can be added and dispersed well into this prepared polymer solution. If it is a nanocomposite, there will be a large possibility for the nanoparticles to get agglomerated. The nanoparticle agglomerations will lead to undesirable electrical or material properties if they are dispersed nonuniformly. Therefore, dispersion of nanoparticles is an extremely important contributor for achieving improved properties. In order to overcome the problem of agglomeration, viscosity of the polymer can be reduced through heating during ultrasonic mixing process. The next step is to transfer this mixture to a suitable open container for the solvent to evaporate completely. After the evaporation of the solvent the film can be peeled off from the container [6]. In the case of nanocomposites, owing to nanometer length scales which minimizes scattering of light, the films will usually be transparent.

2.3 Structural characterization by XRD

Every atom in a crystal scatters the X-ray beam incident upon it in all directions. The condition for X-ray diffraction from a crystal is given by the Bragg equation,

$$2d \sin\theta = n\lambda \qquad (2.1)$$

where d is the distance between each set of atomic planes of the crystal lattice, θ is the angle of diffraction, n is the order of diffraction and λ is the wavelength of X-ray beam. Atoms located exactly on the crystal planes contribute maximally to the intensity of the diffracted beam; atoms exactly halfway between the planes exert maximum destructive interference and those at intermediate locations interfere constructively or destructively depending on their exact location but with less than their maximum effect. The positions of the diffracted beams from a crystal depend only upon the

size and shape of the repetitive unit of a crystal and the wavelength of the incident X-ray beam. No two substances have identical diffraction patterns when we consider both the diffraction and intensity of all diffracted beams; however, some similar, complex organic compounds may have almost identical patterns. The diffraction pattern is a 'fingerprint' of a crystalline compound and the crystalline components of a mixture can be identified individually.

If the X-ray beam is monochromatic, there will be only a limited number of angles at which diffraction of the beam can occur. The actual angles are determined by the wavelength of X-rays and the spacing between various planes of the crystal. In the rotating crystal method, monochromatic X radiation is incident on a single crystal which is rotated about one of its axes. The reflected beams lie as spots on the surface of cones which are coaxial with the rotation axis. By remounting the crystal successively about different axes, the complete distribution of the reciprocal lattice points can be determined. Definitely, one mounting is sufficient if the crystal is cubic, but two or more may be needed if the crystal has lower symmetry [7].

The powder X-ray diffractometer used to study the samples in this work was Bruker AXS D8 Advance diffractometer with angle range 5-360^{o}. The device consists of a stationary X-ray source, Ni filtered radiation with wavelength 1.5404 Å and a movable detector to scan the intensity of the diffracted radiation as a function of the angle 2θ between the incident and the diffracted beam.

2.4 Morphology by Electron Microscopy

In order to understand the particle sizes of the prepared

nanoparticles and to study the morphology of the prepared samples, Scanning and Transmission Electron Microscopies (SEM and TEM) have been employed.

2.4.1 SEM

The SEM analyses of all the prepared samples were done using Jeol JSM 6390LV Scanning Electron Microscope. It gives the morphological information of the samples prepared and also gives solid evidences for the presence of inclusion materials in polymer matrices. A narrow beam of electrons from a tungsten filament scans the sample surface. The intensity of back scattered or secondary electron beam is noted as a function of the primary beam. In order to ensure that the electrons are not scattered by gas molecules inside the chamber, the scanning is carried out at low pressure [8]. Images from comparatively large area of the sample can be obtained by using a SEM.

2.4.1.1 Elemental analysis by EDS

Elemental analyses of some prepared samples have been carried out using an Electron Diffraction Spectrometer (Make: Jeol, Model: JED 2300) attached to the SEM instrument.

2.4.2 TEM

In the Transmission Electron Microscopy a focused beam of high energy electrons is transmitted through a thin sample to bring out the information about its internal structure, crystallography, particle size distribution and its elemental composition. Lattice images with atomic scale resolution and chemical information at a spatial resolution of the order of one nm or better can be produced by a TEM. Using TEM a single

nanoparticle in a sample can be focused and it is possible to identify and quantify directly its chemical and electronic structure. Definitely the most important application of TEM is the real space imaging of nanoparticles with atomic scale resolution [9]. In our investigations we have used a high resolution TEM of Jeol Make, Model JEM 2100.

2.5 Thermal analysis by DSC

In Differential Scanning Calorimetry the sample and a reference material are subjected to a closely controlled programmed temperature. In the event that a transition induced by temperature variation occurs in the sample, thermal energy is added to or removed from the sample or reference containers in order to maintain both sample and reference at the same temperature. Because this energy input is precisely equivalent in magnitude to the energy absorbed or evolved in the particular transition, a recording of this balancing energy yields a direct calorimetric measurement of the transition energy. The DSC apparatus used in our studies is Mettler Toledo Make, Model DSC 822^e machine.

2.6 Analysis by FTIR

The IR spectra provide valuable information regarding the structure and nature of the functional groups present in the sample. So it can be used as an effective tool for sample analysis. The IR radiation is guided through an interferometer. After passing through the sample the detected signal is the interferogram signal. By the application of the mathematical Fourier Transform on this signal we will get a spectrum identical to that from conventional IR spectroscopy. Measurement with a single spectrum is faster here because the information of all frequencies is collected simultaneously.

This allows multiple samples to be collected and averaged together resulting in an improvement in sensitivity. In our studies the transmittance in the region 1000–400 cm^{-1} were recorded using Thermo Nicolet make Avatar 370 Fourier Transform Infrared Spectrophotometer.

2.7 Measurement of dielectric properties

In the case of materials used as thermal/IR detectors it is important to evaluate their dielectric response and characteristics.

The dielectric constants of all the prepared samples were measured by the capacitance method. The sample under study was used as the dielectric medium of a parallel plate capacitor. In order to ensure the electrical contact between the sample and the capacitor electrodes, both sides of the samples were coated with silver paste. The capacitance values (C) and the dissipation factors ($tan\ \delta$) at various frequencies from 100 Hz to 5 MHz were measured using an Impedance analyzer (Make: Hioki, Model: IM3570). From these capacitance values the dielectric constants (ε) were calculated using the expression,

$$\varepsilon = \frac{Cd}{A\varepsilon_0} \qquad (2.2)$$

where d is the sample thickness, A is the electrode area of the sample and ε_0 is the permittivity of free space (= 8.854×10^{-12} F/m) [10, 11]. The dielectric loss (ε') is calculated by the expression,

$$\varepsilon' = \varepsilon \tan\delta \qquad (2.3)$$

In the complete study both the dielectric constants and dielectric losses

were calculated for room temperature.

2.8 Sample poling

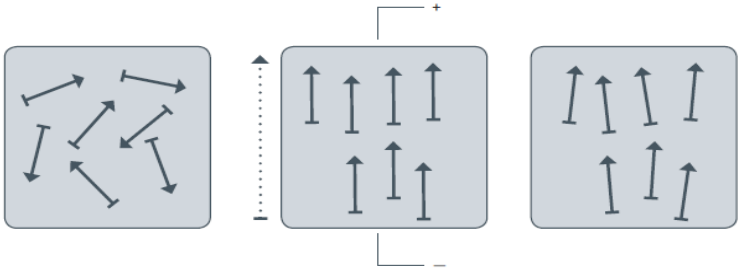

Fig. 2.1 Electric dipoles in pyroelectric materials before, during and after poling

In order to align electric dipoles in the samples a very high electric field is applied at room temperature or elevated temperatures for a definite period of time. This process is called poling. Before poling, the particle inclusions, which are the active particles in a composite, are randomly aligned. Thus the composite possesses a zero net dipole moment, just as in the case of centre of symmetry. During poling the space charge in the polymer will drift and accumulate at the matrix-inclusion interface to compensate for the discontinuity of the electric displacement at the interface and to stabilize the dipole orientation in the inclusion phase. This is the main reason for the long poling time requirement for some composite samples. Though the dipoles in the inclusion phase can be aligned without the interfacial charge, they will relax back to the random orientation due to the development of depolarizing fields [12, 13]. The alignment of the dipoles before, during and after poling is demonstrated in Fig. 2.1.

There are different poling techniques that can be employed to achieve high dipolar orientation in polymer composite samples, such as

thermal poling, electric field poling, electronic beam poling, contact poling, corona poling, plasma and hysteresis poling [14, 6]. The most advanced technique for poling (or charging) film samples is Corona poling. So in our investigations we have adopted the corona poling technique. This is an efficient non-contact poling process for both ferroelectric and non-ferroelectric polymer materials [15-18]. Corona is a self-sustainable discharge occurring when a sufficiently high voltage is applied to asymmetric electrodes such as a point and a plate [19]. Surrounding the corona point, depending on the corona polarity being either positive or negative, ions are produced in the ionization area. The ions bombard a non-metalized film surface, so that the metallic electrode is not required on this surface of the film sample. The process takes place at atmospheric pressure, so the ions have an average thermal energy. The samples are exposed for a few minutes to a few hours at room temperature or elevated temperatures. The ions do not penetrate into the film sample but they only transfer their charge and leave the surface as neutral atoms or molecules. The excess charges either reside on the surface or injected in to the film sample. The poling process is completed by freezing the dipole orientation in the glassy state of the polymer.

The poling conditions for each samples prepared in the form of free standing films, for the present investigation, are given in the respective chapters, as these vary with the sample.

2.8.1 Poling set up

Fig. 2.2 shows the schematic diagram of the experimental set-up employed for performing corona poling, assembled in the laboratory. The

set-up consists of a sharp edged corona electrode fixed within a chamber, 1 cm above the polymer sample. When the needle is elevated to a high enough potential the air around it becomes ionized. These ions then drift down towards the polymer film sample.

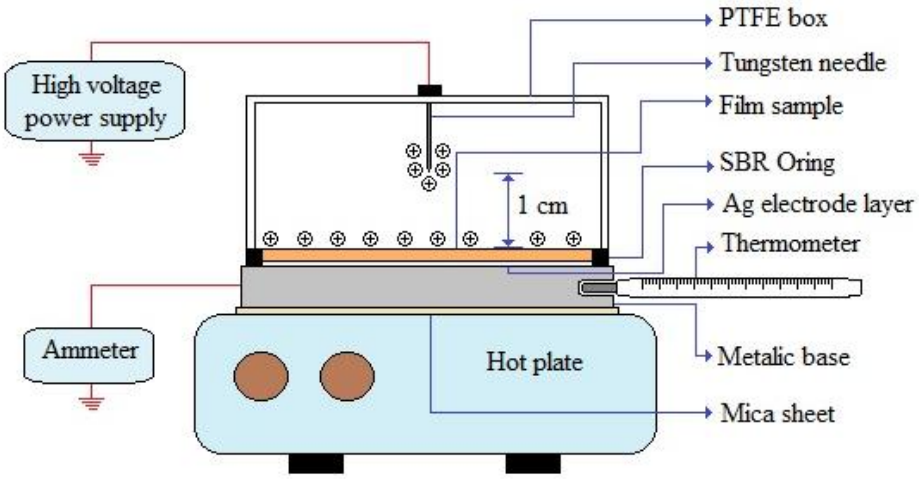

Fig. 2.2 Schematic diagram of corona poling system

The poling chamber is made of a very high insulating material which causes any free ions that come in contact with it to attach onto its surface. This collected ions results in a charge build-up on the inner surface of the chamber, which in turn repels other drifting ions forcing them down towards the sample. On the underside of the polymer film there is a grounded base that enables the ions to produce an electric field through the sample and thus pole the polymer film. Between the grounded base and the polymer film there is a silver electrode layer provided to increase the electrical conductivity between the polymer film and the metallic base. The base is grounded through an ammeter, so that the current flowing from the electrode can be measured. As the polymer chains reorganize and the dipoles become aligned, fewer and fewer charges will be able to travel

through the sample and thus the current flowing through the electrode will decrease. When this current becomes nearly zero, the polymer is completely poled. Here the Styrene Butadiene Rubber (SBR) O ring prevents the charges on the surface of the polymer film from travelling around the material and directly into the electrode, which result in an incorrect measurement of current [20].

2.9 Measurement of pyroelectric coefficient: Byer-Roundy method

Pyroelectricity is the ability of certain materials to generate temporary electric charges on their surfaces when they are heated or cooled. Here the induced charges will be proportional to the temperature gradient. The pyroelectric activity can be measured by various techniques such as heating by electromagnetic radiation, temperature-modulated excitation, capacitive charge integration, quasi-static measurement method, radiative dynamic method, etc. [21-24]. In our studies, to measure the pyroelectric current *p(T)* of the prepared film samples, the quasi-static *direct method,* originally implemented by Byer and Roundy, was adopted [25]. This method is more straight forward than the *dynamic method* in which the current produced by an absorbed radiation pulse is measured [26] or, the charge integration method (*static method*), in which the current produced during heating is integrated in an operational amplifier and the resultant curve is differentiated to obtain the pyroelectric coefficient [27-31].

A schematic diagram of the experimental set up used for the measurement of pyroelectric current is shown in Fig. 2.3. The measurement cell consists of a sample holder kept in it. This sample holder is attached to

a heater so that we can increase or decrease the temperature of the specimen at a constant rate. The rate of increase of temperature can be controlled and monitored using a programmable PID temperature controller (Make: Lakeshore Cryotronics, Model: DRC 82C). The temperature sensor used here was a PT100 sensor. In this method, the sample under study, with metallic electrodes coated on both sides, was kept between two copper electrodes, in which one is spring loaded. From the two electrodes connection wires are taken and are given to a BNC connector which is connected to an auto-ranging picoammeter (Make: Keithley, Model: 485) from which we can get the pyroelectric current directly. By knowing the electrode area of the sample and the rate of change of temperature, we can calculate the pyroelectric coefficient of the sample using the expression (1.1) given in section 1.5.1 of Chapter 1.

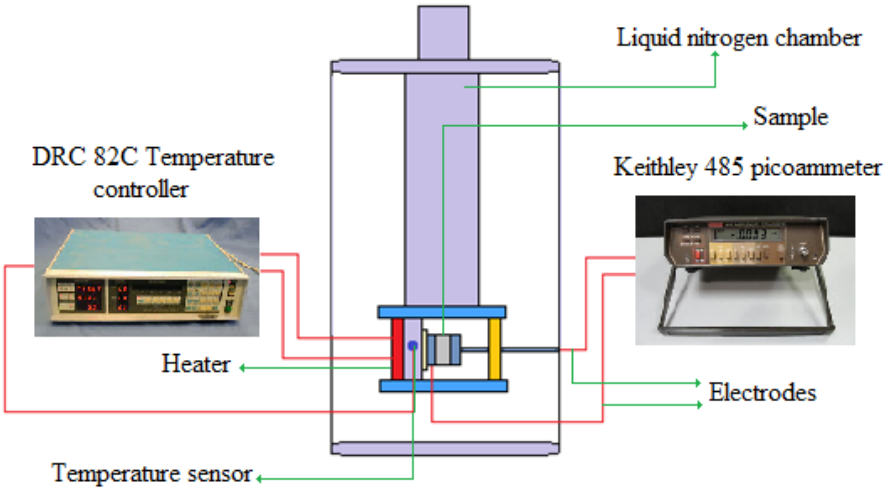

Fig. 2.3 Schematic diagram of pyroelectric current measurement set up

In order to measure the pyroelectric coefficients of all the prepared samples, the samples were poled at temperatures which are just above the

glass transition temperatures of the selected host polymers. It is well known that during pyroelectric measurements if we increase the temperature of the sample above glass transition temperature the pyroelectric coefficient vanishes. So, in order to ensure that samples are kept below their glass transition temperature we limited all our measurements to 60^{o}C. Normally, for poled pyroelectric materials the total current is usually made up of two non-identifiable contributions such as irreversible depolarization current due to space charge relaxation and the true reversible pyroelectric current [32].

In order to make sure that the pyroelectric current is due to its ferroelectricity (and not due to the trapped charges), the pre-poled samples were heated at a constant rate with its electrodes shorted and the short-circuit current monitored with a picoammeter. The first run provides irreversible current due to space charges injected during poling process. But this current is subsequently reduced in subsequent measurements. When no appreciable reduction is observed, the reversible and repeatable pyroelectric current is established. So, for all the samples we performed the measurements during cooling also, in which the pyroelectric current due to the trapped charges disappear almost completely.

2.10 Thermal properties by Photopyroelectric technique

The thermal properties such as thermal conductivity (k) and specific heat capacity (C) of all samples were measured employing an improved photopyroelectric (PPE) technique [33]. The PPE technique is a fairly established one to measure thermal properties of materials in the form of thin discs [33-35]. The PPE effect is based on the use of a pyroelectric film

transducer to detect the periodic temperature rise in a sample when it is irradiated by an intensity modulated beam of light. The laser source used in our experiments was Kimmon's IK series He-Cd laser (wavelength 442 nm) and the laser beam was modulated with an optical chopper (Model: SR540, Make: Stanford Research Systems). In order to ensure the maximum absorption of the incident radiation, a thin layer of carbon coating was provided on the illuminating surface of the sample. The sample configuration in a back detection PPE experiment is shown in Fig. 2.4.

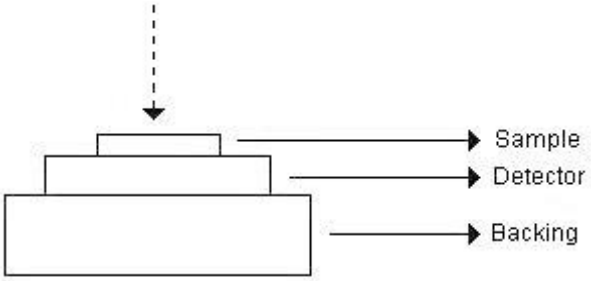

Fig. 2.4 Sample configuration of back detection photopyroelectric (PPE) experiment

The modulated radiation absorbed by the sample at its surface gets converted into thermal waves, which propagate through the sample and are detected by the pyroelectric detector. The temperature variations sensed by the detector give rise to an electrical current, which is proportional to the rate of change of the average heat content given by,

$$i_d = PA\left(\frac{\partial\theta(t)}{\partial t}\right) \qquad (2.4)$$

where P is the pyroelectric coefficient of the detector and A is its area. $\theta(t)$ is the spatially averaged temperature variation over the thickness of the detector L_d and is given by,

$$\theta(t) = \left(\frac{1}{L_d}\right)\int_0^{L_d} \theta(x,t)dx \qquad (2.5)$$

One can draw an electrical equivalent circuit for this configuration and obtain expressions for the output signal amplitude and phase. These expressions are considerably simplified if one assumes physically realistic boundary conditions. Assuming that the sample and the pyroelectric detector are thermally thick, with their thermal diffusion lengths (defined mathematically as $\sqrt{\alpha/\pi f}$ where α is the thermal diffusivity and *f* is the modulation frequency) smaller than their physical thicknesses, one can obtain the following expressions for the PPE signal amplitude and phase at the output of the detector [33]:

$$V(f,T) = \frac{I_0 \eta_s A R_d}{L_d\left[1+\left(f/f_c\right)^2\right]^{1/2}} \frac{P(T)}{\rho_d(T) C_d\ (T)} x \frac{\exp\left[-\left(\pi f/\alpha_s\right)^{1/2} L_s\right]}{e_s(T)/e_d(T)+1} \qquad (2.6)$$

$$\phi(f,T) = -\tan^{-1}\left(f/f_c\right) - \left(\frac{\pi f}{\alpha_s(T)}\right)^{1/2} L_s \qquad (2.7)$$

Here *f* is the modulation frequency of light, *T* is the temperature, I_o is the intensity of the radiation falling on the sample, η_s is a constant for a sample, R_d is the detector leakage resistance, f_c is the critical frequency at which the sample goes from a thermally thin to a thermally thick regime and *L*, ρ and *C* are the thickness, density and specific heat capacity for the medium with subscripts *d* and *s* stand for detector and sample respectively.

The detector used in the present experiments is a PVDF film of thickness 28 μm, coated on both sides with Ni-Cr alloy. The pyroelectric

coefficient of the detector is P = 30 μCm^{-2}K^{-1} at room temperature. The parameter $P(T)/[P_d(T)C_d(T)]$ for the detector has been determined by measuring the PPE amplitude and phase at a fixed frequency as a function of temperature from 25 ^{o}C to 50 ^{o}C in a calibration run.

From equations (2.6) and (2.7) it is clear that the thermal diffusivity α_s of the sample can be determined from the variation of phase with frequency of the PPE signal. Mathematical fitting of experimental PPE phase curve with equation (2.7) yields α_s. Substitution of α_s into the amplitude expression gives the thermal effusivity e_s of the sample. From these, the thermal conductivity and specific heat capacity can be obtained from the following relations [33]:

$$k_s(T) = e_s(T)[\alpha_s(T)]^{1/2} \qquad (2.8)$$

$$C_s(T) = \frac{e_s(T)}{\rho_s(T)[\alpha_s(T)]^{1/2}} \qquad (2.9)$$

A temperature calibration of the PPE detector is necessary as all the parameters in equations (2.6) and (2.7) are temperature dependent. The experimental set up and technique have been tested and calibrated with reference materials such as copper (α = 1.12×10^{-4} m^{2}s^{-1}) and polymer nylon (α = 1.26×10^{-7} m^{2}s^{-1}) with widely different thermal diffusivity values.

The sample-detector-backing configuration was carefully aligned and mounted in a specially designed chamber with an optical window so that light from the laser source can fall directly on the sample. Good thermal contacts between the sample and detector were ensured by applying

a very thin layer of a heat sink compound between them. A photopyroelectric spectrometer of the type shown in Fig. 2.5 was used for the PPE measurements in this work.

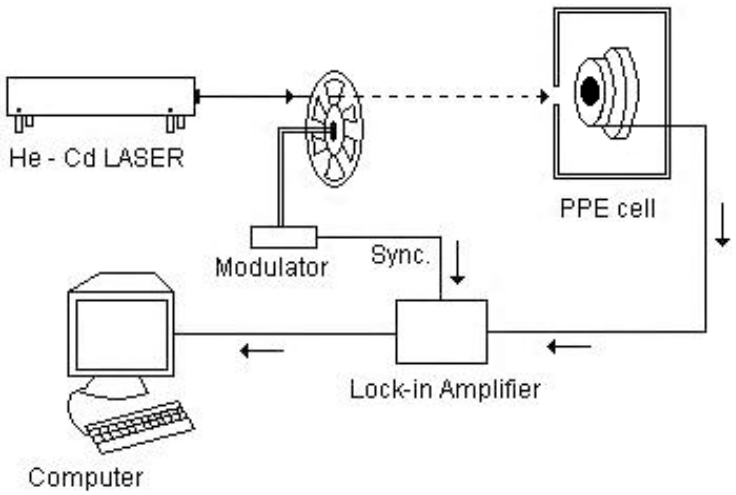

Fig. 2.5 Block diagram of a PPE experimental set up

In the experiment we measure the variations of the PPE amplitude and phase with modulation frequency. From these curves the characteristic frequency f_c for each sample is determined as the frequency at which a peak in amplitude is obtained. These values of f_c along with other known quantities are substituted in equations (2.7) to evaluate α_s. This is substituted along with other known quantities in equation (2.6) to evaluate e_s. These values of α_s and e_s are then substituted in equations (2.8) and (2.9) to obtain k and C values for each sample.

2.11 Measurement of Hardness

Hardness is not a simple property to define; its measure gives a good idea about the mechanical properties of a material. There are several

hardness scales based on the Vickers, Brinell, Knoop, Janka, Meyer, Barcol, Rockwell and Shore measurement tests [36]. Metals have variable hardness values ranging from very soft (copper) to very hard (certain metal alloys). Semiconductors generally have average hardness. Minerals have variable hardness. Ceramics are generally harder than the preceding classes. Polymers have wide ranging hardness values. Generally, hardness of polymers is expressed as Shore hardness values. Normally, Shore hardness reduces as temperature rises.

The hardness of a material characterizes its resistance to the penetration of a needle under a defined spring force. It also characterizes the strengths of atomic bonds, structure and crystallization. It may be measured by the impression of an indenter of known geometry (tempered steel billet, square based diamond pyramid or tempered diamond cone) applied to the surface of a material. The smaller the indentation left behind, the harder is the material. On the other hand, a material that is not hard is easily deformable, penetrable, or abraded.

Albert F. Shore, in 1920s, developed an instrument known as Durometer indenter to measure the Shore hardness of polymers, rubbers and elastomers [37]. In this instrument, the Shore hardness is measured as a number from 0 to 100 on the scales A or D. The higher the value the higher will be the hardness. Though the scales for A and D do have some overlap, scale A is used for flexible type and scale D for rigid type polymers, rubbers and elastomers.

In the studies presented in this thesis, the Shore hardness values for all the samples were measured following indentation method, measuring the

penetration depth of a Durometer indenter with a Shore hardness meter (Make: Hardmatic Mitutoyo, Model: 321JAA283).

2.12 Pyroelectric figures of merit

Pyroelectric figures of merit are important parameters for the selection of materials for pyroelectric thermal/IR detection applications. A detailed description of the relevant figures of merit for the materials investigated in this work is given in the section 1.5.3 of Chapter 1.

References:

1. N. S. Gajbhiye, P. K. Pandey and P. Smitha, *Synthesis and Reactivity in Inorganic, Metal-Organic and Nano-Metal Chemistry* **37**, 431 (2007)

2. G. Xu, W. Jiang, M. Qian, X. Chen, Z. Li and G. Han, *Crystal Growth and Design* **9**, 13 (2009)

3. A. C. Pierre, "Introduction to Sol-Gel processing", Kluwer, Boston, MA (1998)

4. M. T. Reetz and W. Helbig, *J. Am. Chem. Soc.* **116**, 7401 (1994)

5. A. Holden and P. Singer, "Crystals and crystal growing", (1982)

6. A. K. Batra, M. D. Aggarwal, M. E. Edwards and A. Bhalla, *Ferroelectrics* **366**, 84 (2008)

7. H. H. Willard, L. L. Merritt (Jr.), J. A. Dean and F. A. Settler (Jr.), "Instrumental methods of analysis", 7th Ed., Wadsworth Publishing Company, Ney York (1988)

8. S. Amelinckx, D. V. Dyck, J. Vanlanduyt and G. V. Tandeloo, "Electron microscopy: Principles and fundamentals", Wiley-VCH (2003)

9. Z. L. Wang, *J. Phys. Chem. B* **104**, 1153 (2000)

10. C. J. Dias and D. K. Das-Gupta, *IEEE Trans. Diel. & Elect. Insul.* **3**, 706 (1996)

11. S. B. Lang and D. K. Das-Gupta, *Ferroelectrics Rev.* **2**, 217 (2000)

12. S. T. Lau, K. W. Kwok, H. L. W. Chan and C. L. Choy, *Sens. Actuators. A: Phys.* **96**, 14 (2002)

13. T. Furukawa, *IEEE Trans. Electr. Insul.* **24**, 375 (1989)

14. G. M. Sessler, *Key Engn. Mat.* **92-93**, 249 (1994)

15. J. M. Marshal, Q. Zhang and R. W. Whatmore, *Thin Solid Films* **516**, 4679 (2008)

16. J. Kulek, Cz. Pawlaczyk and E. Markiewicz, *Journal of Electrostatics* **56**, 135 (2002)

17. S. Yun, J. H. Kim, Y. Li and J. Kim, *J. Appl. Phys.* **103**, 083301 (2008)

18. S. Arora and S. Kumar, *Optoelectronics and Advanced Materials – Rapid Communications* **2**, 360 (2008)

19. L. B. Loeb, "Electrical coronas", University of California, Berkeley (1965)

20. T. Miller, "Design of corona poling apparatus", (2011)

21. N. P. Hartley, P. T. Squire and E. H. Putley, *J. Phys. E: Sci. Instrum.* **5**, 787 (1972)

22. L. E. Garn and E. J. Sharp, *J. Appl. Phys.* **53**, 8974 (1982)

23. S. G. Porter, *Ferroelectrics* **33**, 193 (1981)

24. C. J. Dias, M. Simon, R. Quad and D. K. Das-Gupta, *J. Phys. D: Appl. Phys.* **26**, 106 (1993)

25. R. L. Byer and C. B. Roundy, *Ferroelectrics* **3**, 333 (1972)

26. A. G. Chynoweth, *J. Appl. Phys.* **27**, 78 (1956)

27. A. M. Glass, *J. Appl. Phys.* **40**, 4699 (1969)

28. W. Ackermann, *Ann. Physik.* **46**, 197 (1915)

29. V. V. Gladkii and I. S. Zheludev, *Sov. Phys. Cryst.* **10**, 50 (1965)

30. N. D. Gavrilova, *Sov. Phys. Cryst.* **10**, 278 (1965)

31. G. Chanussot and L. Godefroy, *Comptes Rendu* **265B**, 1189 (1967)

32. D. K. Das-Gupta and M. J. Abdullah, *Ferroelectrics* **87**, 213 (1988)

33. C. P. Menon, J. Philip, *Meas. Sci. Technol.* **11**, 1744 (2000)

34. F. Mercuri, M. Marinelli, U. Zammit, F. Scudieri, *J. Therm. Anal. Calorim.* **52**, 739 (1998)

35. D. Dadarlat, C. Neamtu, V. Tosa, M. Streza, *Acta Chim. Slov.* **54**, 149 (2007)

36. http://en.wikipedia.org/wiki/Indentation_hardness

37. S. Sandrucci and B. Mussa, "Peripherally inserted central venous catheters", Springer, Italy (2014)

Chapter 3

Pyroelectric Properties of $LiTaO_3$/Poly(vinylidene fluoride) (LT/PVDF) Nanocomposites

Selection of the appropriate ceramic additive and the polymer matrix is the key to the success for the development of the best material for any application. The aim of this work is to develop highly sensitive, at the same time flexible, polymer nanocomposites for pyroelectric infrared detector applications by dispersing the well known pyroelectric material, Lithium Tantalite ($LiTaO_3$) in nanocrystalline form, in an inherently pyroelectric host polymer matrix, Poly(vinylidene fluoride) (PVDF). $LiTaO_3$ nanoparticles are synthesised and dispersed in PVDF at varying volume fractions, and composite materials cast in the form of films for experimentation.

3.1 Introduction

Polymer-ceramic nanocomposites with good pyroelectric properties are proposed as promising materials for the detection and measurement of thermal waves, including infrared radiation. Composite materials made from ferroelectric ceramic particles embedded in polymers possess hybrid properties of the components. These hybrid properties include high

pyroelectric coefficients of the ceramic material and the excellent mechanical strength, formability, flexibility, light weight and robustness of the polymer, eventually useful for thermal and infrared detection applications [1]. Different combinations of ceramic-polymer composites with 0-3 connectivity have been investigated with the aim to enhance their pyroelectric and piezoelectric performance, and other desirable physical properties for use in various devices. A 0-3 connectivity ceramic-polymer composite is easy to fabricate, which allows for commercial production of the composites in a cost-effective manner [2]. Of late efforts have been expended to synthesize ceramics in nanocrystalline form so as to further enhance the detection sensitivity and mouldability of the composites.

All ferroelectric materials show pyroelectric as well as piezoelectric properties with varying degrees depending upon the structure and internal polarization of the material. So ferroelectric materials are intrinsically multifunctional and have found a broad range of applications. Some well known pyroelectric thermal/infrared detecting materials belonging to the ceramic class are Lead Zirconate Titanate (PZT), Lithium Tantalate (LT), Triglycine Sulphate (TGS), Strontium Barium Niobate (SBN) etc. Host polymer matrix like Poly(vinylidene fluoride) (PVDF) and its co-polymers are known to be electro-active with good values for their pyroelectric coefficients. Bare PVDF films are widely used commercially as thermal and infrared detectors [3, 4].

$LiTaO_3$ (LT) is one of the interesting ferroelectric materials which find applications as pyroelectric infrared detectors. For sensitive pyroelectric detectors made from ferroelectric materials, the temperature

dependence of the pyroelectric output voltage is related to the temperature dependence of their spontaneous polarization. The useful temperature range is below the Curie point in these materials [5]. Different $LiTaO_3$-polymer composites have been prepared and their pyroelectric and dielectric properties investigated by different research groups earlier [6, 7]. LT has aroused great deal of interest among researchers due to its excellent ferroelectric, piezoelectric, pyroelectric and nonlinear optical properties. Periodically poled LT has attracted considerable attention as optical superlattices for quasi-phase matching because of its high damage threshold and small photo-elastic properties [8, 9]. Low temperature and nanostructure processing of LT have been under intensive investigation in recent years [10].

PVDF, one of the representative ferroelectric electro-active polymers, is selected as the host polymer in the present work because of its inherently high pyroelectric properties. It is often introduced to have possibilities of applications for next generation memory devices, micro-sensors and miniature actuators. PVDF is one of the semicrystalline polymers with at least four crystalline phases; well known for its pyroelectric, piezoelectric and ferroelectric properties. These crystalline phases include nonpolar α phase, polar β and γ phases and the δ phase. The structure of the common α and β forms of PVDF are shown in Fig. 3.1. The β phase exhibits the pyro, piezo, dielectric and related properties. An easy method to get the β crystalline phase of PVDF films is mechanical stretching. Also, use of certain solvents like dimethyl sulfoxide (DMSO), N,N -Dimethylformamide (DMF) etc. results in β phase PVDF films after casting.

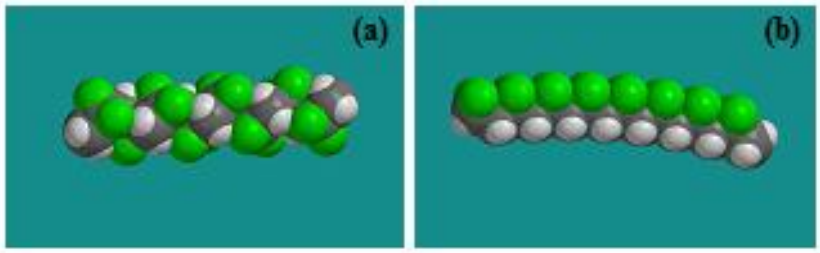

Fig. 3.1 (a) α-form and (b) β-form of PVDF polymer

The aim of this investigation is to prepare polymer-ceramic nanocomposites of LT/PVDF by dispersing nanoparticles of LT in the β phase of PVDF with varying concentrations of LT and measure their structural, dielectric, thermal, mechanical and pyroelectric properties and estimate their pyroelectric figures of merit. The investigations are aimed at developing nanocomposites of this category with high enough pyroelectric figure of merit and low enough mechanical hardness to keep the material flexible so that mouldable thermal and infrared detectors can be developed for commercial applications. The objective of preparing LT as nanoparticles is to attain high flexibility and detection sensitivity for the composite for lower concentrations of the ceramic.

3.2 Experimental techniques

Procedures followed to prepare the samples and experimental methods employed to study their properties are outlined below.

3.2.1 Sample preparation

The sample preparation includes the synthesis of $LiTaO_3$ nanopowders, preparation of the PVDF polymer solution and synthesis of the LT/PVDF nanocomposite films.

3.2.1.1 Synthesis of $LiTaO_3$ nanopowders

For the synthesis of $LiTaO_3$ nanoparticles, Ta_2O_5 (99.999%, Sigma Aldrich), HF (40% v/v), standard ammonia (25% v/v), ammonium oxalate (99.99% w/w, Sigma Aldrich) and Li(OH) (Sigma Aldrich) were used as the starting materials. Nanoparticles of LT were prepared following a known chemical route which was similar to the one followed by Muthurajan *et al* [11]. For this a required amount of Ta_2O_5 was dissolved in HF with heating in an oil bath for 10 hours. After that, aqueous ammonium hydroxide was added drop wise into the TaF_5 solution to precipitate tantalum as hydroxide under basic conditions. This precipitate was washed several times free of anions and dried at 100^{o}C in an oven. A stoichiometric quantity of Li(OH) was mixed with $(Ta(OH))_5.xH_2O$ and ground well for 1 hour using acetone as the grinding medium, in an agate mortar. Thus prepared white powders were calcined at 450^{o}C for 6 hours.

3.2.1.2 Preparation of PVDF polymer solution

The polymer matrix used in this study was commercially available PVDF in powder form (Sigma Aldrich, with average molecular weight ~ 5,34,000). Required quantity of PVDF powder was dissolved in N,N-Dimethylformamide (DMF), which is a suitable polar solvent for it, at 80^{o}C for 1 hour. Thus prepared polymer solution was kept undisturbed for some time to obtain clear bubble free solution.

3.2.1.3 Synthesis of LT/PVDF nanocomposite films

A solvent cast method was used to prepare the LT/PVDF nanocomposites as flexible free standing films [12]. For this, as mentioned in section 2.2.3 of chapter 2, required quantity of the LT ceramic

nanopowder was added into the PVDF polymer solution and mixed/ dispersed well with constant stirring followed by ultrasonic agitation. Utmost care was taken to face the problems during mixing, which are linked to poor dispersion of the ceramic inclusions and poor adhesion of the component phases. Again this mixture was kept undisturbed to get bubble free composite solution. The mixture so obtained was then poured into a glass petridish and was kept in a hot air oven set at 80^{o}C, for two and half hours for the solvent to evaporate completely. We could overcome the possibility for agglomerating the ceramic particles by lowering the polymer viscosity by heating the mixture during stirring and ultrasonic mixing. Here the LT nanoparticles at required volume fractions (0.001, 0.01, 0.05, 0.09, 0.15, and 0.25) were dispersed in PVDF solution and each of the LT/PVDF nanocomposite films including a pure PVDF film were cast at the same temperature and same atmospheric conditions. Free standing films of thickness about 40μm were peeled off. Films with only up to volume fraction 0.25 of LT could be fabricated due to problems of particle agglomeration and nonuniformity of the cast films at higher concentrations.

3.2.2 Sample characterization

The newly prepared $LiTaO_3$ nanopowders and the cast nanocomposite films were characterized using the standard characterization techniques such as powder X-ray Diffraction (XRD), Fourier Transform Infrared Spectroscopy (FTIR), Differential Scanning Calorimetry (DSC), Scanning Electron Microscopy (SEM) and Transmission Electron Microscopy (TEM).

3.2.2.1 Dielectric measurements

Small pieces of dry composite samples were coated with silver paste on both sides for dielectric measurements. The dielectric constants were measured by a capacitance method. Samples having area 1 cm^2 each were used as the dielectric medium for a parallel plate capacitor and the capacitance and *tanδ* values were measured as a function of frequency. The experimental details are given in the section 2.7 of chapter 2. The dielectric constants (ε) and dielectric losses (ε') of the samples were measured with an impedance analyzer in the frequency range 100 Hz - 5 MHz. All the dielectric measurements were carried out in room temperature.

3.2.2.2 Pyroelectric measurements

Pyroelectric coefficients *p(T)* of the prepared nanocomposite films were measured by the Byer and Roundy method, the direct method [13]. Theory and working principle of pyroelectric/ thermal IR detectors is explained in section 1.5.1 of chapter 1. The pyroelectric current I_P is proportional to the electrode area *A* of the sample and the temperature change with time *(dT/dt)*, from which the pyroelectric coefficient can be determined using the expression (1.1) given in section 1.5.1 of chapter 1. In our measurements the sample heating rate fixed was 2^oC/min.

The pyroelectric properties of PVDF film can be enhanced by poling. Poling is a process of converting a multidomain single crystal to single domain one with the application of an external electric field far greater than the coercive field in the direction of the polarization axis. Enhancement of nonvolatile polarization in LT/PVDF nanocomposite by applying a high DC field has already been reported by Satapathy *et al* [14].

The PVDF material can retain its pyroelectric properties only up to a certain value of the electric field. Beyond this it gets de-poled (loses its pyroelectric/piezoelectric properties). Poling technique adopted for our study was the corona poling in which the LT/PVDF sample film had an electrode fixed only to one side and a sharp corona needle is placed at a certain distance away from the other side. When a very high voltage was applied across the needle and the bottom electrode, ionization of air took place around the needle and the generated charges got accumulated on the film surface established a poling electric field in the film [15-17]. In our investigations, for corona poling the samples we had a home built setup and all the samples were poled at 80^{o}C at a DC electric field of 16.5 MVm^{-1}.

The performance as well as sensitivity of pyroelectric detectors is limited by noise. Noise due to temperature fluctuations sets a fundamental limit for all pyroelectric detectors. This is the same limit for all thermal detectors in general. However, when the matrix and inclusions are poled in parallel or in the same direction, pyroelectricity of the two phases reinforce while piezoelectric activity almost cancels or disappears, thereby reducing vibration-induced electrical noise in pyroelectric sensors [18].

3.2.2.3 Thermal studies

Thermal properties of LT/PVDF nanocomposites were measured following a photothermal technique, with a pyroelectric detector used as the thermal detector [19]. Here, when a periodically modulated light beam from a source impinges on the surface of the sample, the sample absorbs part of the incident energy. The sample undergoes a nonradiative de-excitation process and the sample gets correspondingly heated. This

periodic temperature variation in the sample can be directly detected with a sensitive pyroelectric transducer kept in intimate contact with the sample. A 120 mW He-Cd laser of wavelength 442 nm, intensity modulated by a mechanical chopper, was used as the optical heating source. A nickel-chromium alloy coated PVDF film was used as the pyroelectric detector. The sample-detector assembly was mounted on a thermally thick backing. The modulation frequency of light was kept above 60 Hz to ensure that the detector, the sample and the backing were thermally thick during measurements. The output signals as amplitude and phase were recorded with a dual-phase lock-in amplifier (Make: Stanford Research Systems, Model: SR830). Measurement of amplitude and phase of the output signal enabled us to determine the thermal diffusivity *(α)* and thermal effusivity *(e)*, from which the thermal conductivity *(k)* and specific heat capacity *(C)* of the samples could be obtained.

3.2.2.4 Hardness measurements

Fluoropolymers like PVDF fall under the category of thermoplastics. Filler materials in the form of powders can be added to thermoplastics to provide improvement of their specific properties like strength, stiffness, lubricity etc. Hardness of polymers (rubbers, plastics) is usually measured by the Shore scales. The Shore A scale is used for 'softer' rubbers while the Shore D scale is for 'harder' elastomers/thermoplastics. The Shore hardness values of all the prepared nanocomposite film samples were measured following an indentation technique by measuring the penetration depth of the durometer indenter with a Shore D hardness meter. Shore hardness is often used as a proxy to flexibility for the specification of elastomers/plastics.

3.3 Results and discussions

Results of the investigations as well as the pyroelectric figures of merit of the prepared compositions are presented and discussed in the following sections. Also theoretical calculations for thermal conductivity (k), specific heat capacity (C) and dielectric constant (ε) are carried out and are compared with the experimental results. The theoretical values are calculated using effective medium theory. The effective medium theory expressions used for the calculations are [20-22],

$$\varepsilon_{eff} = \varepsilon_m \frac{2\varepsilon_m + \varepsilon_f + 2\varphi_f(\varepsilon_f - \varepsilon_m)}{2\varepsilon_m + \varepsilon_f - \varphi_f(\varepsilon_f - \varepsilon_m)} \quad (3.1)$$

$$\varphi_m \frac{k_m - k_{eff}}{k_m + 2k_{eff}} + \varphi_f \frac{k_f - k_{eff}}{k_f + 2k_{eff}} = 0 \quad (3.2)$$

$$C_{eff} = \varphi_f C_f + (1-\varphi_f) C_m \quad (3.3)$$

were φ is the volume fraction and subscripts m, f and eff stand for the matrix, filler and composite respectively. Since the assumptions and approximations of effective medium theory are well documented in cited references, they are not discussed any further here.

3.3.1 Material identification, structure and morphology

The powder XRD pattern of pure PVDF sample (Fig. 3.2(a)) shows a major peak at 20.5^o (corresponding to the (200) plane), which is the prominent peak for β PVDF [23]. The FTIR spectrum of pure PVDF sample is shown in Fig. 3.3. Here the absorption peaks at 511 and 840 cm^{-1} are the characteristic ones for β PVDF [20, 21]. From the figure it is clear that the characteristic peaks corresponding to α (766, 795, 856 and 976

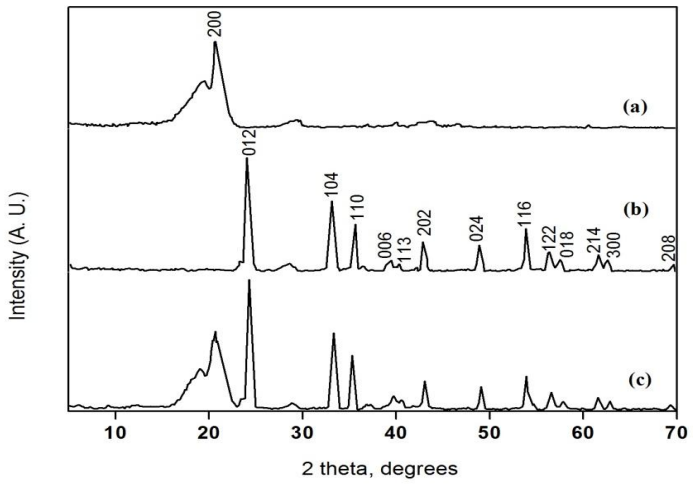

Fig. 3.2 XRD pattern of (a) pure PVDF film, (b) LT nanopowder, (c) LT/PVDF nanocomposite with volume fraction 0.01 of LT

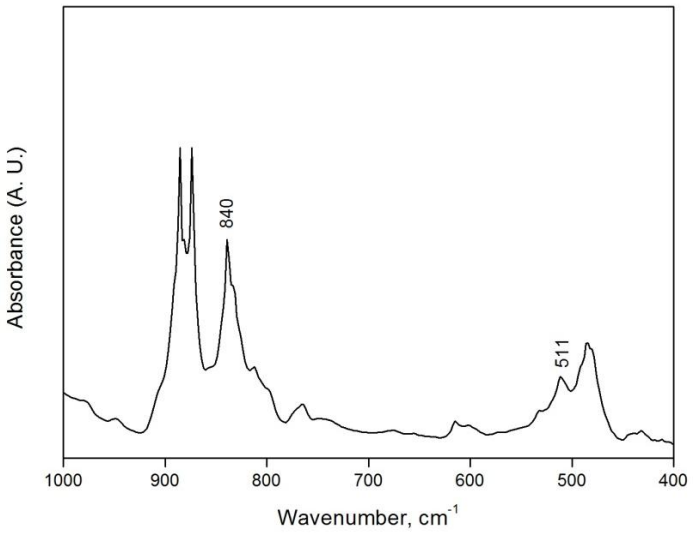

Fig. 3.3 FTIR spectrum of pure PVDF film

cm^{-1}) and γ (778, 812 and 834 cm^{-1}) phases of PVDF are absent in the FTIR spectrum [24]. This shows that PVDF formed is predominantly β phase.

From the DSC analysis (Fig. 3.4) it is found that the melting point of the PVDF film cast from DMF solvent is 161.18^{o}C. No other transition peak has been found in the temperature region of the measurements.

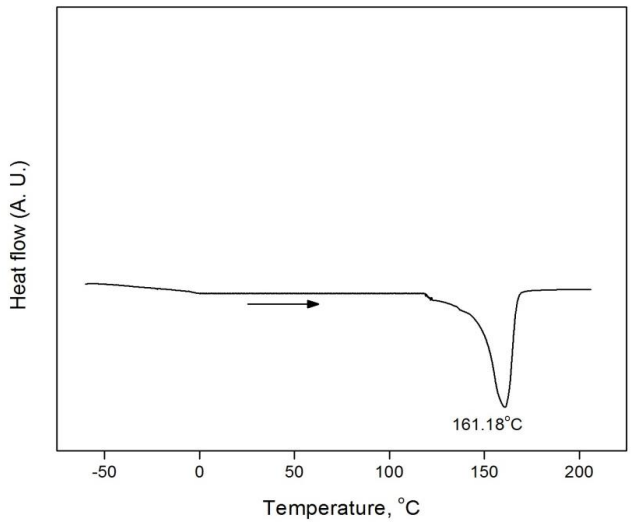

Fig. 3.4 DSC curve of pure PVDF film during heating cycle (Heating rate 10 ^{o}C/min)

XRD patterns of pure $LiTaO_3$ nanoparticles are shown in Fig. 3.2(b). The XRD pattern matches well with that of $LiTaO_3$ (JCPDS Card No: 29-0836). The average diameter of the particles, calculated using the Debye - Scherrer formula, is in the range 35–50 nm.

Each of the polymer nanocomposite samples has also been subjected to powder XRD measurements. The XRD pattern for one sample (with volume fraction 0.01) is also shown in Fig. 3.2(c). Peaks in the XRD pattern for this sample confirm the presence of LT nanoparticles in the polymer matrix.

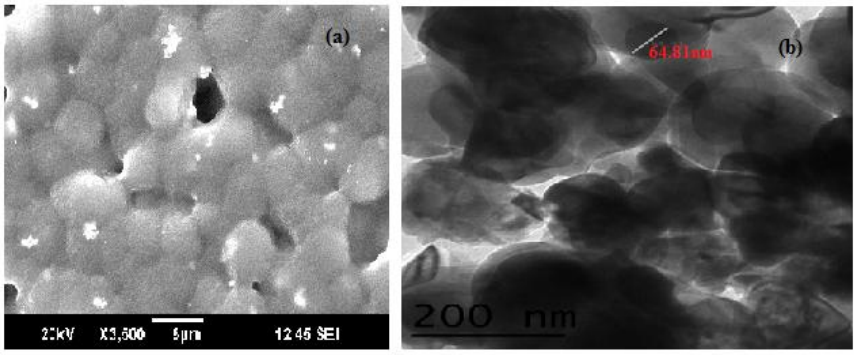

Fig. 3.5 (a) SEM image of the 0.05 volume fraction of LT/PVDF composite film and (b) TEM image of the $LiTaO_3$ nanoparticles prepared

The SEM image of one of the LT/PVDF nanocomposite films (0.05 volume fraction) cast by solvent casting is shown in Fig. 3.5(a). This figure gives direct evidence for the presence of LT nanoparticles in PVDF polymer matrix. Fig. 3.5(b) is the TEM image of the prepared nanoparticles. Form the TEM image the particle size obtained is in the range 64.81nm.

3.3.2 Sample density

The theoretical and experimental densities of the composites with varying volume fractions of LT are shown in Fig. 3.6. Theoretical densities of the composites are calculated using the rule of mixtures

$$\rho_{eff} = \varphi_f \rho_f + (1-\varphi_f)\rho_m \qquad (3.4)$$

where ρ is the density. Density of LT is taken as 7.43 gcm^{-3} and that of PVDF as 1.74 gcm^{-3} in the calculations. Densities have also been measured directly. It can be inferred that the density increases with filler

concentration, and it is slightly lower than the theoretical density. This could be due to the possible presence of voids and defects in the composites

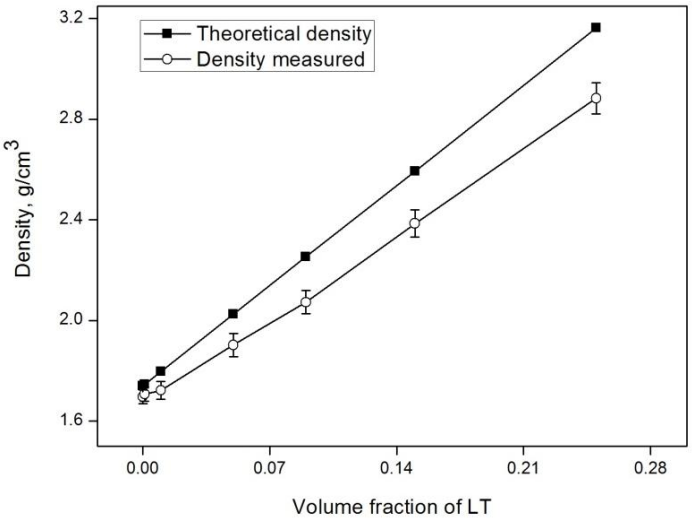

Fig. 3.6 Variations of theoretical and experimental densities of LT/ PVDF nanocomposites with varying volume fractions of LT

during preparation, which are not accounted for in the theoretical calculations. At high filler loadings, certainly there is a possibility for the ceramic particles to form aggregates, which may tend to settle. This will cause some nonuniformity in the density of the samples, reducing the density in the upper regions of the cast films. However, all of the prepared samples have attained a density in the range of 94-90% of the theoretical density as the filler volume fraction increases from 0 to 0.25.

3.3.3 Dielectric properties

Variations of dielectric constant and dielectric loss with frequency for samples with different concentrations of nano LT in PVDF are shown in figures 3.7 and 3.8.

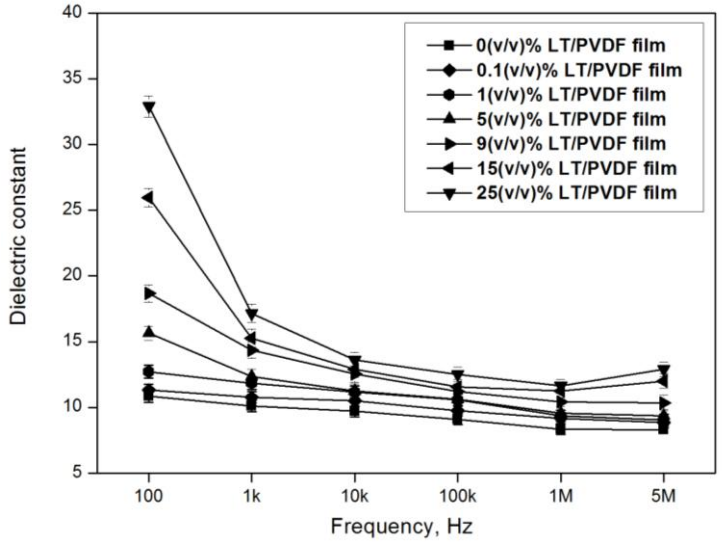

Fig. 3.7 Variations of dielectric constant with frequency for different LT/PVDF nanocomposites

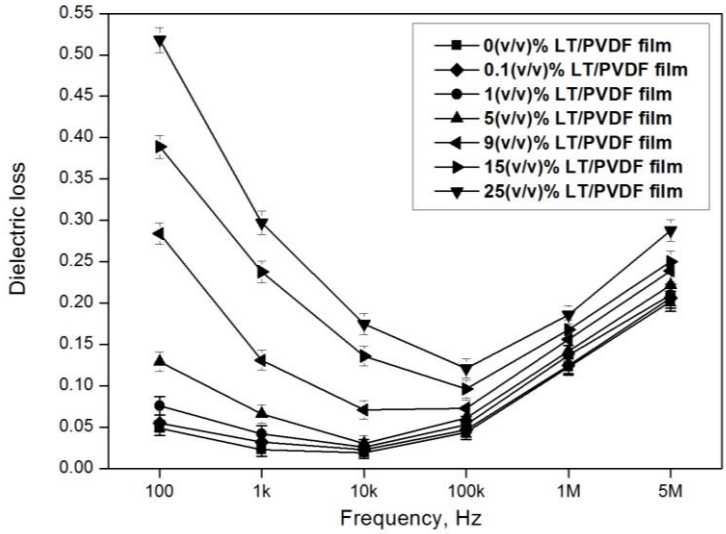

Fig. 3.8 Variations of dielectric loss with frequency for different LT/PVDF nanocomposites

It can be seen that both dielectric constant and loss increase at all frequencies as the LT content in the PVDF matrix increases. Dielectric

constant varies from 10.09 to 17.16 as the volume fraction of LT increases from 0 to 0.25 at 1 kHz, whereas the corresponding variations in dielectric loss are from 0.023 to 0.297. The reported value of dielectric constant for pure PVDF film is 11 at 1 kHz [25], in our measurements it is 10.09, which is rather close to the reported value. It is found that both dielectric constant and loss decrease as frequency increases, but above 100 kHz the dielectric loss shows an increase. It can also be noticed that the dielectric constant decreases sharply as the frequency increases for higher filler concentrations, but in the high frequency region, the decrease is much less. More or less similar variation occurs for dielectric loss as well.

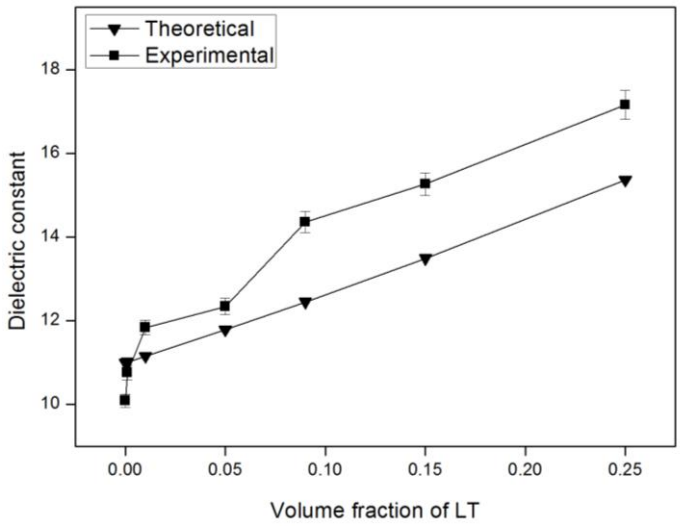

Fig. 3.9 Comparison of theoretical and experimental dielectric constants at 1 kHz for SBN30/PU nanocomposites with different volume fractions of SBN30

The increase in dielectric constant with increase in LT content can be attributed to an enhancement in internal polarization of the samples. At lower frequencies (say, below 1 kHz) the dielectric constant of the

nanocomposites is higher than the expected values for higher filler concentrations. So it is clear that there must be other contributions to polarization, which enhances the dielectric constant at low frequencies. The observed extra polarization might be from minute space charge polarization [26].

A comparison of the theoretical dielectric constants calculated using the expression (3.1) and experimental results at 1 kHz frequency of the prepared LT/PVDF nanocomposites is shown in Fig. 3.9. The variation of the curves shows that the experimental and the measured values are in good agreement.

3.3.4 Pyroelectric coefficients

It has been shown that the pyroelectric constant of a ferroelectric polymer can be increased by addition of a ceramic component [27, 28]. When LT nanoparticles are added to PVDF, the polarization of the composites increase compared to PVDF due to the dipolar contribution from LT. The pyroelectric coefficients are measured exactly as mentioned in section 2.9 of chapter 2. Enhancement in pyroelectric coefficient is obtained for the composite films after poling at a temperature about 80^{o}C. It is found that pyroelectric coefficient increases from 39 $\mu Cm^{-2}K^{-1}$ to 327 $\mu Cm^{-2}K^{-1}$ in heating cycle and 32 $\mu Cm^{-2}K^{-1}$ to 308 $\mu Cm^{-2}K^{-1}$ in cooling cycle as the LT concentration in the PVDF matrix increases from 0 to 0.25 volume fraction. The variations are shown in figures 3.10 and 3.11. Here during heating, in addition to the pyroelectric current, a small current due to release of trapped space charges will be present. But during cooling the presence of depolarization currents can be eliminated. From Fig. 3.11 it is

clear that during cooling the pyroelectric coefficients are slightly less compared to those during heating.

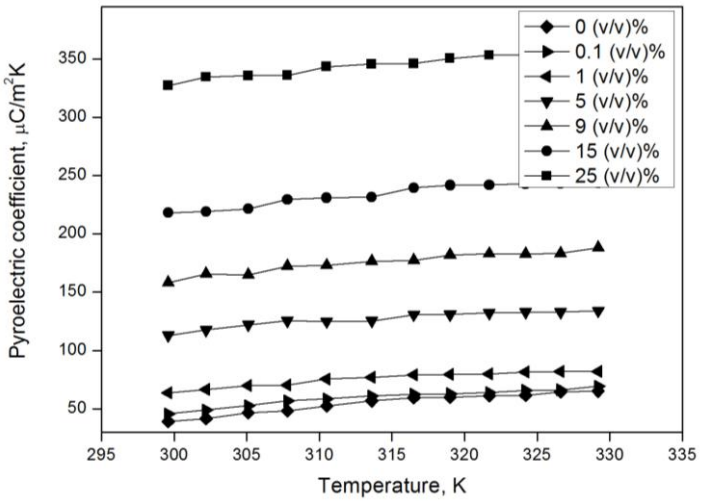

Fig. 3.10 Variation of pyroelectric coefficient during heating for different volume fractions of LT content in PVDF matrix

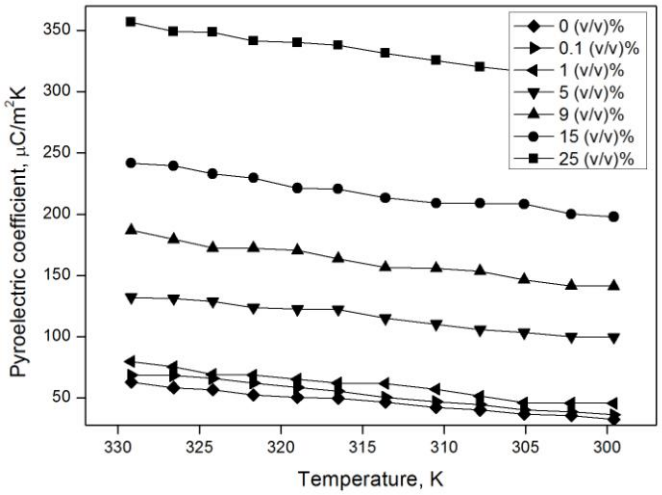

Fig. 3.11 Variation of pyroelectric coefficient during cooling for different volume fractions of LT content in PVDF matrix

The average pyroelectric coefficient varies from 36 $\mu Cm^{-2}K^{-1}$ to 318

$\mu Cm^{-2}K^{-1}$ as the LT content in the polymer matrix increases as shown in Fig. 3.12.

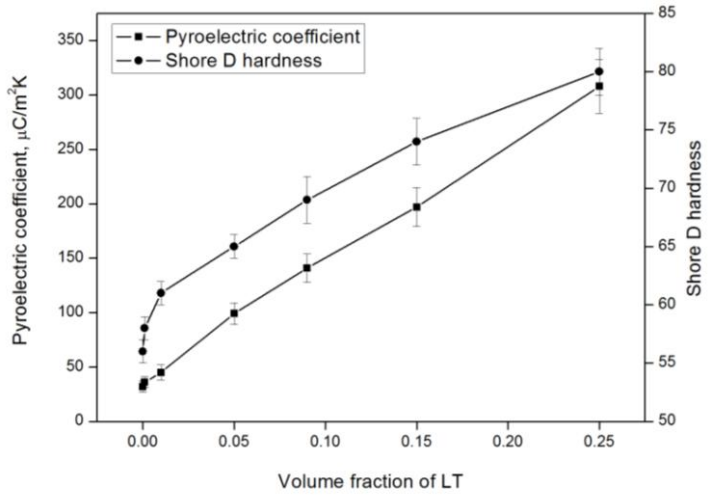

Fig. 3.12 Variations of pyroelectric coefficients and Shore D hardness of LT/PVDF nanocomposites with volume fractions of LT

At higher volume fractions of LT, the pyroelectric coefficient increases because of the presence of a higher proportion of the pyroelectric material and an increased likelihood of ceramic paths connecting the upper and lower electrodes of the sample.

3.3.5 Thermal analysis

In order to calculate the thermal parameters firstly, the photopyroelectric (PPE) amplitude and phase are recorded as functions of frequency, with a dual phase lock-in amplifier. The amplitude and phase curves for 0.15 volume fraction of LT/PVDF film is shown in Fig. 3.13. Same kind of variations is obtained for other samples also. From these amplitude and phase values, thermal conductivity and specific heat capacity were calculated as explained in section 2.10 of chapter 2.

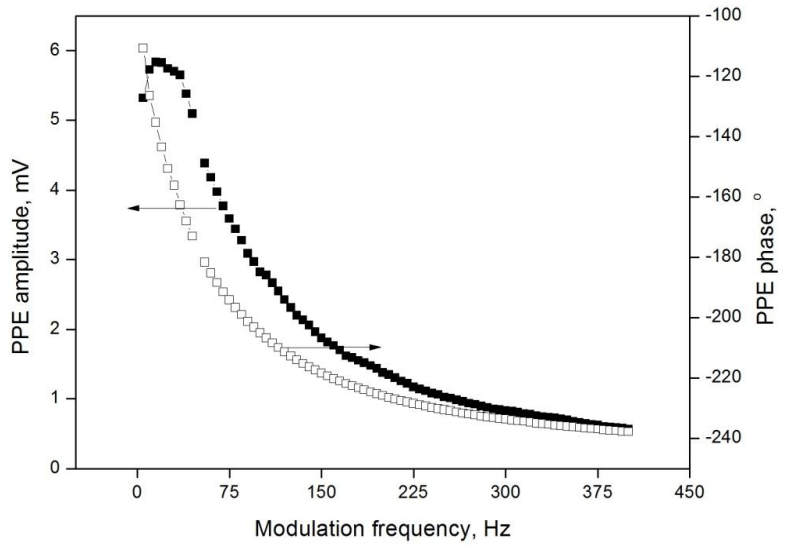

Fig. 3.13 Variations of PPE amplitude and phase as functions of frequency for 0.15 volume fraction of LT in PVDF polymer

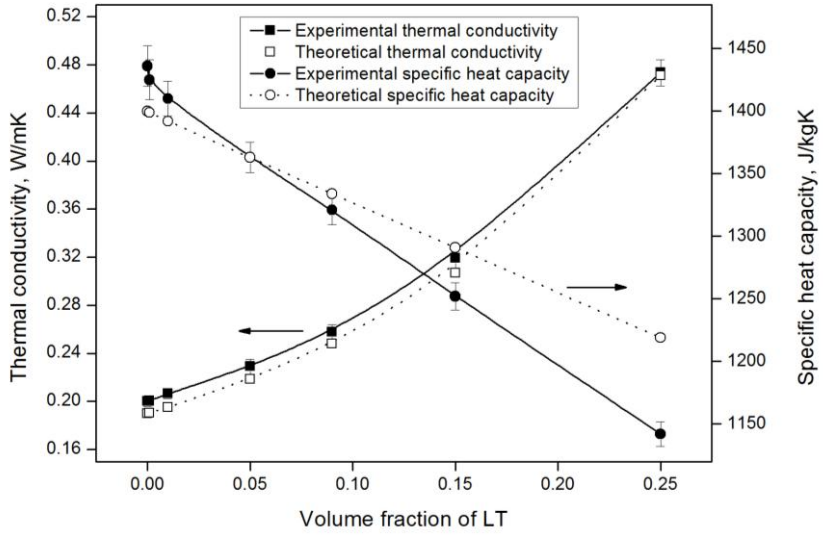

Fig. 3.14 Variations of thermal conductivity and specific heat capacity of LT/PVDF nanocomposites (including theoretical comparison) with volume fractions of LT

It is found that the thermal conductivity of the nanocomposites, increase from 0.20 $Wm^{-1}K^{-1}$ to 0.47 $Wm^{-1}K^{-1}$ with increase in filler concentration, whereas the specific heat capacity decreases from 1436 $Jkg^{-1}K^{-1}$ to 1142 $Jkg^{-1}K^{-1}$. Both the measurements were carried out at room temperature. The variations of thermal conductivity and specific heat capacity with filler concentration are shown in Fig. 3.14 including corresponding theoretical curves. Measured values for both the parameters fairly agree with corresponding theoretical values calculated using the expressions (3.2) and (3.3).

3.3.6 Pyroelectric figures of merit

The important figures of merit for pyroelectric infrared detector materials, i.e., figures of merit for high current sensitivity (F_I), high voltage responsivity (F_V) and high detectivity (F_D) [29-32] are calculated using the expressions (1.2), (1.3) and (1.4) mentioned in section 1.5.3 of chapter 1. These have been calculated for each of the LT/PVDF nanocomposites and found that the figures of merit increase with increase of filler concentration. F_I varies from 25×10^{-3} μCm/J to 278×10^{-3} μCm/J, F_V varies from 2.48×10^{-3} μCm/J to 16.23×10^{-3} μCm/J and F_D varies from 165×10^{-3} μCm/J to 510×10^{-3} μCm/J.

Variations of the above three pyroelectric figures of merit, normalized to the corresponding ones for pure PVDF plotted against the volume fractions of LT nanopowder are shown in Fig. 3.15. It can be seen that all the three figures of merit increase more or less linearly with filler concentration, which is in tune with mean field approximation [33].

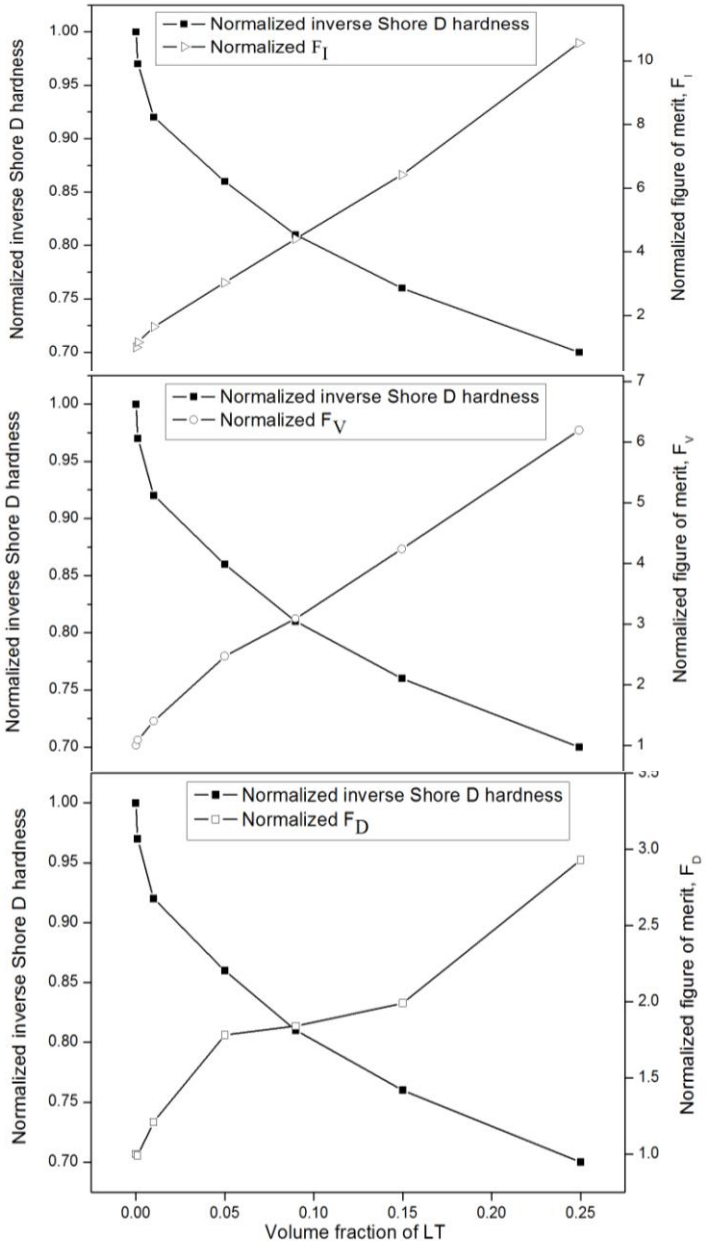

Fig. 3.15 Variations of normalized pyroelectric figures of merit and normalized inverse Shore D hardness for LT/PVDF nanocomposites with volume fractions of LT

3.3.7 Hardness studies

As shown in Fig. 3.12, for LT/PVDF nanocomposite films, increase in Shore D hardness values have been obtained for increasing volume fractions of LT nanopowder in the composite. The variation of inverse Shore D hardness values, normalized to the value for pure PVDF, with varying volume fractions of LT is also shown in Fig. 3.15. Since Shore hardness scales inversely with flexibility of the polymer, one can notice that the samples get harder as the LT concentration increases.

From Fig. 3.15 it is clear that the pyroelectric figures of merit compete with Shore hardness or flexibility of the composite. Depending on the application, the Shore hardness of the composite shall be fixed, which automatically fixes the figure of merit or thermal/infrared detection sensitivity of the material. From the plots shown in Fig. 3.15 it can be noticed that at the volume fraction 0.09, where the Shore hardness curves meet the figure of merit curves, the LT/PVDF nanocomposite possesses good flexibility, at the same time good figures of merit for high current sensitivity, F_I, high voltage responsivity, F_V and high detectivity, F_D. So we can conclude that the volume fraction 0.09 of LT provides the best composition for sensing application with good flexibility. By preparing the filler particles in the nanometer scales, we have been able to obtain simultaneously good thermal sensitivity along with high flexibility for this composite.

3.4 Conclusions

Thin flexible LT/PVDF nanocomposite films with high thermal/ infrared detection sensitivity have been synthesized and their properties

measured. The pyroelectric, dielectric and thermal properties as well as mechanical hardness of LT/PVDF nanocomposites with varying filler concentrations have been investigated. It is found that pyroelectric coefficient, dielectric constant and thermal conductivity increase significantly with filler loading, but specific heat capacity decreases. All the three relevant pyroelectric figures of merit have been evaluated from these parameters for their possible use as pyroelectric thermal/infrared detectors. A comparison with corresponding Shore hardness for these materials shows that improvement in pyroelectric figure of merit is at the expense of the flexibility of the material. So for any application, depending on the requirement, one shall fix the hardness and then settle down with the corresponding sensitivity.

References:

1. K. W. Kwok, S. T. Lau, C. K. Wong and F. G. Shin, *J. Phys. D: Appl. Phys.* **40**, 6818 (2007)

2. M. T. Sebastian and H. Jantunen, *Int. J. Appl. Ceram. Technol.* **7**, 415 (2010)

3. A. Navid, C. S. Lynch and L. Pilon, *Smart Mater. Struct.* **19**, 055006 (2010)

4. A. K. Batra, S. Bhattacharjee, A. K. Chilvery, M. D. Aggarwal, M. E. Edwards and A. Bhalla, *J. Photon. Energy* **1**, 014001 (2011)

5. G. Akcay, S. P. Alpay, J. V. Mantese and G. A. Rossetti, *Appl. Phys. Lett.* **90**, 252909 (2007)

6. A. K. Batra, J. Corda, P. Guggilla, M. D. Aggarwal and M. E. Edwards, *Proc. of SPIE* **7213**, 721313 **(**2009)

7. A. K. Batra, J. Corda, P. Guggilla, M. D. Aggarwal and M. E. Edwards, *Proc. of SPIE* **7419**, 741904 (2009)

8. J. L. He, H. M. Wang, S. D. Pan, J. Liu, H. X. Li and S. N. Zhu, *J. Cryst. Growth* **292**, 337 (2006)

9. F. Rotermund, C. J. Yoon, V. Petrov, F. Noack, S. Kurimura, N. E. Yu and K. Kitamura, *Opt. Express.* **12**, 6421 **(**2004)

10. A. Tarafder, K. Annapurna, R. S. Chaliha, S. Satapathy, V. S. Tiwari, P. K. Gupta and B. Karmakar, *J. Nonlinear Optic. Phys. Mat.* **20**, 49 (2011)

11. H. Muthurajan, H. H. Kumar, N. Natarajan and V. Ravi, *Ceram. Int.* **34**, 669 (2008)

12. G. D. Baird and D. I. Collias, "Polymer processing: Principles and Design", John Wiley & Sons Inc., New York (1998)

13. R. L. Byer and C. B. Roundy, *Ferroelectrics* **3**, 333 (1972)

14. S. Satapathy, P. K. Gupta and K. B. R. Varma, *J. Phys. D: Appl. Phys.* **42**, 055402 (2009)

15. L. B. Loeb, "Electrical Coronas: Their Basic Physical Mechanisms", University of California Press, Berkeley (1965)

16. J. M. Marshall, Q. Zhang and R. W. Whatmore, *Thin Solid Films* **516**, 4679 **(**2008)

17. S. Yun, J. H. Kim, Y. Li and J. Kim, *J. Appl. Phys.* **103**, 083301 **(**2008)

18. B. Ploss, W. Y. Ng, H. L. Chan, B. Ploss and C. L. Choy, *Compos. Sci. Technol.* **61**, 957 (2001)

19. C. P. Menon and J. Philip, *Meas. Sci. Technol.* **11**, 1744 (2000)

20. I. H. Rizvi, A. Jain, S. K. Ghosh and P. S. Mukherjee, *Heat Mass Transfer* **49**, 595 (2013)

21. Z. Han, Nanofluids with enhanced thermal transport properties. *http://drum.lib.umd.edu/ bitstream/1903/8654/1/umi-umd-5648.pdf 2008*

22. M. E. Hossain, S. Y. Liu, S. O'Brien and J. Li, *Acta Mech* **225**, 1197 (2014)

23. S. H. Lee and H. H. Cho, *Fibers and Polymers* **11**, 1146 (2010)

24. L. Yu, P. Cebe, *Polymer* **50**, 2133 (2009)

25. R. W. Whatmore, *Rep. Prog. Phys.* **49**, 1335 (1986)

26. P. Murugaraj, D. Mainwaring and N. Mora-Huertas, *J. Appl. Phys.* **98**, 054304 (2005)

27. L. F. Malmonge, J. A. Malmonge, and W. K. Sakamoto, *Mater. Res.* **6**, 469 (2003)

28. B. Ploss, B. Ploss, F. G. Shin, H. L. W. Chan and C. L. Choi, *Appl. Phys. Lett.* **76**, 2776 (2000)

29. B. L. Sidney and D. K. Das-Gupta, *Ferroelectrics Review* **2**, 217 (2000)

30. R. W. Whatmore and R. Watton, "Pyroelectric Materials and Devices" in "Infrared Detectors and Emitters: Materials and Devices", Kluwer Academic Publishers, The Netherlands, 99 (2001)

31. P. Guggilla, A. K. Batra, J. R. Currie, M. D. Aggarwal, M. A. Alim and R. B. Lal, *Materials Letters* **60**, 1937 (2006)

32. A. Rogalski, *Prog. Quantum Electron.* ***27***, 59 (2003)

33. P. Barber, S. Balasubramanian, Y. Anguchami, S. Gong, A. Wibowo, H. Gao, H. J. Ploehn and H. C. Z. Loye, *Materials* **2**, 1697 **(**2009)

Chapter

4

Pyroelectric Properties of $LiNbO_3$/Poly(vinylidene fluoride) (LN/PVDF) Nanocomposites

The pyroelectric properties of polymer-ceramic nanocomposites of Lithium Niobate/Poly(vinylidene fluoride) abbreviated as LN/PVDF for thermal/infrared sensing applications are studied and reported in this chapter. The composites are prepared by dispersing nanoparticles of $LiNbO_3$ in β PVDF matrix at varying volume fractions and cast in the form of flexible films. The thermal, pyroelectric and dielectric properties are measured. From these data the pyroelectric figures of merit of the composite films have been determined and their values compared with corresponding values for pure PVDF film. The Shore hardness of the films has been measured to estimate the extent to which the flexibility of the films is affected by the addition of ceramic.

4.1 Introduction

Even though the remarkable thermal and electrical properties of pyroelectric materials have been known for years, surprising new effects and practical applications are being discovered with advent of materials in their nanoforms [1-6]. Among many fundamental properties of

nanomaterials, the pyroelectric properties are being exploited for technological applications ranging from basic sensing and detection to security systems. Pyroelectric materials take the most important role as pyroelectric infrared detectors [7-9]. Under equilibrium conditions the bound polarization charges at the surface of a pyroelectric material are screened by mobile compensation charges. A temperature change results in a change in the magnitude of polarization leading temporarily to an imbalance between bound polarization charges and the remaining screening charges at the surface [10, 11]. This effect is employed in various thermal and infrared detectors whereby the pyroelectric potential is converted into a current signal through the electrical contacts at opposite surfaces of the pyroelectric element [12, 13]. Pyroelectric single crystals, ferroelectric ceramic materials as well as electro-active polymers have been used since the 1960s for thermal and infrared (IR) detection applications and a variety of materials used for this application can be found in literature [13-15].

Thermal detectors measure IR radiation indirectly by measuring the temperature change due to absorption of radiation. They are widely used for contact-less temperature measurements such as security detectors, human presence sensors and thermal imaging. Although mostly promoted by military interest in night time warfare, low-cost IR imaging techniques based on pyroelectric detectors also have a number of industrial, medical and other civil applications where useful information is obtained by detecting IR radiation [15-18]. A good amount of work has already appeared in literature on the preparation and properties of polymer/ceramic composites as pyroelectric thermal/IR detectors [19]. Polymer detectors such as PVDF film detectors are available commercially. However,

commercial detectors based on polymer/ceramic composites have not yet appeared in the market.

$LiNbO_3$ (LN) is a well known ferroelectric material with very wide technological applications for its interesting physical properties like birefringence, high piezoelectricity, pyroelectricity, and acousto-optic, electro-optic as well as photo-elastic coefficients [20-23]. Compared to other commonly used pyroelectrics like Triglycine Sulfate, Barium Titanate, or Lead-based Titanates or Germanates, the rare combination of several material properties and technological advantages make LN the most favoured material for a variety of applications in technology. The material can be prepared in the laboratory without much difficulty and its polarization is highly stable even in unidirectional poled material at nanometer scales. LN is a naturally stable material because it has no phase transition below its high Curie temperature (1200^oC) [24]. At room temperature it has a rhombohedral symmetry with *R*3*c* space group.

As mentioned in the previous chapter, PVDF is a semi-crystalline polymer with four crystalline phases which include α, β, γ and δ in which the β phase exhibits the pyro, piezo and dielectric properties [25, 26]. The β phase PVDF is currently available commercially as thermal and strain sensors which respectively employ the pyroelectric and piezoelectric properties of this material. Being a representative ferroelectric electro-active polymer with inherently high pyroelectric and piezoelectric properties and with dynamic response for use in touch/tactile sensors, infrared detectors and vidicon/imaging devices, PVDF is selected as the host polymer matrix in this study also [27, 28]. Nowadays, high efficiency

becomes a prerequisite in many application fields such as sensors, information storage, etc. To meet this end it is very easy to prepare thin films of PVDF containing high content of β phase. This is also a reason for selecting PVDF as the polymer matrix part for these studies.

A survey of literature on polymer-ceramic composites for sensor applications reveal that most of the work in this area have been on composites prepared by mixing the polycrystalline ceramic with an electro-active polymer. Such composites have many of the shortcomings of the parent ceramic, like high hardness and brittleness; at the same time less sensitivity due to large volume of the material occupied by the polymer matrix. However, if the ceramic is prepared in the nanocrystalline form, with particle sizes typically less than 100 nm, one can develop polymer-ceramic nanocomposites with better sensitivity. At the same time, such a composite has all the desirable properties of the polymer matrix, such as flexibility, robustness and possibility to cast in the form of thin sheets or even films. Moreover, since the inclusions have particle sizes in the nanometer range, one can hope to achieve higher sensitivity at lower concentrations of the ceramic, compared to the corresponding polymer-polycrystalline ceramic. It is only recently that scientists developed techniques to prepare pyroelectric ceramics in the nanocrystalline form with control over particle sizes. But it is also known that the pyroelectricity in a ceramic vanishes when particle sizes are reduced below typically 20-10 nm, depending on the material. Serious works on the development of such smart materials has begun only recently, and commercial sensors based on them are likely to appear shortly.

As polymers possess high strength, good flexibility, easy processing and low cost, combining LN with polymers like PVDF would be promising for the development of sensor materials [29]. This work aims at the preparation of polymer/ceramic nanocomposites of LN/PVDF with varying concentrations of LN nanoparticles and studying their properties. The objective of preparing the ceramic inclusions as nanoparticles is to attain better flexibility without compromising on the detection sensitivity for lower concentrations of the ceramic.

4.2 Experimental techniques

Experimental techniques adopted for the entire study of LN/PVDF nanocomposites are given in this section. Since all the experimental techniques are explained in detail in chapter 2, they are presented briefly.

4.2.1 Sample preparation

The synthesis techniques for LN nanoparticles, PVDF polymer matrix and their composites are outlined in the following subsections.

4.2.1.1 Synthesis of $LiNbO_3$ nanoparticles

In order to prepare LN nanoparticles, analytically pure Nb_2O_5 (99.999%, Sigma Aldrich), Hydrofluoric acid (HF) (40% v/v), standard Ammonia (25% v/v), Ammonium oxalate (99.99% w/w, Sigma Aldrich) and Li(OH) (Sigma Aldrich) were used as the starting materials. Nanopowders of LN were prepared following a simple and novel synthesis method. For this, stoichiometric amount of Nb_2O_5 was dissolved in minimum amount of HF after heating in a hot water bath at 98^oC for 20 hours. The ratio of Nb_2O_5 to HF was taken as one. It was then mixed with 1.2 mol/litter Ammonium oxalate solution by keeping the ratio Ammonium

oxalate:Nb_2O_5 (V/W) = 5 litter:1.5 mol. During addition of Ammonia solution, $Nb(OH)_5$ began to precipitate. This precipitate was washed several times with dilute Ammonia solution and plenty of hot water. Then this filtered cake was dried in an oven at about 65^oC for 2 hours. Then the two hydroxides Li(OH) and $Nb(OH)_5$ were taken in stoichiometric ratio and mixed, ground well several times in an agate mortar using acetone as grinding medium for 2 hours. Finally the mixture obtained was heated at several temperatures and found out that the optimum sintering temperature is 850^oC for 4 hours.

4.2.1.2 Preparation of PVDF polymer matrix

The same polymer used in the study of LT/PVDF (i.e., commercially available PVDF powders (Sigma Aldrich) with average molecular weight ~ 5,34,000) explained in chapter 3 is used as the matrix in this study also. The preparation steps are given in section 3.2.1.2 of chapter 3.

4.2.1.3 Synthesis of LN/PVDF nanocomposite films

The solvent cast method was used to prepare the LN/PVDF nanocomposite flexible free standing films [30]. In order to investigate the variations in properties of the composites with concentration of LN, different volume fractions of LN (0.001, 0.01, 0.05, 0.09, 0.15 and 0.25) were dispersed in PVDF matrix so as to synthesize LN/PVDF nanocomposites. A sample of pure PVDF film was also synthesized for comparison with the composites. The synthesis technique of LN/PVDF nanocomposite films is similar to that of LT/PVDF films which is explained in section 3.2.1.3 of chapter 3.

4.2.2 Sample characterization

Powder X-ray Diffraction was employed to characterize the newly prepared nanopowders. XRD patterns were recorded for LN nanoparticles sintered at different temperatures. The Transmission Electron Microscopic images are used to find out the exact particle size range of the prepared nanoparticles.

The electroactive β phase of the cast PVDF films were confirmed by powder XRD, FTIR and DSC analyses. The SEM images of the prepared composite films were also taken for the direct evidence of the presence of LN nanoparticles in the PVDF matrix and also to understand the equal dispersion of the ceramic inclusion in the polymer matrix.

4.2.2.1 Dielectric measurements

In order to take electrical contacts from both sides of the samples, small pieces of dry composite film samples were coated with a thin layer of silver paste. Then the samples were dried in a hot air oven for 5 minutes to dry the silver paste. These samples were used as the dielectric medium of a parallel plate capacitor, for the dielectric studies. The dielectric constant (ε) and dielectric loss (ε') of the samples were measured with an Impedance analyzer in the frequency range 100 Hz - 5 MHz. The dielectric studies were carried out in room temperature.

4.2.2.2 Pyroelectric measurements

The pyroelectric coefficients *p(T)* of the nanocomposite films were measured by the Byer and Roundy method, the quasi static direct method [31]. For this the sample was heated up to a certain temperature, but below the transition temperature of the polymer film, by keeping the heating at a

constant rate. The heating rate selected for this study was 2^{o}C/min. The pyroelectric current which depends on this temperature change with time and the electrode area was measured using a highly sensitive picoammeter from which the pyroelectric coefficient was calculated using the expression (1.1) given in chapter 1.

In order to enhance the pyroelectric properties of pure and LN composite PVDF films, all the samples were poled using corona poling technique in which the very high voltage applied across the corona needle and the bottom electrode on which the sample is kept, ionizes the air in between the needle and the electrode and the generated charges get accumulated on the film surface establishing a poling electric field in the film [32, 33]. For our study all the film samples in circular shape having diameter 4 cm were uniformly poled by a single corona point under a high DC electric field of 23 MVm^{-1} at 80^{o}C for one hour and then the temperature source was switched off to cool down the samples to room temperature by keeping the DC power supply on.

4.2.2.3 Thermal studies

Thermal properties of LN/PVDF nanocomposites were measured following the photopyroelectric (PPE) technique, explained in section 2.10 of chapter 2 [34]. In PPE measurements a mechanically chopped light beam from a 120 mW He-Cd laser of wavelength 442 *nm*, impinges on the surface of the sample. The sample absorbs part of the incident energy and undergoes a non-radiative de-excitation process and gets heated. This periodic temperature variation in the sample is directly detected with a sensitive pyroelectric nickel-chromium coated PVDF film transducer

(pyroelectric coefficient 30 $\mu Cm^{-2}K^{-1}$) kept in contact with the sample. The output signal in the form of amplitude and phase was measured with a dual-phase lock-in amplifier from which the thermal parameters such as thermal conductivity *(k)* and specific heat capacity *(C)* of the sample could be calculated.

4.2.2.4 Hardness measurements

The Shore D hardness values for the samples, including pure PVDF, were measured following indentation method by measuring the penetration depth of the durometer indenter with a Shore hardness meter.

4.3 Results and discussions

Results of the complete study of the LN/PVDF nanocomposites in order to use them as materials for pyroelectric thermal/IR detectors are given in the following sections and discussed.

4.3.1 Material identification, structure and morphology

The powder XRD patterns recorded with step size: 0.020^o and step time: 31.2s for the LN nanoparticles sintered at different temperatures are shown in Fig. 4.1. The X-ray powder diffraction patterns of the newly prepared samples show only the reflection peaks of the hexagonal $LiNbO_3$ structure. All the *d*-line patterns match with reported values (JCPDS-20-631) (Fig. 4.2(b)). As can be seen in Fig. 4.1, the beginning of crystallization can be detected starting from 400 ^oC, and at 650°C all the reflections are observed. The intensity of the reflections increases with increasing sintering temperature which indicates a higher degree of crystallinity for the material and maximum observed at 850^oC. The average particle size obtained using

the Debye-Scherrer formula is in the range 45-65 nm.

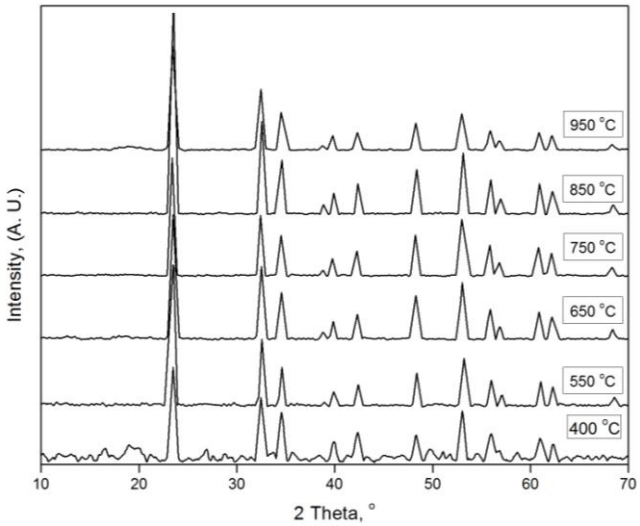

Fig. 4.1 X-ray diffraction patterns of LN nanopowders sintered at different temperatures

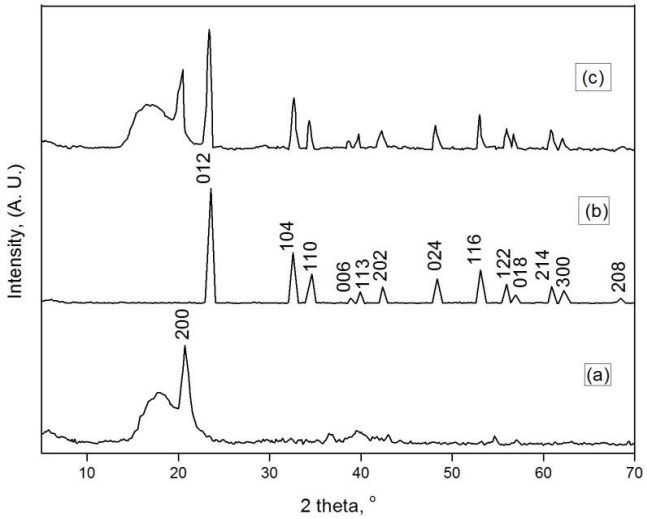

Fig. 4.2 X-ray diffraction pattern of (a) pure PVDF film, (b) LN nanopowder, (c) LN/PVDF nanocomposite with volume fraction 0.05 of LN

The powder XRD pattern of pure PVDF sample shown in Fig. 4.2(a), the major peak is at 20.5^{o} and is corresponding to the (200) plane, which indicates the prominent peak for the β phase of PVDF [35]. Each of the LN/PVDF nanocomposite films has also been subjected to powder XRD measurements. The XRD pattern for one LN/PVDF composite sample (with volume fraction 0.05) is also shown in Fig. 4.2(c). Peaks in the XRD pattern for this sample confirm the presence of LN nanoparticles in PVDF matrix.

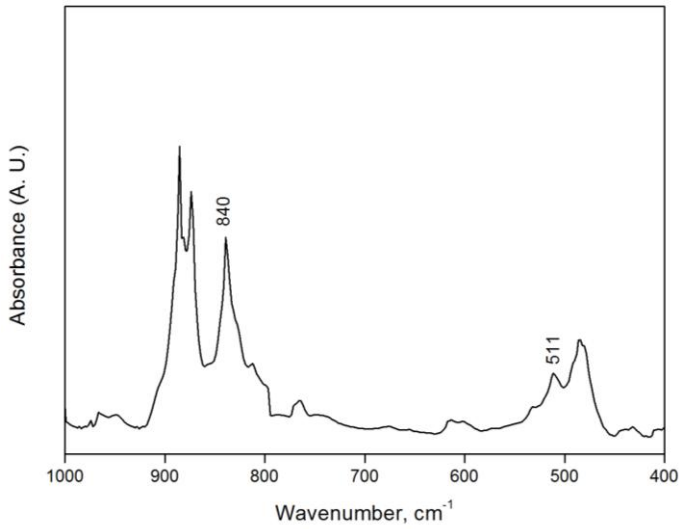

Fig. 4.3 FTIR spectrum of pure PVDF film

The FTIR spectrum of pure PVDF sample is shown in Fig. 4.3. In the FTIR spectrum recorded, the absorption peaks at 511 and 840 cm^{-1} are the characteristic ones for β PVDF [35, 36]. The characteristic peaks corresponding to α phase (766, 795, 856 and 976 cm^{-1}) and γ phase (778, 812 and 834 cm^{-1}) of PVDF are absent in the FTIR spectrum [36]. These results show that PVDF formed is predominantly in β phase. From the DSC curve (Heating rate 10^{o}C/min) shown in Fig. 4.4 it is found that the melting

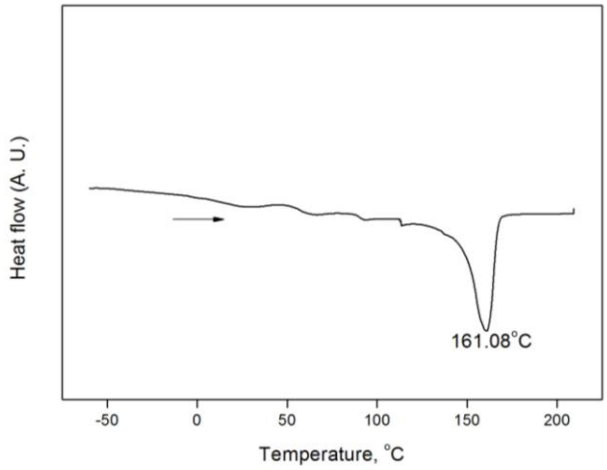

Fig. 4.4 DSC curve of pure PVDF film during heating cycle

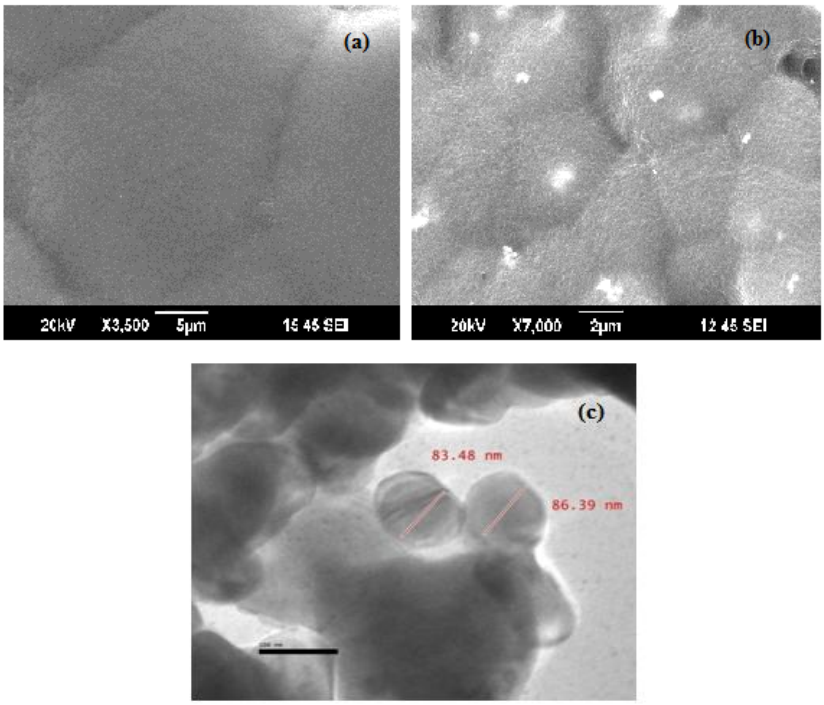

Fig. 4.5 SEM image of (a) pure PVDF film and (b) 0.05 volume fraction of LN/PVDF film and (c) TEM image of LN nanoparticles synthesized

point of the PVDF film cast from DMF solvent is 161.08^{o}C. No other transition peak is found in the temperature region of the measurements.

The SEM images of the pure PVDF film and LN/PVDF film with 0.05 volume fraction is shown in Fig. 4.5(a) and (b) and the TEM image of the prepared LN nanoparticles is shown in Fig. 4.5(c). The Fig. 4.5(b) is a solid evidence for the presence of LN particles in PVDF matrix. From the TEM image the particle size of the prepared nanoparticles is ~ 80 nm.

4.3.2 Sample density

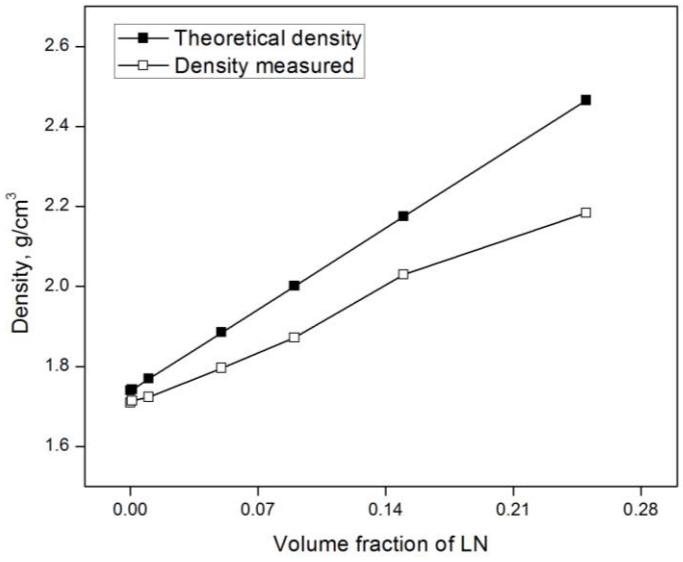

Fig. 4.6 Variations of theoretical and experimental densities of LN/ PVDF nanocomposites with varying volume fractions of LN

Densities of all the prepared samples were measured and compared with theoretical values. Fig. 4.6 gives the comparison of the theoretical and experimental densities of the composites with varying volume fractions of LN. Theoretical densities of the composites are calculated following the

rule of mixtures and the expression for calculating theoretical densities is given in section 3.3.2 of chapter 3. The density increases as the filler loading in the composite increases and just as in the case of LT/PVDF nanocomposites here also the experimental density is slightly lower than the theoretical density in all volume fractions due to the possible particle agglomerates and defects that occur in the composites during synthesis which will cause nonuniformity in the density of the samples. Anyway, all of the prepared samples have attained a density in the range 95-90% of the theoretical density as the filler volume fraction increases from 0 to 0.25.

4.3.3 Dielectric properties

Figures 4.7 and 4.8 show the nature of dielectric constant and dielectric loss properties of the prepared LN/PVDF nanocomposites with frequency and varying sample concentrations of nano LN in PVDF. The dielectric constant increases at all frequencies as the LN content in the matrix increases which is due to the enhancement in internal polarization of the samples. At lower frequencies, below 1 kHz, the dielectric constants of the nanocomposites are higher than the expected values for higher filler concentrations due to the space charge effects [37, 38]. The dielectric loss also increases with filler concentration. At 1 kHz, the dielectric constant varies from 10.19 to 15.53 as the volume fraction of LN increases from 0 to 0.25 and the dielectric loss increases from 0.034 to 0.318. The value of dielectric constant for the pure PVDF film is 10.19, which is rather close to the previously reported value [13]. Both dielectric constant and loss decrease as frequency increases. Above 1 MHz the dielectric constant and above 100 kHz the dielectric loss show a slight increase. As in the case of LT/PVDF nanocomposites, the LN/PVDF nanocomposites also show a

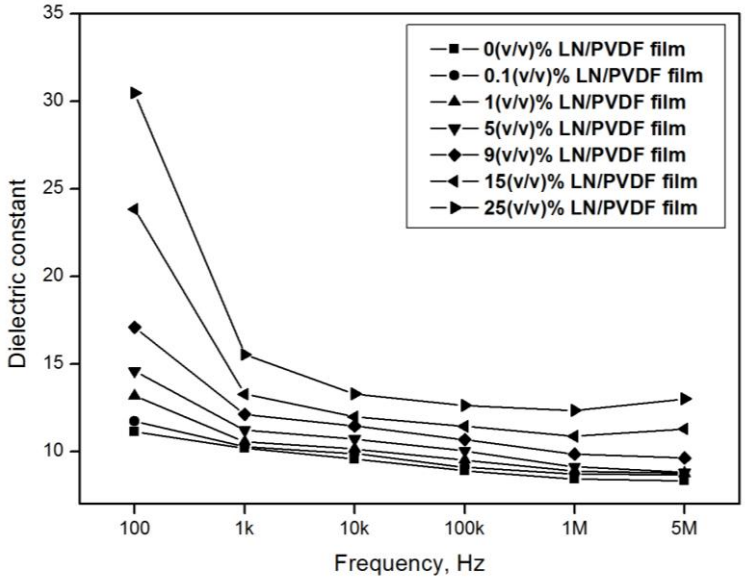

Fig. 4.7 Variations of dielectric constant with frequency for different LN/PVDF nanocomposites

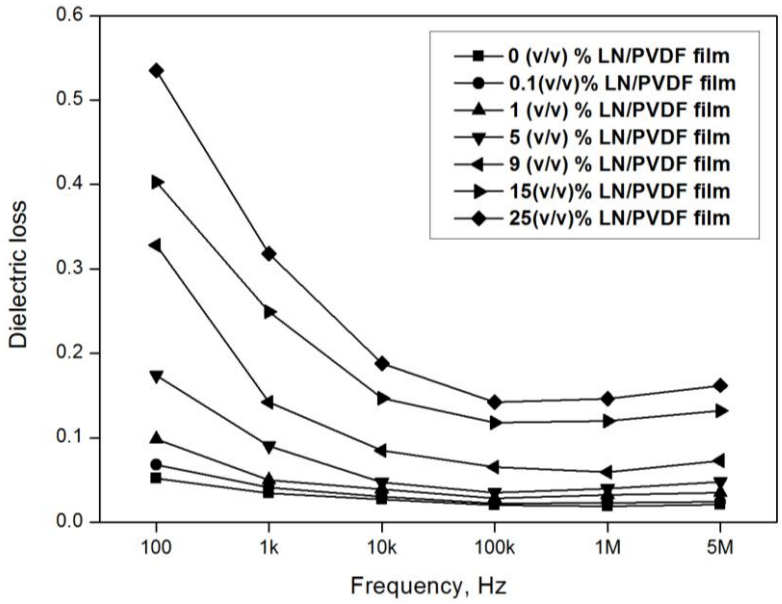

Fig. 4.8 Variations of dielectric loss with frequency for different LN/PVDF nanocomposites

sharp decrease in the dielectric constant at lower frequencies for higher filler concentrations. As the frequency increases to higher values the decrease in dielectric constant is much less. A similar kind of variation occurs for dielectric loss also.

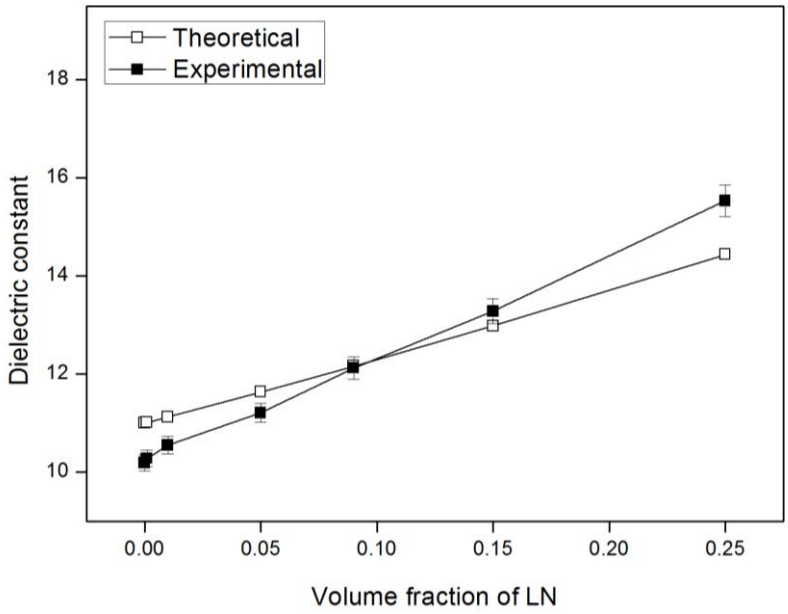

Fig. 4.9 Comparison of theoretical and experimental dielectric constants at 1 kHz for LN/PVDF nanocomposites with different volume fractions of LN

The theoretical dielectric constants for all the prepared LN/PVDF nanocomposites were calculated using the expression (3.1) given in section 3.3 of chapter 3. Experimentally measured dielectric constant values are compared with the theoretical values and noticed that they fairly agree with theoretical values. Comparison of theoretical and experimental dielectric constants is shown in Fig. 4.9.

4.3.4 Pyroelectric coefficients

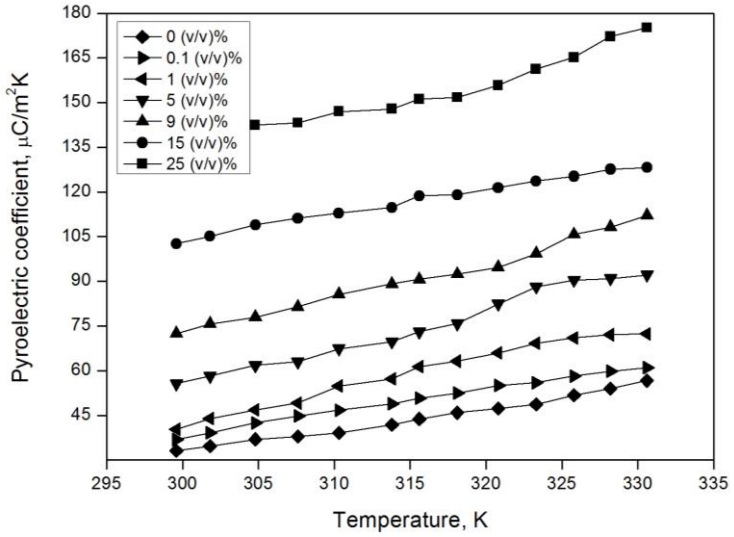

Fig. 4.10 Variations of pyroelectric coefficient of LN/PVDF nanocomposites with temperature for heating

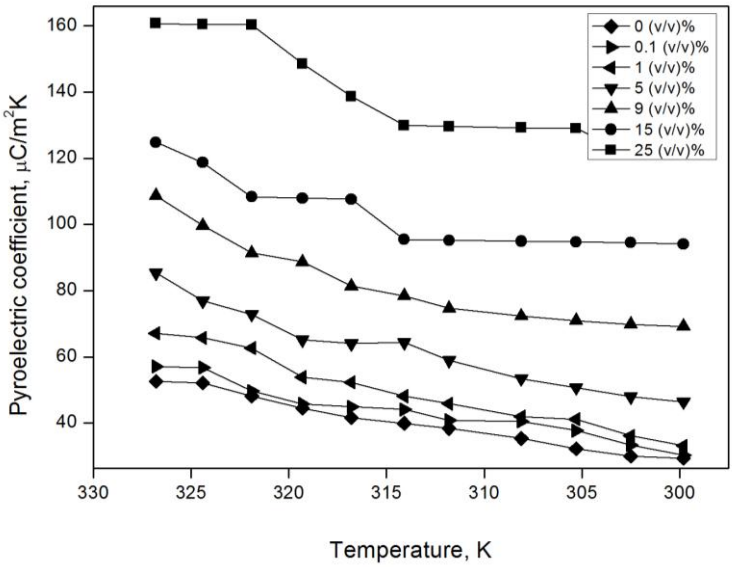

Fig. 4.11 Variations of pyroelectric coefficient of LN/PVDF nanocomposites with temperature for cooling

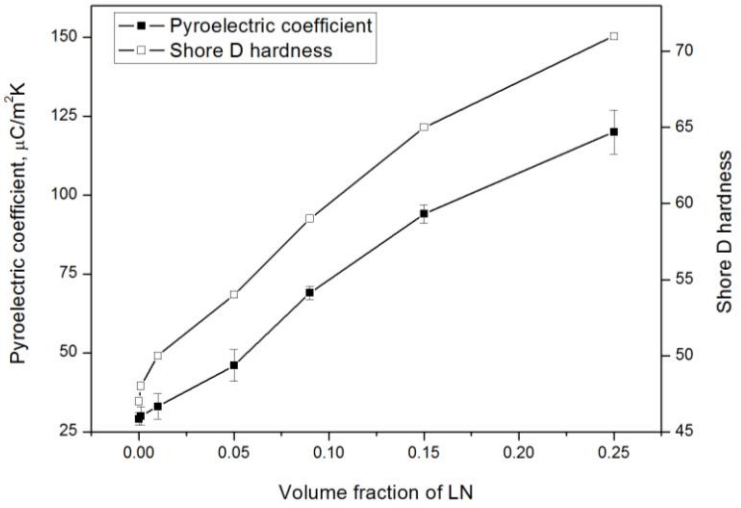

Fig. 4.12 Variations of pyroelectric coefficient and Shore D hardness of LN/PVDF nanocomposites with volume fractions of LN

The quantity of accumulated charges depends on the polarity of the polymer. When LN nanoparticles are added to PVDF, the polarization of the composites increase compared to PVDF due to the dipolar contribution from LN. The pyroelectric coefficients of all the samples were measured after poling in order to get enhancement in property. Pyroelectric coefficients for all the samples (having area $1cm^2$ and thickness ranging from 55-80μm) were measured and verified on heating (Fig. 4.10) as well as cooling (Fig. 4.11). During heating the pyroelectric coefficient varies from 33 $\mu Cm^{-2}K^{-1}$ to 134 $\mu Cm^{-2}K^{-1}$ and during cooling the variation is from 29 $\mu Cm^{-2}K^{-1}$ to 120 $\mu Cm^{-2}K^{-1}$. During heating, pyroelectric coefficient will be slightly higher than that during cooling. That is mainly due to the release of trapped space charges during heating. But in cooling the presence of depolarization currents can be eliminated. It is found that the average value of pyroelectric coefficient increases from 31 $\mu Cm^{-2}K^{-1}$ to 127 $\mu Cm^{-2}K^{-1}$ as

the LN concentration in the PVDF matrix increase from volume fraction 0 to 0.25. Fig. 4.12 shows the variation of average pyroelectric coefficients for varying volume fractions of LN/PVDF nanocomposites.

4.3.5 Thermal analysis

The PPE amplitude and phase recorded for the 0.09 volume fraction of LN in PVDF is shown in Fig. 4.13. Similar kinds of variations are recorded for other combinations of LN/PVDF. From these amplitude and phase values we have calculated thermal parameters.

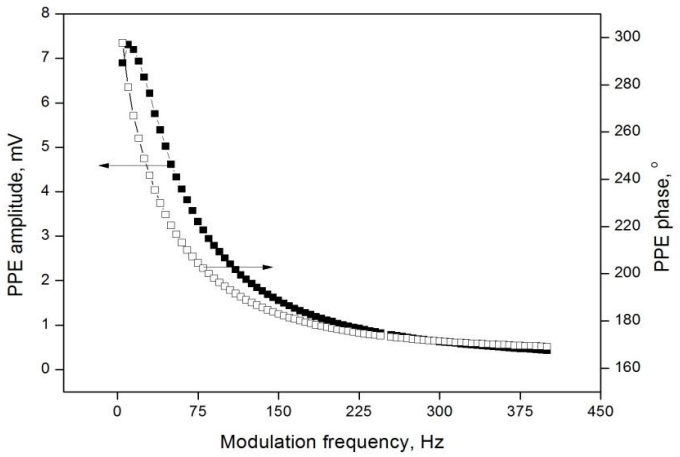

Fig. 4.13 Variations of PPE amplitude and phase as functions of frequency for 0.15 volume fraction of LN in PVDF matrix

It is found that thermal conductivity of the nanocomposites increase from 0.2 $Wm^{-1}K^{-1}$ to 0.47 $Wm^{-1}K^{-1}$ with increase in LN ceramic filler concentration, whereas the specific heat capacity decreases from 1428 $Jkg^{-1}K^{-1}$ to 1210 $Jkg^{-1}K^{-1}$. The variations of thermal conductivity and specific heat capacity with filler concentration are shown in Fig. 4.14. Thermal conductivity and specific heat capacity are also calculated theoretically,

using expressions (3.2) and (3.3) given in section 3.3 of chapter 3. Theoretical curves are also included in Fig. 4.14 and it is clear that the experimental and theoretical values are in good agreement.

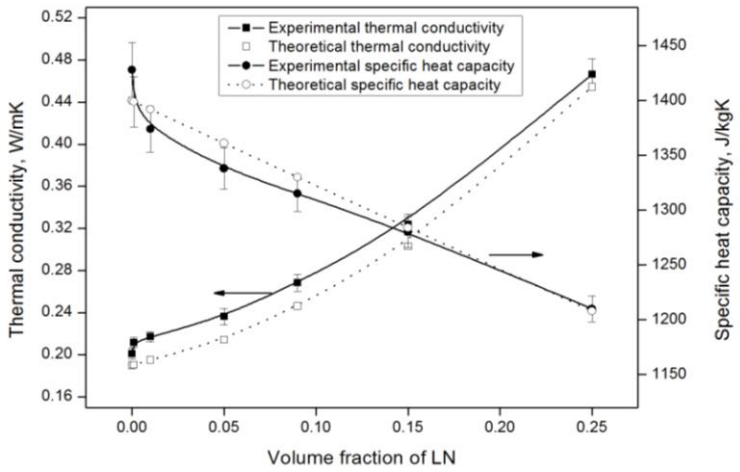

Fig. 4.14 Variations of thermal conductivity and specific heat capacity of LN/PVDF nanocomposites (including theoretical comparison) with volume fractions of LN

4.3.6 Pyroelectric figures of merit

The important properties to look for in a thermal/infrared sensor material are, low dielectric constant and loss, high pyroelectric coefficient, low specific heat capacity and thermal conductivity. The important figures of merit for infrared pyroelectric detector materials F_I, F_V and F_D i.e., figures of merit for high current sensitivity, high voltage responsivity and high detectivity have been calculated for each of the LN/PVDF nanocomposites and in the calculations the values of the dielectric constant and dielectric loss at 1 kHz were used [39-42]. Figures of merit are found to increase with increasing filler content. Variations of the above mentioned figures of merit F_I, F_V and F_D for varying volume fractions of LN are 21×10^{-3} μCm/J to

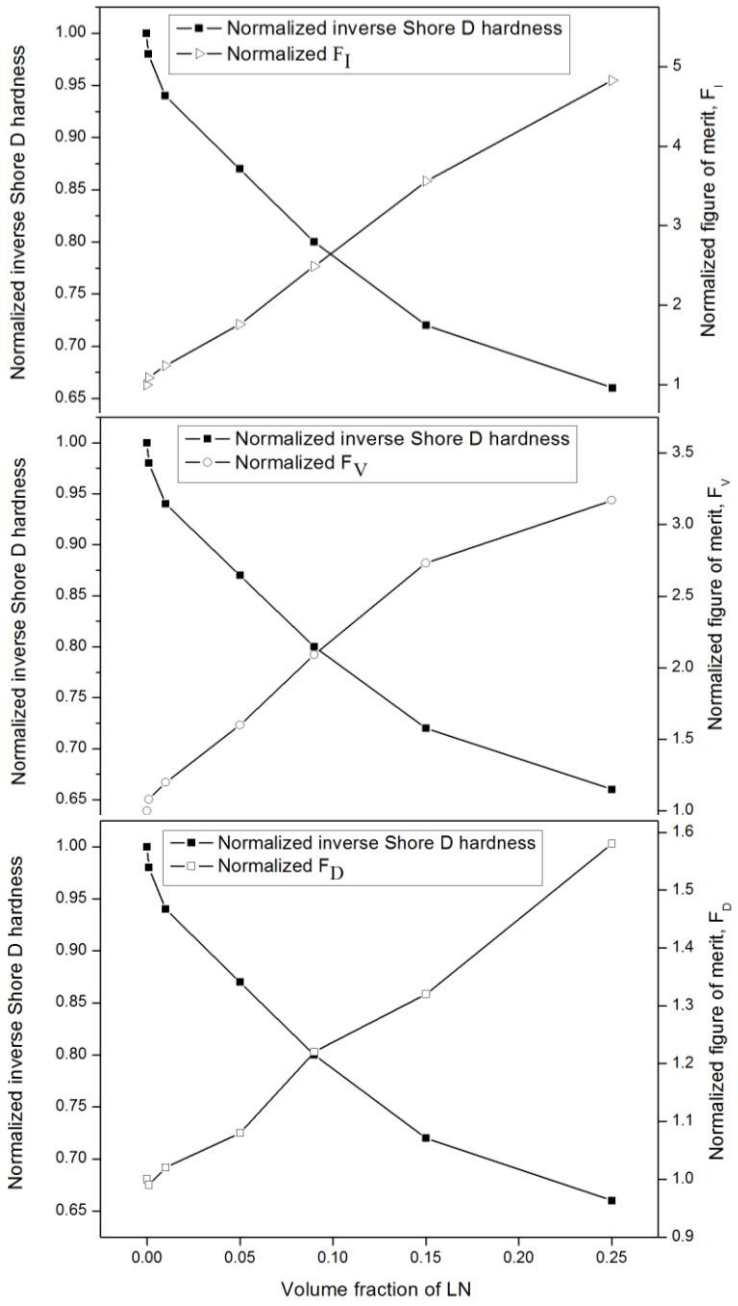

Fig. 4.15 Variations of normalized pyroelectric figures of merit and normalized inverse Shore D hardness for LN/PVDF nanocomposites with volume fractions of LN

104×10^{-3} μCm/J, 2.13×10^{-3}μCm/J to 6.76×10^{-3} μCm/J and 117×10^{-3} μCm/J to 186×10^{-3} μCm/J respectively.

Variations of the figures of merit mentioned above normalized to the corresponding one for pure PVDF, plotted against the volume fractions of LN nanopowder are shown in Fig. 4.15. In the case of LN/PVDF nanocomposites also the figure of merit increases more or less linearly with filler concentration and is also in tune with mean field approximation [43].

4.3.7 Hardness studies

Filler materials in the form of powders or fibres can be added to thermoplastic fluoropolymers like PVDF to accomplish improvement in specific properties like strength, stiffness, lubricity etc. Hardness of polymers like PVDF is usually measured by the Shore D scales. Shore hardness is often used as a proxy to flexibility for the specification of elastomers/plastics. For LN/PVDF nanocomposite films the Shore D hardness increases with increasing volume fractions of LN nanopowder in the composite, as shown in Fig. 4.12. The variation of inverse Shore D hardness, normalized to the value for pure PVDF, with varying volume fractions of LN is also shown in Fig. 4.15. Here it can be noticed that at the volume fraction of about 0.10, where the Shore hardness curve meets the figures of merit curve, the LN/PVDF nanocomposite possesses good flexibility as well as good figures of merit.

4.4 Conclusions

In this study, investigations have been carried out on the development of LN/PVDF nanocomposites with high enough pyroelectric figures of merit and low enough mechanical hardness to keep the material

flexible so that mouldable thermal and infrared detectors can be developed for commercial applications. LN nanopowders are prepared following a novel technique. The pyroelectric coefficients and figures of merit for LN/PVDF nanocomposite films with variable volume fractions have been reported. In this chapter the thermal conductivity, specific heat capacity, dielectric constant, dielectric loss and Shore D hardness of these nanocomposites have also been reported. All the three relevant pyroelectric figures of merit have been evaluated from these parameters for their possible use as pyroelectric thermal/infrared detectors. All these properties are compared with those of pure β PVDF film, which is commercially available currently for the same application. Significant enhancement in pyroelectric sensitivity has been obtained with increase in volume fraction of $LiNbO_3$ nanoparticles.

References:

1. J. Lee, S. Mahendra and P. J. J. Alvarez, *ACS Nano* **4**, 3580 (2010)
2. V. S. Saji, H. C. Choe and K. W. K. Yeung, *Int. J. Nano and Biomaterials* **3**, 119 (2010)
3. X. Chen, S. Xu, N. Yao and Y. Shi, *Nano Lett*. **10**, 2133 (2010)
4. I. Iavicoli, L. Fontana, V. Leso and A. Bergamaschi, *Int. J. Mol. Sci.* **14**, 16732 (2013)
5. X. Huang, L. Li, T. Liu, N. Hao, H. Liu, D. Chen and F. Tang, *ACS Nano* **5**, 5390 (2011)
6. M. Sethi, D. B. Pacardo and M. R. Knecht, *Langmuir* **26**, 15121 (2010)
7. M. Orvatinia and M. Heydarianasl, *Sens. Actuators. A: Phys.* **174**, 52 (2012)
8. A. K. Batra and M. D. Aggarwal, "Pyroelectric materials: Infrared detectors, particle accelerators, and energy harvesters", *SPIE Press Book*, ISBN: 9780819493316 (2013)
9. A. Rogalski, "Infrared detectors", 2nd edn. CRC Press, Taylor & Francis Group, USA (2011)
10. J. Goniakowski, F. Finocchi and C. Noguera, *Rep. Prog. Phys.* **71**, 016501 (2008)
11. G. Rosenman, D. Shur, Y. E. Krasik and A. Dunaevsky, *J. Appl. Phys.* **88**, 6109 (2000)
12. S. B. Lang, *Phys. Today* **58**, 31 (2005)
13. R. W. Whatmore, *Rep. Prog. Phys.* **49**, 1335 (1986)
14. P. Muralt, *Rep. Prog. Phys.* **64**, 1339 (2001)

15. C. Corsi, *Advances in Optical Technologies* **2012**, 838752 (2012)

16. J. Cilulko, P. Janiszewski, M. Bogdaszewski and E. Szczygielska, *Eur. J. Wildlife Res.* **59**, 17 (2013)

17. R. S. Kad, *IJAREEIE* **2**, 988 (2013)

18. M. J. Suriani, A. Ali, A. Khalina, S. M. Sapuan, S. Abdullah and Haftirman, *Materials Testing* **54**, 340 (2012)

19. T. Hanemann and D. V. Szabo, *Materials* **3**, 3468 (2010)

20. M. P. F. Graca, P. R. Prezas, M. M. Costa and M. A. Valente, *J. Sol-Gel Sci. Technol.* **64**, 78 (2012)

21. P. Rabiei and P. Gunter, *Appl. Phys. Lett.* **85**, 4603 (2004)

22. Q. Peng and R. E. Cohen, *Phys. Rev: B.* **83**, 220103 (2011)

23. B. Jaffe, W. R. Cook (Jr.) and H. Jaffe, "Piezoelectric Ceramics", Academic Press Inc., London (2012)

24. A. Mohimi, P. Richardson, P. Catton, T. H. Gan, W. Balachandran and C. Selcuk, *Key Engineering Materials* **543**, 117 (2013)

25. I. N. Bhatti, M. Banerjee and I. N. Bhatti, *IOSR-JAP* **4**, 42 (2013)

26. S. Satapathy, S. Pawar, P. K. Gupta and K. B. R. Varma, *Bull. Mater. Sci.* **34**, 727 (2011)

27. L. Seminara, M. Capurro, P. Cirillo, G. Cannata and M. Valle, *Sens. Actuators. A: Phys.* **169**, 49 (2011)

28. I. Graz, M. Krause, S. B. Gogonea, S. Bauer, S. P. Lacour, B. Ploss, M. Zirkl, B. Stadlober and S. Wagner, *J. Appl. Phys.* **106**, 034503 (2009)

29. J. Jeon, H. B. R. Lee and Z. Bao, *Adv. Mater.* **25**, 850 (2013)

30. M. D. Sanchez-Garcia, E. Gimenez and J. M. Lagaron, *Carbohydr. Polym.* **71**, 235 (2008)

31. R. L. Byer and C. B. Roundy, *Ferroelectrics* **3**, 333 (1972)

32. J. M. Marshall, Q. Zhang and R. W. Whatmore, *Thin Solid Films* **516**, 4679 (2008)

33. S. Yun, J. H. Kim, Y. Li and J. Kim, *J. Appl. Phys.* **103**, 083301 (2008)

34. C. P. Menon and J. Philip, *Meas. Sci. Technol.* **11**, 1744 (2000)

35. S. H. Lee and H. H. Cho, *Fibers and Polymers* **11**, 1146 (2010)

36. L. Yu and P. Cebe, *Polymer* **50**, 2133 (2009)

37. P. Murugaraj, D. Mainwaring and N. Mora-Huertas, *J. Appl. Phys.* **98**, 054304 (2005)

38. H. Sakai, K. Konno and H. Murata, *Appl. Phys. Lett.* **94**, 073304 (2009)

39. B. L. Sidney and D. K. Das-Gupta, *Ferroelectrics Review* **2**, 217 (2000)

40. R. W. Whatmore and R. Watton, "Pyroelectric Materials and Devices" in "Infrared Detectors and Emitters: Materials and Devices", Kluwer Academic Publishers, The Netherlands (2001)

41. P. Guggilla, A. K. Batra, J. R. Currie, M. D. Aggarwal, M. A. Alim and R. B. Lal, *Mater. Lett.* **60**, 1937 (2006)

42. A. Rogalski, *Prog. Quantum Electron.* **27**, 59 (2003)

43. P. Barber, S. Balasubramanian, Y. Anguchami, S. Gong, A. Wibowo, H. Gao, H. J. Ploehn and H. C. Z. Loye, *Materials* **2**, 1697 (2009)

Chapter

5

Pyroelectricity in Strontium Barium Niobate/Polyurethane Nanocomposites

This chapter presents the improvement in electric field-induced pyroelectric properties of Polyurethane (PU) elastomer, brought about by the incorporation of Strontium Barium Niobate, $Sr_{0.3}Ba_{0.7}Nb_2O_6$ (SBN30) nanopowders. Attempts have been made to develop highly sensitive and flexible thermal/IR detector materials with SBN30/PU nanocomposites prepared in the form of cast films with varying the volume fraction of SBN30. Pyroelectric coefficients of poled samples were determined by Byer and Roundy method. The dielectric properties and thermal properties are measured following photopyroelectric (PPE) technique. The figures of merit for the material to act as a thermal/infrared detector are calculated. In order to understand the corresponding change of flexibility, Shore hardness for each composite has been measured.

5.1 Introduction

Thermal/IR detectors based on pyroelectric effect have potential advantages such as room temperature operation and wide spectral response. In the past decades major thrust in this area has been on development of

materials for infrared detection and thermal imaging for military night vision, target acquisition and missile guidance. In recent years the thrust has shifted more towards biomedical applications, waste energy harvesting, human movement detection etc [1-5]. Crystalline pyroelectric materials such as Triglycine Sulphate (TGS) and deuterated TGS have extensively been used as thermal/IR detectors for many years owing to their high pyroelectric coefficient [6, 7]. However, they suffer from serious disadvantages such as susceptibility to humidity and other environmental conditions. Ceramic/polymer based pyroelectric composite materials have the potential to be used as commercial thermal/IR detectors mainly due to the possibility to fabricate large area light weight detectors with enhanced strength and immunity to humidity and environment, eventually useful for thermal/infrared detection applications without use of substrates [8, 9].

Electro-active polymers (EAPs) have been widely studied for the past few years for various sensor applications, owing to their high field-induced polarization [10-12]. In this chapter, commercially available Polyurethane (PU), an electro-active polymer, is selected as the host polymer matrix. PU was invented during 1930s, as a result of research efforts to develop polymeric fibre materials similar to but different from nylon fibres. It was discovered even earlier but was protected by US patents [13]. Polyurethanes are one of the most versatile classes of materials today. Their industrial demand continues to grow, as they are unique materials that offer elasticity of rubber combined with the toughness and durability of hard plastics. Because urethane is available in a very broad hardness range, it allows engineers to replace rubber or plastics with the ultimate material in abrasion resistance as well as other desirable physical properties [13].

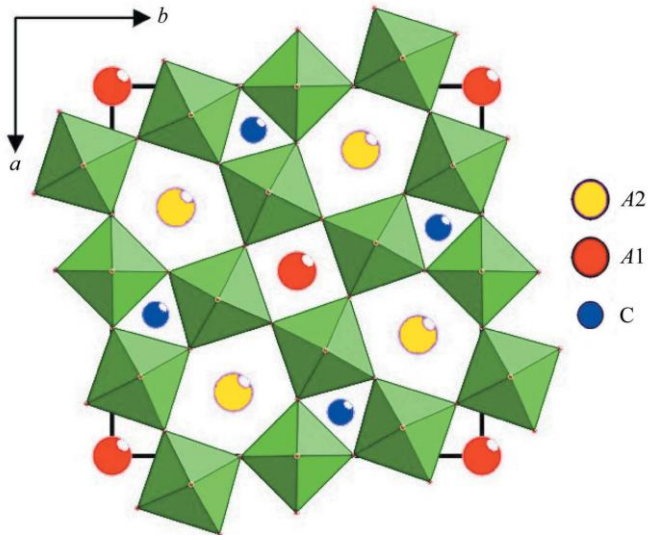

Fig. 5.1 Crystal structure of the tetragonal tungsten bronze

Ferroelectric materials with tetragonal tungsten bronze (TTB) structures are important due to their superior pyroelectric, piezoelectric and excellent electro-optic properties with very fast response times [14-17]. Strontium Barium Niobate ($Sr_xBa_{1-x}Nb_2O_6$, $0.25 \leq x \leq 0.75$) or SBN, is one such interesting ferroelectric material with TTB crystal structure, which finds applications in thermal/infrared detection and diverse device applications including memory devices, surface acoustic wave (SAW) devices and so on. Moreover, SBN possesses excellent pyroelectric properties with very fast response times [18]. At low annealing temperatures, say below 950^{o}C, SBN crystallizes into a mixture of orthorhombic and TTB phase and transforms completely into TTB phase at higher temperatures, say above 1000^{o}C, and longer annealing times ($\approx$ 5 hours) [19]. The structure of tetragonal tungsten bronze is shown in Fig. 5.1. The characteristic feature of the TTB crystal structure is interconnected

corner sharing oxygen octahedral with three types of pseudo symmetric open channels i.e., three fold, four fold and fivefold as shown in the Fig. 5.1. All ferroelectric materials show good performance below their Curie temperatures. In the case of SBN the temperature of transition (T_C) from ferroelectric tetragonal to paraelectric phase depends on the concentration of strontium. As the strontium content in SBN increases the Curie temperature decreases [20]. SBN with 30 wt. percent Sr, $Sr_{0.30}Ba_{0.70}Nb_2O_6$ (or SBN30), has a high transition temperature, compared to other SBNs with higher percentages of strontium content. It is suitable for applications below 230^{o}C, which is the Curie temperature for SBN30. Below T_C, SBN exhibits TTB crystal structure. Even though the pyroelectric coefficient increases with strontium content in SBN series, it is also known that SBN compositions with lower strontium content presents lower relative dielectric constants at room temperature [21]. Even for a slight increase in strontium content, there is drastic increase in dielectric constant. So, in SBN series, SBN30 composition possesses good pyroelectric coefficient, at the same time low permittivity, which are the most important factors to improve the figures of merit for a material to act as a pyroelectric infra-red/thermal detector.

Though different combinations of polymers (mostly PVDF and its co-polymers) and pyroelectric ceramics (mostly titanates, niobates and TGS) have been tried to develop sensitive thermal/IR sensor materials [22], no efforts have been made so far to develop SBN/ PU based polymer-ceramic nanocomposites for this application. This work is a part of an effort to develop more sensitive, polarisable and flexible composites, than already reported in literature. Different compositions of SBN30/PU have been

prepared and relevant properties measured to estimate their pyroelectric performance and compare with results reported on similar materials.

5.2 Experimental techniques

The various experimental techniques used to study the properties of the prepared SBN30/PU nanocomposite samples, including the synthesis of SBN30 and its polymer composite preparation are outlined below.

5.2.1 Sample preparation

Sample preparation includes the synthesis of nanoparticles of SBN30, the polyurethane polymer matrix preparation and fabrication of SBN30/PU nanocomposites with varying volume fractions of SBN30 ceramic inclusion in PU polymer matrix.

5.2.1.1 Synthesis of SBN30 nanopowders

Analytically pure Barium nitrate ($Ba(NO_3)_2$, Aldrich), Strontium nitrate ($Sr(NO_3)_2$, Aldrich), Niobium pentoxide (Nb_2O_5, Aldrich), Ethylene Diamine Tetra Acetic acid (EDTA, Merck), ammonia solution (Merck) and citric acid (Merck) were used as raw materials for synthesis of SBN30 nanoparticles. Nanopowder was prepared by a known aqueous organic gel route [23]. Here the citric acid and EDTA are used as the chelating agents. First the Ba-EDTA and Sr-EDTA complex solutions have to be prepared. For this, $Ba(NO_3)_2$ and $Sr(NO_3)_2$ powders are separately dissolved in deionised water and mixed with aqueous EDTA. Then in order to get transparent complex solutions, pH of both the solutions were adjusted to greater than 7 using ammonia solution. Then the pH of each of the solutions was adjusted to 7 by the addition of nitric acid.

Next step is the preparation of the Nb-citrate solution. For this Nb_2O_5 was dissolved in hydrofluoric acid by heating for 48 hours. Then aqueous solution of ammonium oxalate was added into the solution, followed by ammonia solution with continuous stirring to form precipitate of $Nb_2O_5.nH_2O$. This precipitate was filtered and washed with water to make it fluoride free. After this the precipitate was aged at 80^oC for 12 hours. The powder thus obtained was then dissolved in aqueous solution of citric acid by continuous stirring and heating at 60^oC to form a transparent pale yellow Nb-citrate complex.

Then for the preparation of SBN30 ceramic nanopowders, stoichiometric amounts of Ba-EDTA, Sr-EDTA and Nb-citrate solutions were mixed together followed by the addition of citric acid in the molar ratio of citric acid:Nb = 3:1. Then the pH was adjusted to 8 by the addition of ammonia solution. A clear transparent Sr-Ba-Nb precursor solution had high stability and no precipitation was obtained with continuous stirring. This precursor solution was then heated at 80^oC for 24 hours to produce a gelatinous precursor which was then calcined at 800^oC for 2 hours in air to form the SBN30 nanopowders.

5.2.1.2 Preparation of PU polymer solution

The polymer matrix used was commercially available PU granules (Otto Chemie Pvt. Ltd.). 15 (weight/volume)% polymer solution was prepared by dissolving required amount of PU granules in N,N-Dimethyl formamide (DMF) of S. D. Fine Chem. Ltd., solvent under continuous stirring at a constant temperature of about 75^oC for one hour. (The glass transition temperature of PU elastomer obtained from DSC analysis was

76.43^{o}C). Thus prepared solution was kept undisturbed for some time to get bubble free polymer solution.

5.2.1.3 Synthesis of SBN/PU nanocomposite films

In order to measure properties of SBN30/PU nanocomposites, the samples were prepared in the form of free standing films. Ceramic-polymer nanocomposite films with different volume fractions SBN30 (0, 0.001, 0.01, 0.05, 0.09, 0.15 and 0.25) were fabricated by solvent cast technique [24]. The same 15(w/v)% PU matrix was used for fabricating each composites. Required quantities of the SBN30 nanopowder was added to it and dispersed well by sonication to avoid agglomeration of nanoparticles. The as prepared composite solution was then poured into an open glass container for the solvent to evaporate completely. Finally, free-standing films of SBN30/PU nanocomposites of thickness in the range 35-50 μm were peeled off from the container. We restricted our composite films preparation with up to the volume fraction 0.25 of SBN30 due to problem of excess particle agglomeration.

5.2.2 Sample characterization

Synthesized SBN30 nanopowders were characterized by powder XRD and elemental analysis was done by EDS. All the composite film samples were subjected to SEM and TEM analyses to estimate dispersion of nanoparticles in polymer matrix and to understand their exact range of particle size.

5.2.2.1 Dielectric measurements

Circular pieces (diameter ≈10 mm) of dry composite film samples were coated with silver paste on both sides which acted as electrical

contacts for the specimen. Electrode coated samples were mounted between two spring loaded copper discs (diameter ≈10 mm) for dielectric and pyroelectric measurements. The relative dielectric constant and dielectric loss were measured by capacitance method with an Impedance analyzer. Capacitance and *tanδ* values were measured in the frequency range 100 Hz-5 MHz in room temperature. Values of dielectric constant and loss were calculated using these parameters. The necessary expressions are given in section 2.7 of chapter 2.

5.2.2.2 Pyroelectric measurements

The pyroelectric coefficients of the samples were determined by Byer and Roundy method [25]. For this the sample was placed in a homemade cell and the heating rate was maintained uniform at 2^{o}C/min with the help of a temperature controller and the pyroelectric current developed was monitored with an auto-ranging picoammeter. The expression used to determine pyroelectric coefficient *p(T)* is given in section 1.5.1 of chapter 1.

Before measuring the pyroelectric coefficient of the samples, they were electrically poled in a very high DC field. The poling technique adopted was corona poling, generally used for poling thin polymer films [26]. Corona discharge is a partial breakdown of air, usually at atmospheric pressure, and is initiated by a discharge in an inhomogeneous electric field. Usually corona poling is done at elevated temperatures. Raising the temperature in a polymer guest-host system close to or just above its glass transition temperature before poling increases the mobility of the guest molecules and allows rotation to occur during poling. In this work circular

film samples of diameter 40 mm got uniformly poled into ferroelectric domains by a single point corona by heating them up to 78^{o}C and applying an electric field of 16 MV/m for 1 hour, and then slowly cooling the samples back to room temperature before removing the electric field.

5.2.2.3 Thermal studies

Thermal properties such as thermal conductivity and specific heat capacity are important parameters for a thermal/IR detector. These properties for the prepared samples were measured following the photopyroelectric (PPE) technique mentioned in chapter 2. Here the measurements are carried out with a commercially available pyroelectric detector used as thermal detector [27]. Sample was attached to the pyroelectric detector with a thermally thin layer of a heat sink compound whose contribution to the signal was negligible. The output signal was measured with a dual-phase lock-in amplifier in the form of amplitude and phase. From these parameters the thermal conductivity and specific heat capacity of the samples could be obtained. All measurements were carried out at room temperature.

5.2.2.4 Hardness measurements

Measurement of Shore hardness is used to understand the flexibility and hardness of polymers. Generally Shore A scale is used for 'softer' rubbers/plastics and Shore D for 'harder' ones. In the case of polyurethane selected for the study, we measured the Shore A hardness. The Shore A values for all samples were measured following indentation method.

5.3 Results and discussions

The results of the studies undertaken on SBN30/PU nanocomposite film samples are given and discussed in this section. Besides the experimental measurements, the theoretical values of thermal conductivity (*k*), specific heat capacity (*C*) and dielectric constant (ε) were calculated using effective medium theory [28-30]. The effective medium theory expressions used for the calculations are given in section 3.3 of chapter 3. Here the values used for the calculations of *k*, *C* and ε of the composites are 0.22 $Wm^{-1}K^{-1}$, 1662 $Jkg^{-1}K^{-1}$ and 7.13 respectively for PU mtrix and the corresponding values for SBN30 ceramic filler are 1.17 $Wm^{-1}K^{-1}$, 210 $Jkg^{-1}K^{-1}$ and 930 respectively.

5.3.1 Material identification, structure and morphology

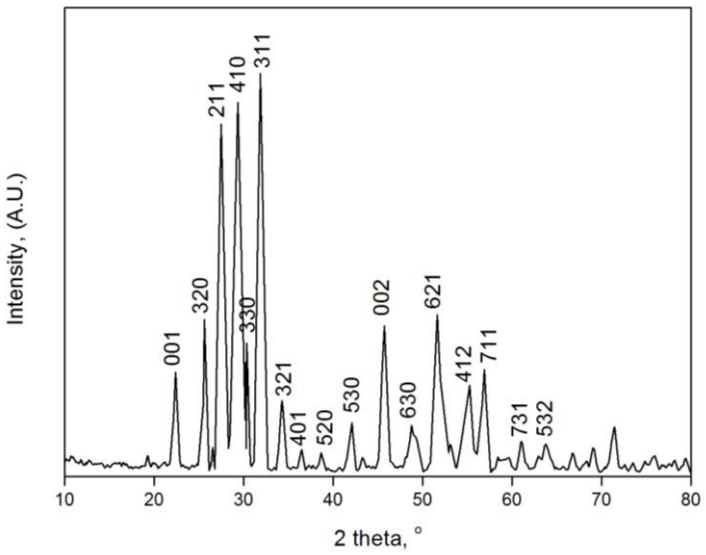

Fig. 5.2 Powder XRD pattern of the SBN30 nanopowder (step size: 0.020°, step time: 31.2 s)

The tetragonal tungsten bronze structure and concentrations of strontium and barium are confirmed from powder XRD and EDS analyses. The powder X-ray Diffraction pattern reproduced in Fig. 5.2 has been indexed according to JCPDS File No.73-126, and the tetragonal tungsten bronze structure for SBN30 powder is confirmed. The particle size calculated using Debye - Scherer formula is in the range 40–90 nm. The diffraction peaks at 2 theta values 27.459^{o}, 29.367^{o}, 31.859^{o}, 45.684^{o} and 51.599^{o} were used to determine particle size. The diffraction peak at 31.859^{o} was used to make correction for instrumental line broadening. The atomic percentages of strontium and barium present in the nanopowder obtained from EDS analysis are 23% (Sr) and 77% (Ba), which correspond to the stoichiometric composition of SBN30.

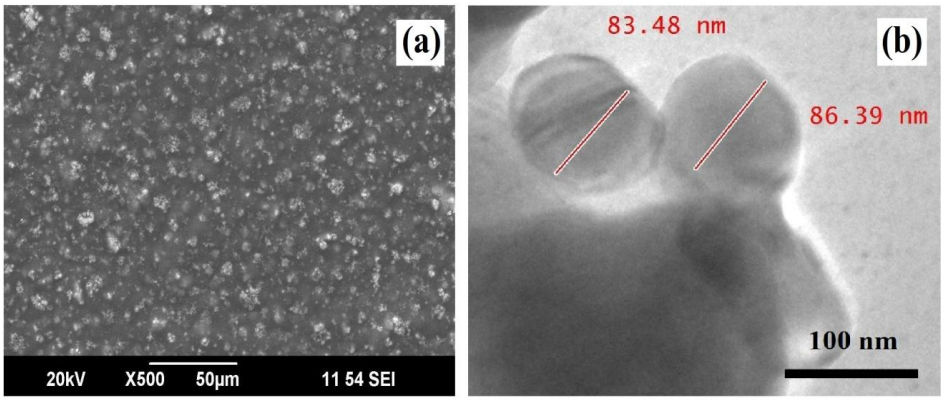

Fig. 5.3 (a) SEM image of a composite film with volume fraction 0.09 of SBN30 and (b) TEM image of SBN30 nanoparticles

The SEM image of composite film with volume fraction 0.09 of SBN30 and TEM image of the prepared SBN30 nanoparticles are shown in Fig. 5.3. From the SEM image it is evident that SBN30 nanoparticles are

dispersed nearly uniformly in the polymer matrix. Since the particles are in nanometer size, it is difficult to prevent particle agglomeration completely. However, at most care was taken to minimize agglomeration by ultrasonicating all composites before casting into films. The SEM images of other compositions also show similar results. From the TEM image it is clear that the particle size is below 100 nm. This is in tune with the average particle size calculated from the XRD pattern.

5.3.2 Sample density

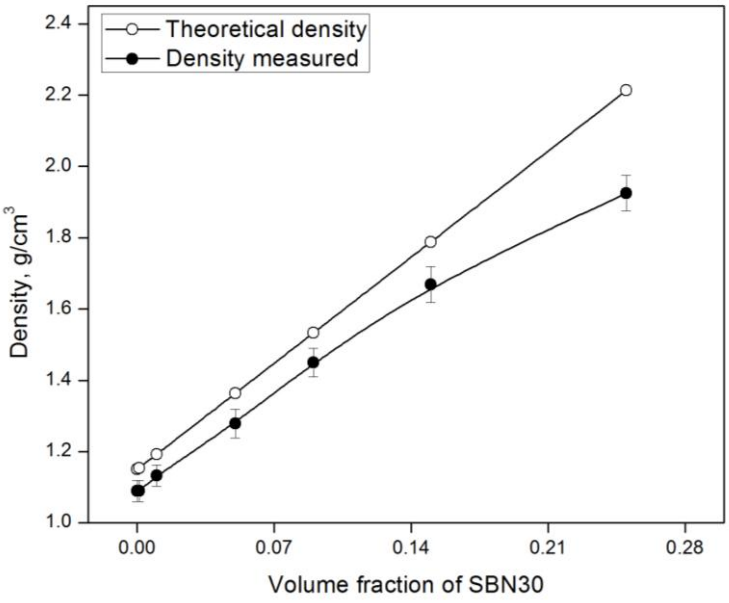

Fig. 5.4 Variations of theoretical and experimental densities of SBN30/PU nanocomposites

The densities of the samples were measured by direct weighing and theoretical densities calculated by the rule of mixtures following the expression given in section 3.3.2 of chapter 3. A comparison of theoretical and measured densities is shown in Fig. 5.4.

As the volume fraction of SBN30 increases, density increases. At higher filler concentrations the measured densities are smaller than corresponding theoretical ones, indicating that lower density is due to possible particle agglomeration and presence of voids as volume fraction of SBN30 increases. But all the samples attained 94–87% theoretical density as the volume fraction of SBN30 nanoparticles increases from 0 to 25%.

5.3.3 Dielectric properties

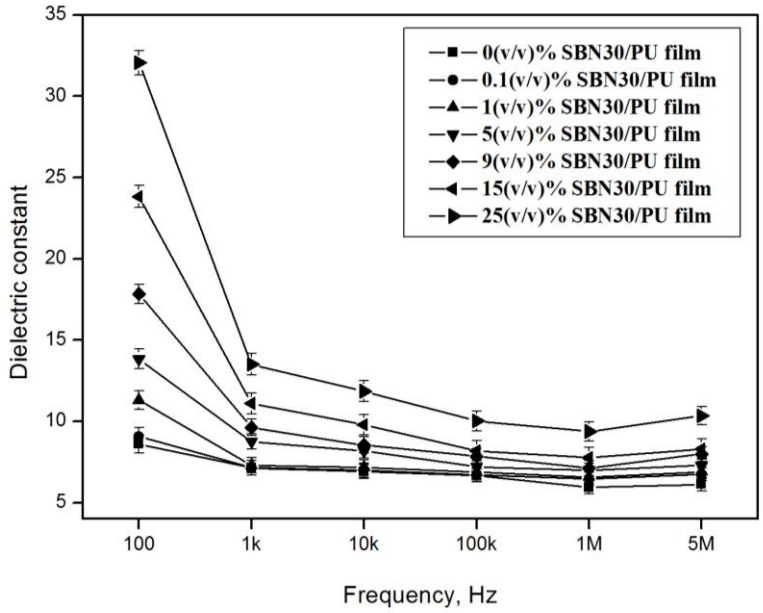

Fig. 5.5 Variations of dielectric constant with frequency for different SBN30/PU nanocomposites

Dielectric properties are key parameters for thermal/IR sensor materials. The variation of the dielectric constant with frequency for pure PU and samples with different concentrations of SBN30 nanoparticles are shown in Fig. 5.5. The dielectric constant of the composite increases as the SBN30 content in PU matrix increases due to the increase in the internal

polarization of the sample. As the frequency increases the dielectric constant decreases. The dielectric loss also show slight increase with increase in SBN30 content, but decrease with frequency for all samples, as shown in Fig. 5.6.

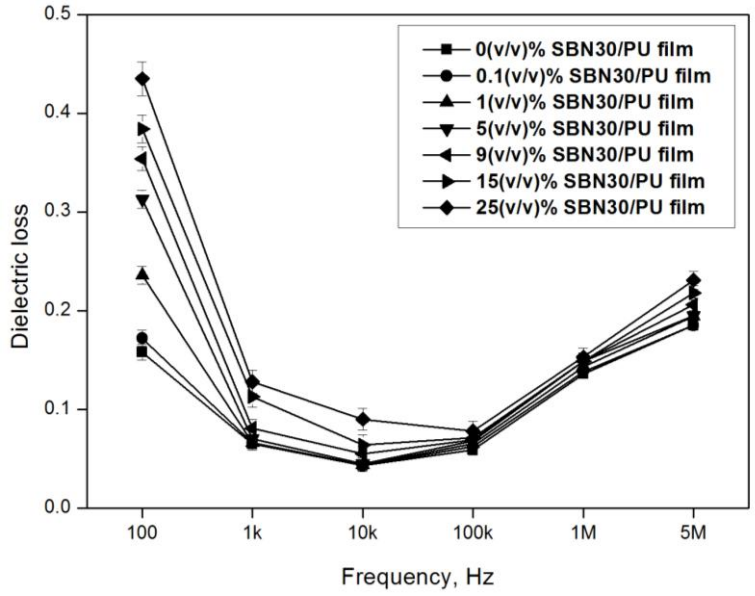

Fig. 5.6 Variations of dielectric loss with frequency for different SBN30/PU nanocomposites

However, beyond frequency 100 kHz, all compositions show an increase in dielectric loss with further increase of frequency. The dielectric constant varies from 7.13 to 13.51 at 1 kHz as the SBN30 volume fraction increases from 0 to 0.25 in the matrix, whereas the corresponding variation in dielectric loss is from 0.065 to 0.128. A comparison of the measured dielectric constants for all compositions at frequency 1 kHz with theoretical values is shown in Fig. 5.7. From this figure it is clear that the measured values are in good agreement with corresponding theoretical values

calculated.

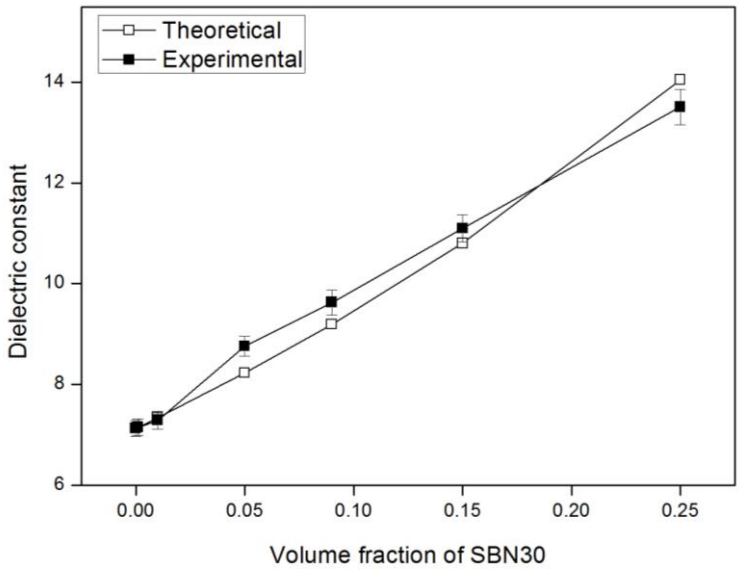

Fig. 5.7 Comparison of theoretical and experimental relative dielectric constants at 1 kHz for SBN30/PU nanocomposites with different volume fractions of SBN30

5.3.4 Pyroelectric coefficients

Pyroelectric coefficients for all the samples with different concentrations of nano SBN30 in PU were measured during heating (Fig. 5.8) as well as cooling cycles (Fig. 5.9). When SBN30 nanoparticles are added to PU the polarization of the composites increase compared to pure PU due to the dipolar contribution from SBN30. It is found that the pyroelectric coefficient during heating increases from 82 $\mu Cm^{-2}K^{-1}$ to 395 $\mu Cm^{-2}K^{-1}$ and during cooling it varies from 79 $\mu Cm^{-2}K^{-1}$ to 380 $\mu Cm^{-2}K^{-1}$ as the SBN30 concentration increases from volume fraction 0 to 0.25. During heating, in addition to the pyroelectric current, a small current due to release of trapped space charges will also be present. During cooling the

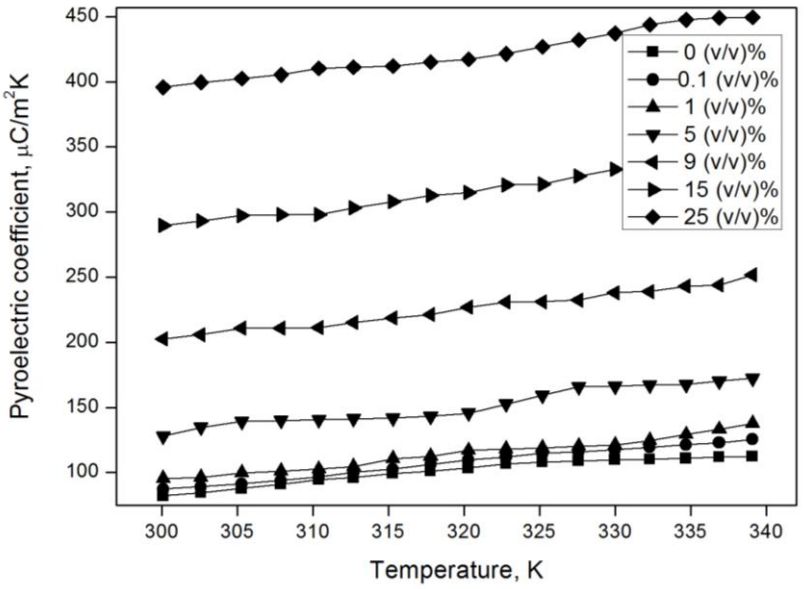

Fig. 5.8 Variations of pyroelectric coefficients during heating with temperature

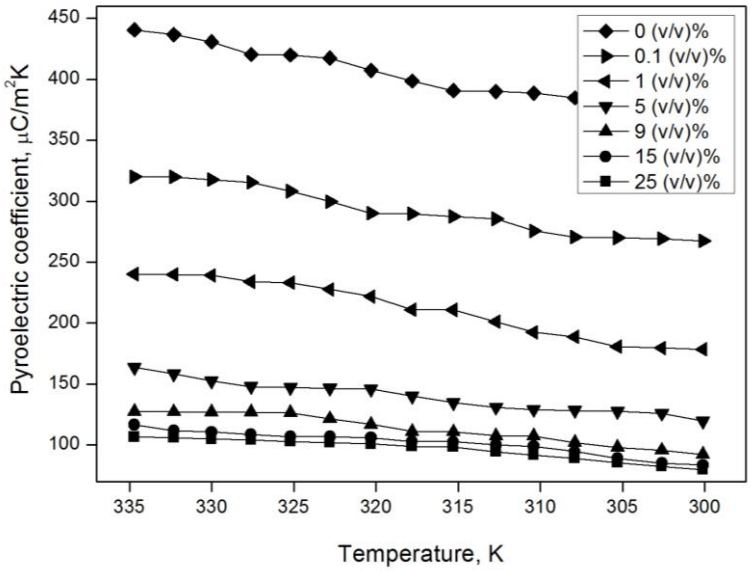

Fig. 5.9 Variations of pyroelectric coefficients during cooling with temperature

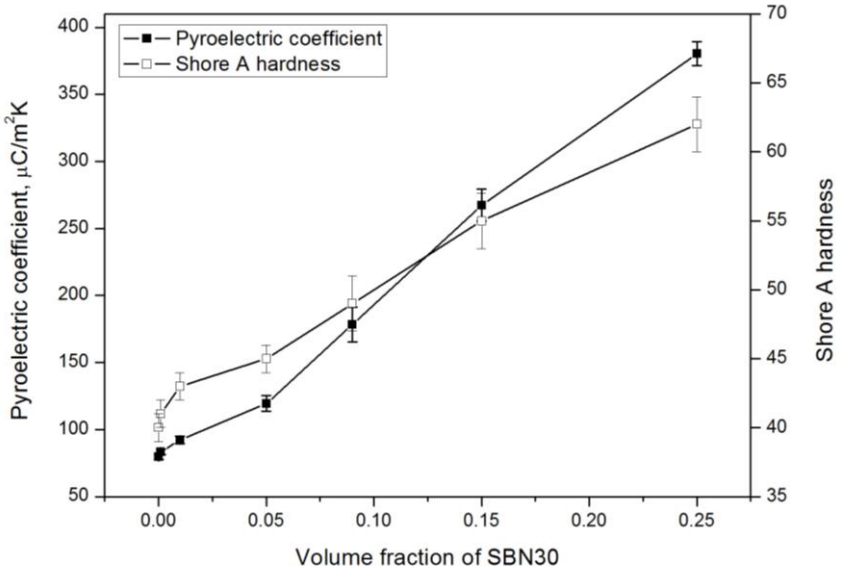

Fig. 5.10 Variation of the average pyroelectric coefficient during heating and cooling and Shore A hardness for SBN30/PU nanocomposites with varying volume fraction of SBN30

presence of depolarization currents can be eliminated. That is why during cooling the pyroelectric coefficients are slightly less compared to those during heating. Fig. 5.10 shows the variation of average of the pyroelectric coefficients during heating and cooling for varying volume fractions of SBN30 in PU. The average value of pyroelectric coefficient increases from 81μCm^{-2}K^{-1} to 388μCm^{-2}K^{-1}. As the volume fraction of SBN30 increases, the pyroelectric coefficient increases due to the presence of higher proportion of the ceramic pyroelectric material.

5.3.5 Thermal analysis

Fig. 5.11 shows the variations of photopyroelectric amplitude and phase with frequency, for the volume fraction 0.25 of SBN30 in PU.

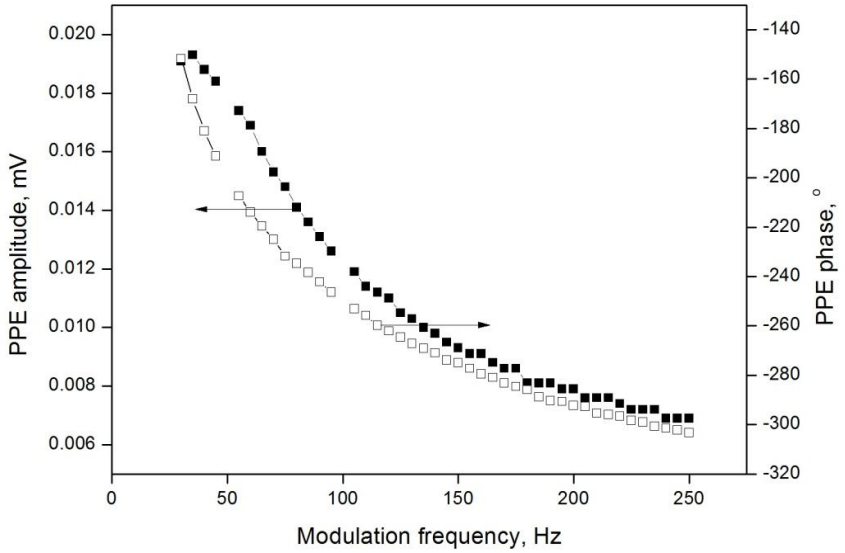

Fig. 5.11 Variations of PPE amplitude and phase as functions of frequency for 0.25 volume fraction of SBN30 in PU polymer matrix

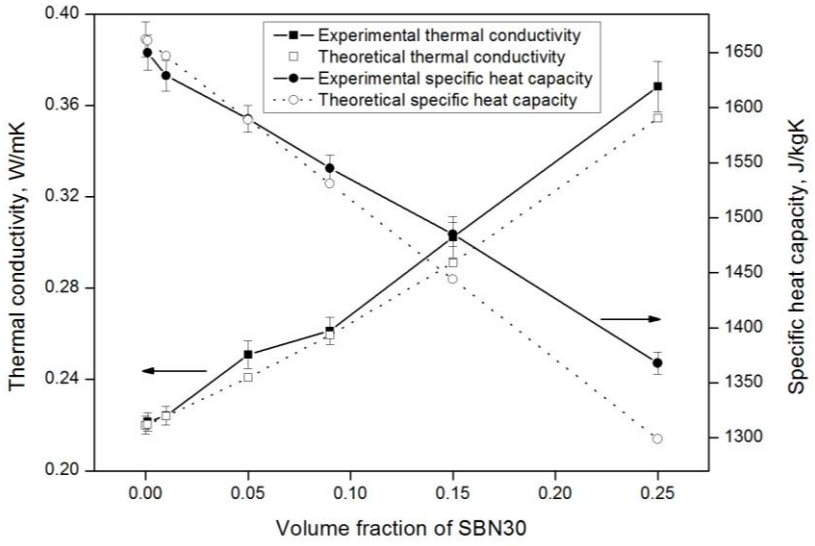

Fig. 5.12 Variations of theoretical and experimental thermal conductivity and specific heat capacity of SBN30/PU nanocomposites with varying volume fraction of SBN30

Similar kinds of variations are observed for other volume fractions also. From these amplitude and phase values the thermal parameters are calculated.

Thermal conductivity and specific heat capacity are two other important parameters to be considered for pyroelectric thermal/IR sensor materials. For a good material, thermal conductivity and specific heat capacity should be low in order to enhance their figures of merit. It is found that thermal conductivity for present nanocomposites increases from 0.22 to 0.37 $Wm^{-1}K^{-1}$ with increase in filler volume fraction from 0 to 0.25, whereas specific heat capacity correspondingly decreases from 1662 to 1368 $Jkg^{-1}K^{-1}$. The variations of thermal conductivity and specific heat capacity with filler concentration are shown in Fig. 5.12. Comparisons with corresponding theoretical values calculated are also shown in this figure. The experimental values follow theoretical ones in both cases.

5.3.6 Pyroelectric figures of merit

The pyroelectric performance of a material is characterized by the relevant figures of merit. Figures of merit are numerical values representing measures of effectiveness, efficiency and performance of the material when used as a transduction device. The figures of merit for high current sensitivity (F_I), high voltage responsivity (F_V) and high detectivity (F_D), which are important for pyroelectric thermal/IR detection applications are calculated [31-34] for each of the SBN30/PU nanocomposites and found that all the figures of merit, in general, increase with increase of filler concentration. F_I increases from 48 to 283, F_V from 6.83 to 20.99 and F_D from 191 to 792 (all in units of $\times 10^{-3}$ μCm/J) as the filler volume fraction

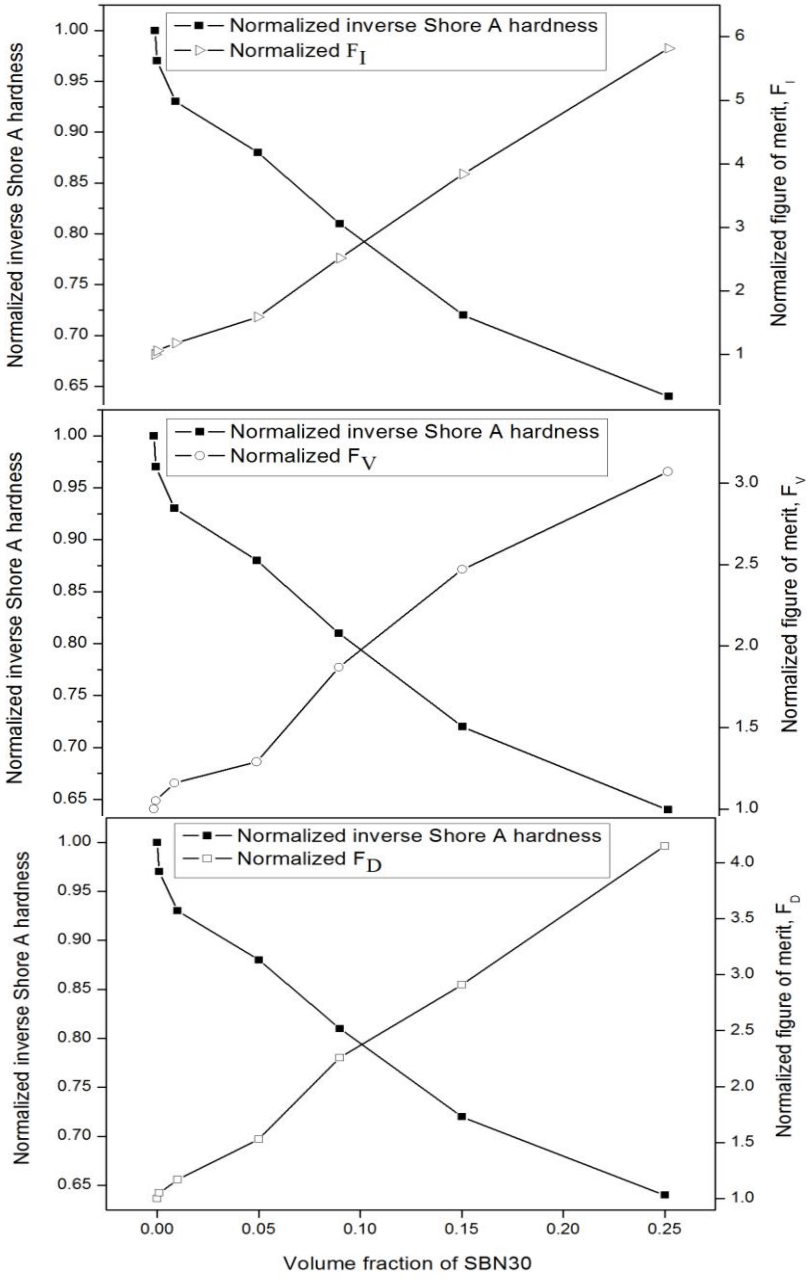

Fig. 5.13 Variations of normalized pyroelectric figures of merit and normalized inverse Shore A hardness for SBN30/PU nanocomposites with volume fractions of SBN30

increases from 0 to 0.25. In the calculations, values of the dielectric constant and dielectric loss at frequency 1 kHz were used.

Variation of each of the pyroelectric figure of merit normalized to the corresponding value for pure PU, plotted against volume fractions of SBN30 nanopowder, are shown in Fig. 5.13. It can be noticed that the figures of merit increase more or less linearly with filler concentration, which is in tune with mean field approximation [35].

5.3.7 Hardness studies

In the present investigations Shore A scale is used to estimate the hardness of SBN30/PU nanocomposites. As shown in Fig. 5.10, for films of SBN30/PU nanocomposites, increase in Shore A hardness from 40 to 62 has been obtained with increasing volume fractions of SBN30 nanopowder from 0 to 0.25. The variation of inverse Shore A hardness, normalized to the value for pure PU, with varying volume fractions of SBN30, is shown in Fig. 5.13. The inverse Shore A hardness curves meet the figure of merit curves nearly at volume fraction 0.10 of SBN30. Thus, this volume fraction can be considered as one with a good balance between high flexibility and high figures of merit. This curve provides guidelines for the selection of the right composite depending upon the envisaged application.

A comparison of the values of figures of merit reported in this work has been done with the corresponding values reported in literature [22]. For the composite with volume fraction 0.10 of SBN30, the values of F_I, F_V and F_D, calculated without division by specific heat capacity for direct comparison, are 190, 19.7 and 667.6 $\mu Cm^{-2}K^{-1}$ respectively, while the corresponding values for TGS (0.43 volume fraction) in P(VDF-TrFE)

composite are 102, 8.3 and 325 respectively, which are the highest reported so far in literature. So these samples hold promise as a high performance detector material.

5.4 Conclusions

SBN30/PU nanocomposites with variable volume fractions could be fabricated as flexible free standing thin films. The pyroelectric, dielectric and thermal properties of various compositions of SBN30/PU nanocomposites are studied. The material figures of merit are determined to evaluate their efficiency for use as pyroelectric detectors. SBN30/PU nanocomposites exhibit high pyroelectric coefficient, low dielectric constant and low thermal conductivity and heat capacity so that they posses comparatively high figures of merit, higher than values reported so far in literature. It is found that the pyroelectric coefficient as well as figures of merit increase by more than 4 times as the volume fraction of SBN30 is increased from 0 to 0.25. In order to understand the changes in flexibility of the polymer with addition of SBN30 nanopowder, Shore hardness measurements are also carried out. The results shown in Fig. 5.13 enable one to identify a composite with right balance between sensitivity and flexibility for the desired sensor applications.

References:

1. Y. Hui and M. Rinaldi, *Proceedings of the 17th international conference on Solid-State Sensors, Actuators and Microsystems (Transducers 2013)*, Spain, 968 (2013)

2. J. Yun and S. S. Lee, *Sensors* **14**, 8057 (2014)

3. J. Yun and M. H. Song, *IEEE Sensors J.* **14**, 1482 (2014)

4. H. Abdollahi, H. Hajghassem and S. Mohajerzadeh, *Microsyst. Technol.* **20**, 387 (2014)

5. K. L. Bing, T. Li, H. H. Hng, F. Boey, T. Zhang and S. Li, "Waste thermal energy harvesting (II): pyroelectric effect and others" in "Waste energy harvesting: Mechanical and thermal energies", Springer-Verlag, Berlin and Heidelberg (2014)

6. J. Li, Y. Li, Z. Zhou, R. Guo and A. Bhalla, *Ceram. Int.* **39**, 8517 (2013)

7. T. Li and X. Long, *J. Am. Ceram. Soc.* , 1 (2014)

8. C. Wu, G. Cai, W. Luo, Q. Peng, X. Sun and W. Zhang, *Sens. Actuators A: Phys.* **199**, 24 (2013)

9. W. C. Gan and W. H. A. Majid, *Smart. Mater. Struct.* **23**, 045026 (2014)

10. Z. Y. Cheng, V. Bharti, T. B. Xu, H. Xu, T. Mai and Q. M. Zhang, *Sens. Actuators A: Phys.* **90**, 138 (2001)

11. J. Wang, C. Wu, R. Liu and S. Li, *Polym. Bull.* **71**, 1263 (2014)

12. J. F. Capsal, J. Galineau, M. Lallart, P. J. Cottinet and D. Guyomar, *Sens. Actuators A: Phys.* **207**, 25 (2014)

13. R. Zevenhoven, "Treatment and disposal of polyurethane wastes: options for recovery and recycling", Helsinki University of Technology, Report TKK-ENY-19 (2004)

14. M. Smirnov and P. S. Gregoire, *Acta. Cryst. A.* **70**, 283 (2014)

15. N. D. Scarisoreanu, M. Dinescu and F. Craciun, "Multifunctional oxides obtained by PLD: applications as ferroelectric and piezoelectric materials. (Lasers in material science", Springer Series in Materials Science (2014)

16. C. J. Huang, K. Li, X. Q. Liu, X. L. Zhu and X. M. Chen, *J. Am. Ceram. Soc.* **97**, 507 (2014)

17. X. Wang, M. Li, C. Zhou, M. Wang and W. Lu, *Ceram. Int.* **40**, 39 (2014)

18. Y. Xu, "Ferroelectric Materials and their Applications", North Holland, Amsterdam (1991)

19. W. Sakamoto, A. Kawase, T. Yogo and S. Hirano, *Jpn. J. Appl. Phys.* **36**, 5930 (1997)

20. M. D. Ewbank, R. R. Neurgaonkar, W. K. Cory and J. Feinberg, *J. Appl. Phys.* **62**, 374 (1987)

21. S. Nishiwaki, J. Takahashi, K. Kodaira and M. Kishi, *Jpn. J. Appl. Phys.* **35**, 5137 (1996)

22. A. K. Batra, M. D. Aggarwal, M. E. Edwards and A. Bhalla, *Ferroelectrics* **366**, 84 (2008)

23. Y. Li, J. Zhao and B. Wang, *Mater. Res. Bull.* **39**, 365 (2004)

24. K. Saha, B. S. Butola and M. Joshi, *J. Appl. Polym. Sci.* **131**, 40824 (2014)

25. R. L. Byer and C. B. Roundy, *Ferroelectrics* **3**, 333 (1972)

26. K. S. Ramadan, D. Sameoto and S. Evoy, *Smart Mater. Struct.* **23**, 033001 (2014)

27. C. P. Menon and J. Philip, *Meas. Sci. Technol.* **11**, 744 (2000)

28. I. H. Rizvi, A. Jain, S. K. Ghosh and P. S. Mukherjee, *Heat Mass Transfer* **49**, 595 (2013)

29. Z. Han, http://drum.lib.umd.edu/bitstream/1903/8654/1/umi-umd-5648.pdf (2008)

30. M. E. Hossain, S. Y. Liu, S. O'Brien and J. Li, *Acta. Mech.* **225**, 1197 (2014)

31. B. L. Sidney and D. K. Das-Gupta, *Ferroelectrics Rev.* **2**, 217 (2000)

32. R. W. Whatmore and R. Watton, "Pyroelectric Materials and Devices" in "Infrared Detectors and Emitters: Materials and Devices", Kluwer Academic Publishers, The Netherlands (2001)

33. P. Guggilla, A. K. Batra, J. R. Currie, M. D. Aggarwal, M. A. Alim and R. B. Lal, *Mater. Lett.* **60**, 1937 (2006)

34. A. Rogalski, *Prog. Quantum Electron*. **27**, 59 (2003)

35. P. Barber, S. Balasubramanian, Y. Anguchami, S. Gong, A. Wibowo, H. Gao, H. J. Ploehn and H. C. Z. Loye, *Materials* **2**, 1697 (2009)

Chapter

6

Pyroelectric Properties of Composites of Microcrystalline TGS and DTGS in Polyurethane for IR/Thermal Detection

Composites comprising of polycrystalline Triglycine Sulphate (TGS) or its deuterated analogue (DTGS) in powder form dispersed in Polyurethane (PU) are synthesized for pyroelectric sensor applications. TGS and DTGS have high pyroelectric coefficients, but are susceptible to humidity. PU also possesses very high pyroelectric coefficient. So composites made of TGS or DTGS dispersed in PU can be expected to have high pyroelectric coefficient as well as immunity to humidity. Composites with varying inclusion volume fractions are prepared and their properties measured.

6.1 Introduction

Triglycine Sulphate (TGS) crystals, with chemical formula $(NH_2CH_2COOH)_3.H_2SO_4$, are promising materials for pyroelectric thermal/ infrared sensor applications due to its high pyroelectric coefficient and relatively low dielectric constant. Pyroelectric sensors based on TGS are

uniformly sensitive to radiation in wavelength range from ultraviolet to far infrared and do not require cooling for operation [1-5]. Pyroelectric IR detectors based on TGS family of crystals provide high figures of merit, but handling difficulties associated with their water solubility, hygroscopic nature and fragility have limited their use to single-element detectors and vidicons, where sensitivity is of prime importance [6-8]. Moreover, the temperature range of operation of these crystals is very limited as the Curie temperature is rather close to room temperature.

In order to improve the ferroelectric and pyroelectric properties and to overcome the drawbacks cited above, many modifications to TGS have been proposed and evaluated for pyroelectric thermal/IR detection applications. One of these is deuteration of TGS [9-12]. Deuteration of TGS by dissolution and re-crystallization in D_2O produces $(ND_2CH_2COOD)_3.D_2SO_4$, which is commonly referred to as partially deuterated TGS (DTGS). In fully deuterated TGS (FDTGS) with chemical formula $(ND_2CD_2COOD)_3.D_2SO_4$, the H atoms in the CH_2 group will also be replaced by deuterium [13]. Use of DTGS crystals allows to extend temperature range of sensing by 5-12^oC due to their higher Curie temperature, depending on the deuteration level [14, 15]. This increase in transition temperature on deuteration occurs because the hydrogen bonding in these materials play a dominant role in the ferroelectric transition mechanism [16]. From literature survey it can be inferred that deuteration of TGS provides a marked improvement in pyroelectric figures of merit of the material. Problems of humidity absorption, fragility etc. exists for DTGS as well. In order to overcome these problems we tried to disperse these crystals in powder form in an electro-active polymer matrix and

investigate their pyroelectric and related properties.

By dispersing these crystal powders in polymer matrix, their direct contact with air can be avoided and thus the problem of humidity absorption could be solved. Moreover, polymers can be processed easily into mechanically flexible and robust components. It is very difficult to achieve high enough pyroelectric/piezoelectric coefficients for composites formed by combining an ordinary polymer with pyroelectric/piezoelectric crystals. But there are many polymers that possess varying degrees of electro-activity. PVDF (Poly(vinylidine fluoride)) and its co-polymers like P(VDF-TrFE) (Poly(vinylidine flouride-Triflouro ethylene)), P(VDF-HFP) (Polyvinylidine difluoride-Hexafluoro propylene), PU (Polyurethane), etc. are a few examples for electro-active polymers. Generally they have low pyroelectric/piezoelectric properties compared to crystals or ceramic materials possessing these properties. At the same time crystals as well as ceramics are very brittle, which is not often desirable for sensor fabrication. Moreover, TGS and DTGS crystals, which possess high pyroelectric coefficients, suffer from humidity absorption. So a good possible solution for the above problems is to combine these crystals with electro-active polymers to form composites. An important attribute of polymers is the ability to modify their inherent physical properties with addition of suitable fillers while retaining their many desirable mechanical properties.

In this work we used the thermoplastic elastomer Polyurethane (PU), an electro-active polymer (EAP), as the matrix for fabricating composites with polycrystalline powders of TGS or DTGS as inclusions. Polyurethanes are unique polymers with a wide range of interesting mechanical, physical and chemical properties. They are one of the most

versatile classes of materials today and their demand as high performance industrial materials continue to grow. PU has a pyroelectric coefficient which is at least 2 to 4 times higher than that of PVDF, another popular electro-active polymer, and has a very low dielectric constant compared to PVDF [17-20]. PU is also famous for its toughness. This toughness comes from high flexibility and elongation of polyurethane chains. The PU polymer elastomer selected for this work is non-piezoelectric and so does not generate piezoelectric noise by picking up vibrations from the environment. Moreover, the pliability of PU provides a cushion effect, which suppresses piezoelectric vibrations from TGS or DTGS crystallites in the composite. Vibration noise is undesirable for any piezoelectric material used for pyroelectric sensor applications. In this regard, the present polymer elastomer-ferroelectric crystals composites, having piezoelectric property, form an alternative pyroelectric sensor material with higher signal to noise ratio. So by dispersing TGS and DTGS in PU matrix the drawbacks of these crystals in their pure form could be overcome and their composites in polymer possess advantages such as flexibility, toughness and immunity to humidity. These desirable properties qualify them for applications in hostile environments.

Pyroelectric thermal/infrared sensors are transducers for radiant energy. The detected energy in the form of temperature rise is transformed into electrical pulses proportional to the temperature difference between the surfaces of the detector. The un-cooled pyroelectric infrared detectors are in great demand for many applications and a few of them are: atmospheric temperature measurement, earth position sensing, infrared detection, fire alarm operation, pollution detection, remote sensing, biomedical imaging

etc [17, 21-25]. One recent and important application is their use is in waste energy harvesting for micro-electric generators [26]. In this chapter we discuss the properties of TGS/PU and DTGS/PU composites for pyroelectric infrared detection applications. A comparison of the pyroelectric properties of these two composites has been done and the experimental results are compared with theoretical predictions. Their properties are also compared with those of a few other ceramic-polymer composites possessing pyroelectric properties.

6.2 Experimental techniques

The sample preparation methods and various experimental techniques adopted for the study of composites of TGS and DTGS microcrystalline powders in polyurethane polymer matrix are given below.

6.2.1 Sample preparation

The sample preparation includes synthesis of small crystals of TGS and DTGS, PU matrix preparation and the preparation of their composites. The synthesis method adopted for TGS and DTGS crystals was crystal growth by conventional slow evaporation from solution technique. Both the crystals were grown at room temperature.

6.2.1.1 Synthesis of TGS and DTGS microcrystalline powders

The starting materials used were Glycine (NH_2CH_2COOH, Sigma-Aldrich) and Sulphuric acid (H_2SO_4, Merck). For the preparation, Glycine and Sulphuric acid were taken in a molar ratio 3:1, dissolved in double distilled water. It was necessary to increase the purity to a reputable level by successive re-crystallization process and maximum attention was paid to

secure high purity for TGS during synthesis. The partially deuterated TGS (DTGS) crystals were synthesised by re-crystallization of pure TGS crystals in 99.9% heavy water (D_2O, Aldrich) more than 6 times. Both TGS and DTGS crystalline samples were made into fine powders using an agate mortar.

6.2.1.2 Preparation of PU polymer solution

The polymer used in the present study was commercially available Polyurethane (PU) transparent beads (Product code: P 2059) supplied by Otto Chemie Pvt. Ltd. 15 (w/v) % polyurethane polymer solutions were prepared for both cases, by dissolving required amount of polymer granules in a suitable solvent (N,N-Dimethyl formamide (DMF) supplied by S D Fine Chem. Ltd. The polymer solutions were prepared by continuous stirring of PU granules in DMF at 75^{o}C.

6.2.1.3 Synthesis of TGS/PU and DTGS/PU composites

Composite samples of TGS/PU and DTGS/PU were prepared in the form of free standing films by solvent cast method [27]. For this the polymer matrix solutions were prepared as described above and then the microcrystalline inclusions were added to it in the form of powders. The mixtures were then stirred well. At most care was taken to avoid agglomeration of the inclusion crystalline powders. These liquid composites were then poured into open containers of uniform depth of 1mm for the solvent to evaporate completely. Finally, polymer composites were peeled off from the containers in the form of films. For both cases we have prepared films of TGS and DTGS with volume fractions 0.001, 0.01, 0.05, 0.09, 0.15 and 0.25, including pure PU films for comparison. All the

free standing films prepared were having thicknesses ranging from 35µm to 85µm for both set of composites.

6.2.2 Sample characterization

All the prepared film samples and TGS/DTGS crystals were characterised using standard characterisation techniques such as powder XRD, DSC and SEM. The results are given in section 6.3.1.

6.2.2.1 Dielectric measurements

For dielectric and pyroelectric measurements, small pieces of dry films having area 1 cm^2 were coated with silver paste on both sides. The dielectric constant and dielectric loss of the samples were measured in the capacitance method using an Impedance analyzer (Hioki, Model: IM3570) in the frequency range 100Hz-5MHz. The measurement details are given in section 2.7 of chapter 2.

6.2.2.2 Pyroelectric measurements

In order to enhance the pyroelectric coefficients, both sets of samples were poled using corona poling technique. Samples in circular shape having diameter 4cm were uniformly poled by a single corona point under a high DC electric field of 8 MV/m at 75^oC. Here all the samples were kept at the same temperature under the electric field for 40 minutes and then the temperature source was switched off maintaining the field while cooling the samples to room temperature. The pyroelectric coefficients of the prepared samples were determined by the Byer and Roundy method, by keeping the heating/cooling rate at 2^oC/min [28].

6.2.2.3 Thermal studies

The important thermal properties that we must consider for pyroelectric thermal/IR detectors, thermal conductivity and specific heat capacity, were measured following a photopyroelectric (PPE) technique explained in chapter 2 [29]. Here the sample was in good thermal contact with the PVDF detector (coated with nickel-chromium alloy) of thickness 28 μm having pyroelectric coefficient 30 $\mu Cm^{-2}K^{-1}$. The modulation frequency of light was kept above 60 Hz to ensure that the detector, the sample and the backing were thermally thick during measurements. The output signal was measured with a dual-phase lock-in amplifier (Stanford Research Systems, Model: SR830). Measurement of amplitude and phase of the output signal enabled us to determine the thermal conductivity (k) and specific heat capacity (C) of the sample were obtained.

6.2.2.4 Hardness measurements

PU used in the study fall under the category of thermoplastic polymers. Filler materials in the form of powders or fibbers can be added to thermoplastics to provide improvement of their specific properties like strength, stiffness, lubricity etc. Hardness of polymers (rubbers/plastics) is usually measured by the Shore scales. As mentioned in the previous chapters Shore hardness is an empirical measurement used to test a polymer's resistance to indentation or penetration under a defined force. Two letters are used to categorize the type of PU: 'A' denotes a flexible type of PU while 'D' refers to more rigid variety. The Shore A hardness values for the samples, including pure PU, were measured in our study. All measurements reported in this work have been carried out at normal environment (room temperature - 28^{o}C and relative humidity 70%).

6.3 Results and discussions

The results of the studies carried out on the two sets of samples, TGS/PU and DTGS/PU are revealed in this section. The thermal conductivity, specific heat capacity and dielectric constants were compared with theoretically calculated values and are given. Theoretical values were calculated using the effective medium theory [30-32] and the corresponding expressions are given in chapter 3.

6.3.1 Material identification, structure and morphology

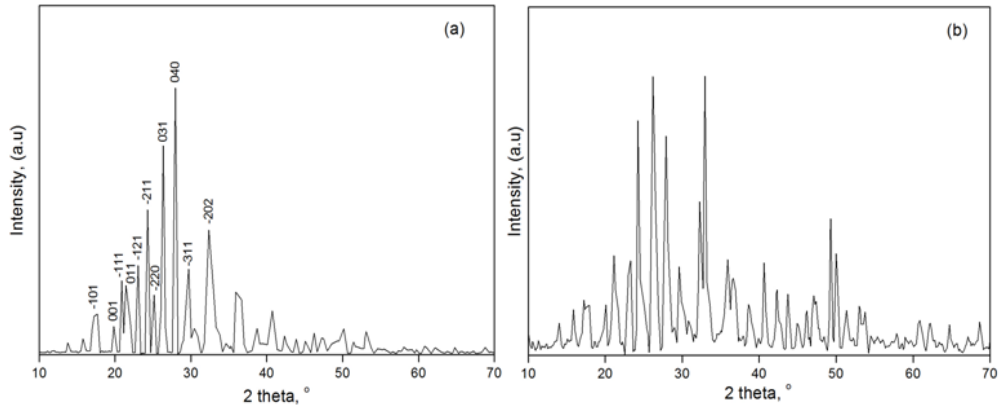

Fig. 6.1 XRD patterns of (a) TGS and (b) DTGS microcrystalline powders (step size: 0.020^{o}, step time: 31.2 s)

TGS/PU and DTGS/PU composite films were characterized following standard methods like powder X-ray Diffraction and Differential Scanning Calorimetry. Powder XRD patterns showed peaks corresponding to TGS/DTGS crystals (Fig. 6.1). From DSC analysis it was found that the transition temperature of the prepared DTGS crystal has increased to 55.7^{o}C, whereas that of pure TGS crystal was 48.65^{o}C. The SEM images of

TGS/PU and DTGS/PU films shown in Fig. 6.2 provide direct evidence for the presence of TGS or DTGS microcrystals in the polymer matrix. From SEM images it was noticed that at 0.25 volume fractions of TGS or DTGS the inclusions started getting agglomerated. In order to avoid this problem we limited volume fractions of TGS and DTGS to 0.25.

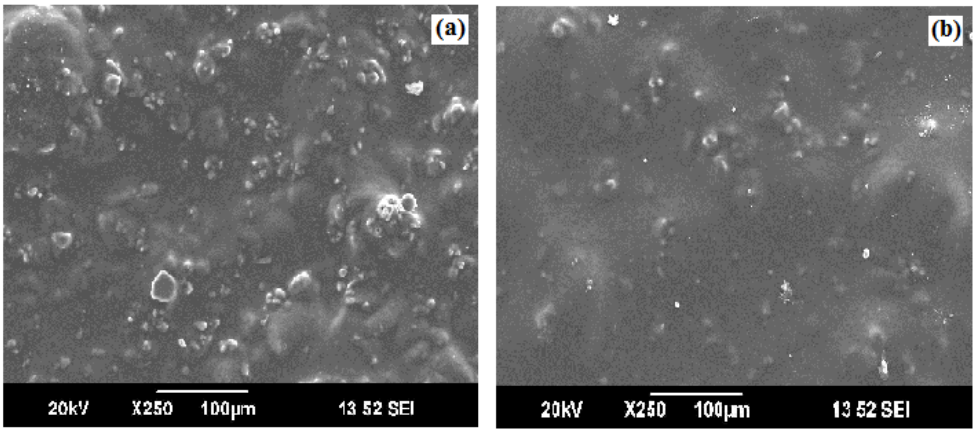

Fig. 6.2 SEM images for (a) TGS/PU and (b) DTGS/PU composites, with inclusion volume fraction 0.25

6.3.2 Sample density

The mass densities of the samples were measured by direct weighing method. The same were calculated theoretically from the densities of TGS and DTGS and PU following the rule of mixtures. The expression is given in chapter 3. The theoretical and experimental densities of the composites with varying volume fractions of TGS and DTGS are shown in Fig. 6.3. The densities increase with filler concentrations, and the experimental densities are lower than the theoretical densities with the increase of filler concentrations due to the possible presence of voids and defects in the prepared composite films at higher filler concentrations. As

the filler volume fractions increased from 0 to 0.25, all the prepared samples attained densities in the range 94 - 88% for TGS/PU and 95 - 90% for DTGS/PU composites.

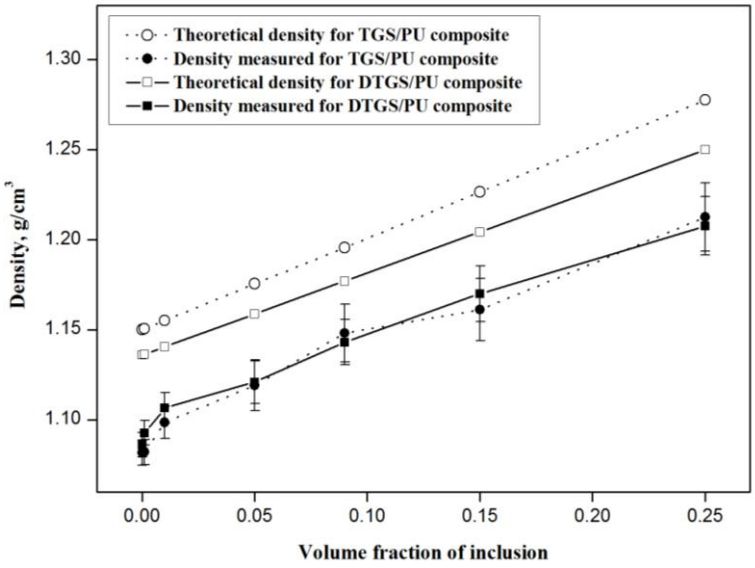

Fig. 6.3 Variations of theoretical and experimental densities of TGS/PU and DTGS/PU composites with varying volume fractions of inclusions

6.3.3 Dielectric properties

Variations of dielectric constant and dielectric loss with frequency for samples with different concentrations of TGS and DTGS in PU are shown in figures 6.4, 6.5, 6.6 and 6.7.

It can be seen that at all frequencies both dielectric constant and loss increase as TGS and DTGS contents in PU matrix increase. For TGS/PU the dielectric constant increases from 6.75 to 10.46 as the volume fraction of TGS increases from 0 to 0.25 at 1 kHz, and for DTGS/PU composites the corresponding variation is from 6.70 to 9.52. The increase in dielectric constant with increase in filler content can be attributed to enhancement

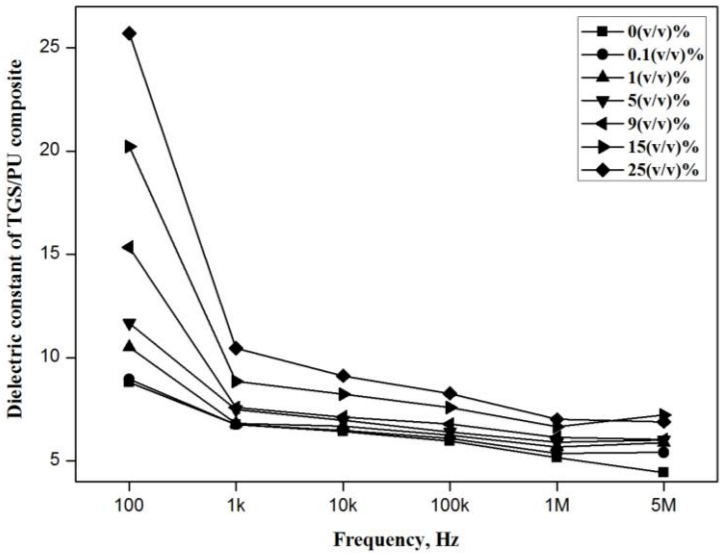

Fig. 6.4 Variations of dielectric constant with frequency for different TGS/PU composites

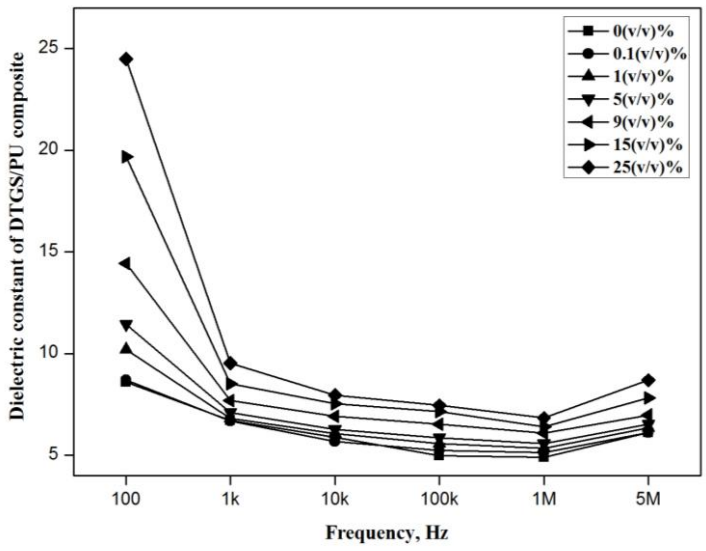

Fig. 6.5 Variations of dielectric constant with frequency for different DTGS/PU composites

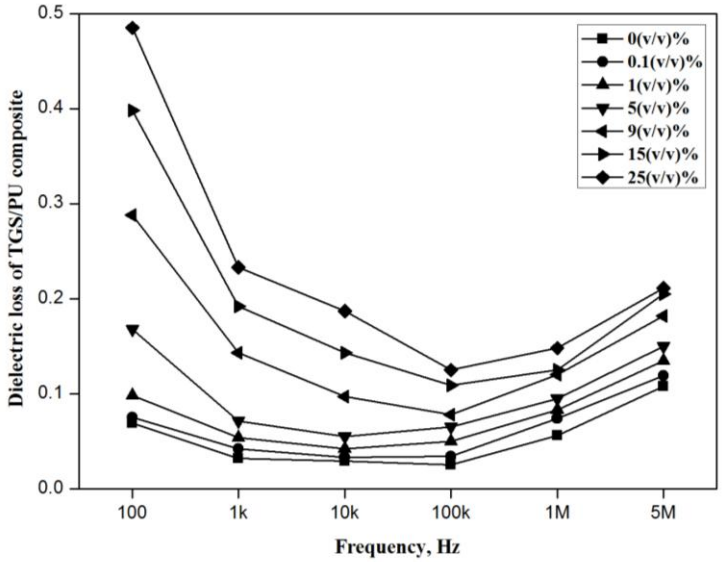

Fig. 6.6 Variations of dielectric loss with frequency for different TGS/PU composites

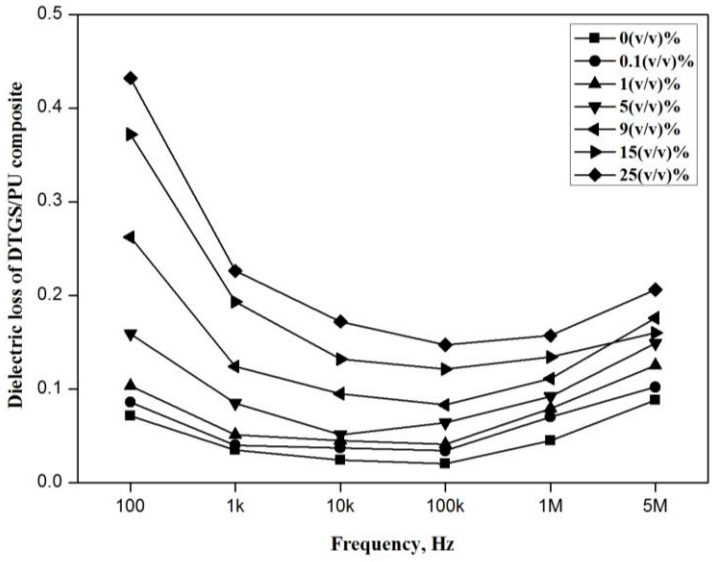

Fig. 6.7 Variations of dielectric loss with frequency for different DTGS/PU composites

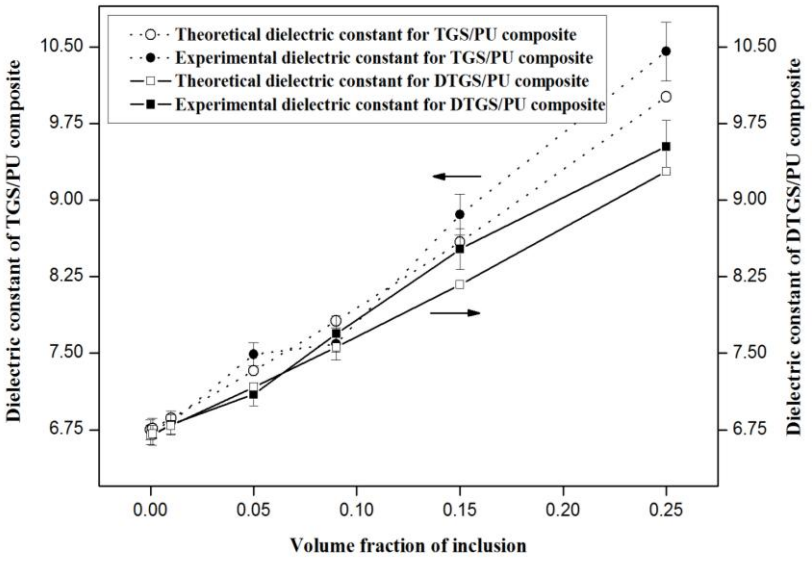

Fig. 6.8 Variations of theoretical and experimental dielectric constants at 1 kHz for TGS/PU and DTGS/PU composites with varying volume fractions of inclusions

in internal polarization of the samples. In the case of dielectric loss the corresponding variations for TGS/PU are from 0.03 to 0.23 and for DTGS/PU composites loss varies from 0.04 to 0.23. For both the composites, dielectric constant and loss decrease as frequency increases. So from present measurements we can say that there is a slight decrease for dielectric constant for DTGS/PU composites compared to TGS/PU composites at higher filler concentrations, and that there exists no appreciable effect for deuteration on the dielectric loss. A comparison with corresponding theoretical values for dielectric constants for TGS/PU and DTGS/PU composites are shown in Fig. 6.8. From this figure it is evident that the experimental results agree fairly well with theoretical values estimated from mean field theory.

6.3.4 Pyroelectric coefficients

Internal polarization of the composites increases due to contributions from inclusion dipoles. Enhancements in pyroelectric coefficients are obtained for the composite films after poling. Pyroelectric coefficients for all the samples were measured and verified during heating as well as cooling cycles (figures 6.9 and 6.10).

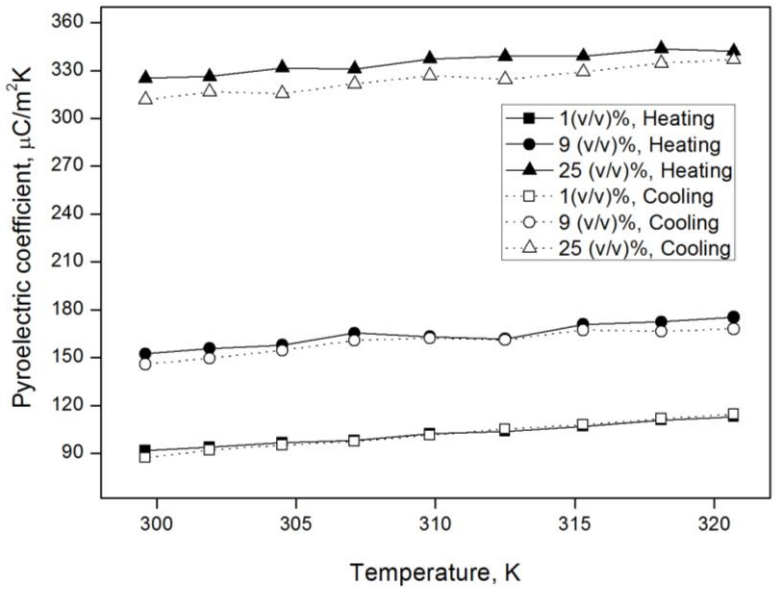

Fig. 6.9 Variation of pyroelectric coefficients of TGS/PU composites with temperature during heating and cooling

During heating, in addition to the pyroelectric current, a small current due to release of trapped space charges will be present. But during cooling the presence of depolarization currents can be eliminated. Fig. 6.11 shows the variation of average pyroelectric coefficients for varying volume fractions of TGS and DTGS in PU matrix.

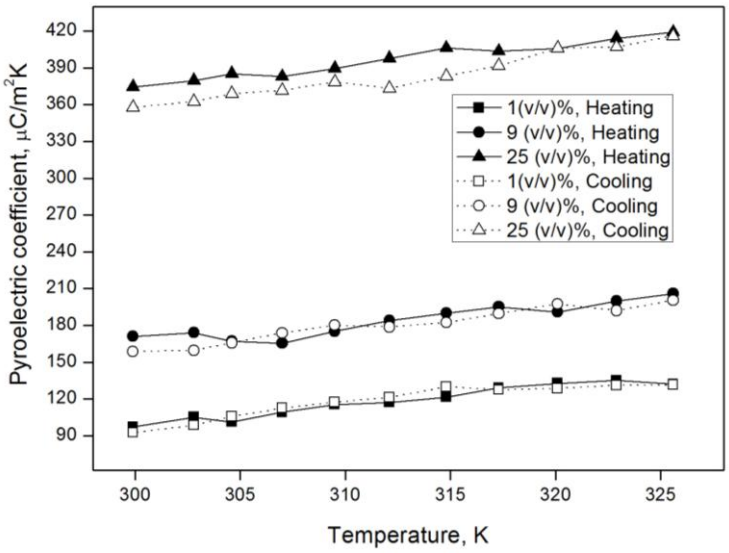

Fig. 6.10 Variation of pyroelectric coefficients of DTGS/PU composites with temperature during heating and cooling

It is found that the average values of pyroelectric coefficients increase from 80 $\mu Cm^{-2}K^{-1}$ to 318 $\mu Cm^{-2}K^{-1}$ as the TGS concentration in the PU matrix increase from volume fraction 0 to 0.25 and the corresponding variation for DTGS/PU composites is from 82 $\mu Cm^{-2}K^{-1}$ to 365 $\mu Cm^{-2}K^{-1}$. At higher volume fractions of inclusions, the pyroelectric coefficient increases because of the presence of higher proportions of pyroelectric materials. But when compared to the pyroelectric coefficient for volume fraction 0.25 of TGS/PU composite, the value for DTGS/PU composite is only 365 $\mu Cm^{-2}K^{-1}$. This value is lower than expected. The reason may be that in the case of ferroelectric crystals that are pyroelectric, there is a possibility for a single domain crystal to become multi-domain one during application, leading to reduction of internal polarization in the sample [33].

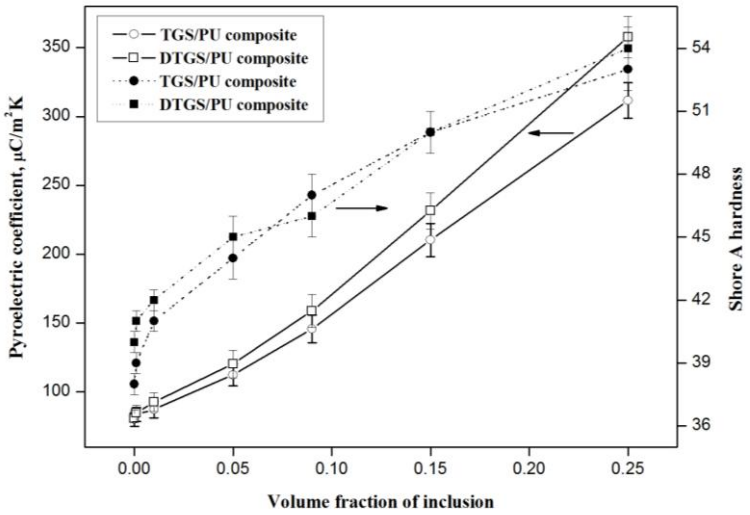

Fig. 6.11 Variations of average pyroelectric coefficients and Shore A hardness of TGS/PU and DTGS/PU composites with volume fractions of inclusion

6.3.5 Thermal analysis

Specific heat capacity and thermal conductivity are important parameters to be considered for a pyroelectric sensor. A good pyroelectric sensor is required to possess low specific heat capacity and low thermal conductivity. It is found that for TGS/PU composites the specific heat capacity, obtained from photopyroelectric measurements, decreases from 1652 $Jkg^{-1}K^{-1}$ to 1584 $Jkg^{-1}K^{-1}$with increase in filler concentration, whereas the corresponding thermal conductivity increases from 0.22 $Wm^{-1}K^{-1}$ to 0.66 $Wm^{-1}K^{-1}$. For DTGS/PU composites the specific heat capacity decreases from 1645 $Jkg^{-1}K^{-1}$ to 1561 $Jkg^{-1}K^{-1}$ with increase in filler concentration, while thermal conductivity increases from 0.26 $Wm^{-1}K^{-1}$ to 0.90 $Wm^{-1}K^{-1}$. The variations of specific heat capacity and thermal conductivity with filler concentration for both these composites, including theoretical predictions, are shown in figures 6.12 and 6.13.

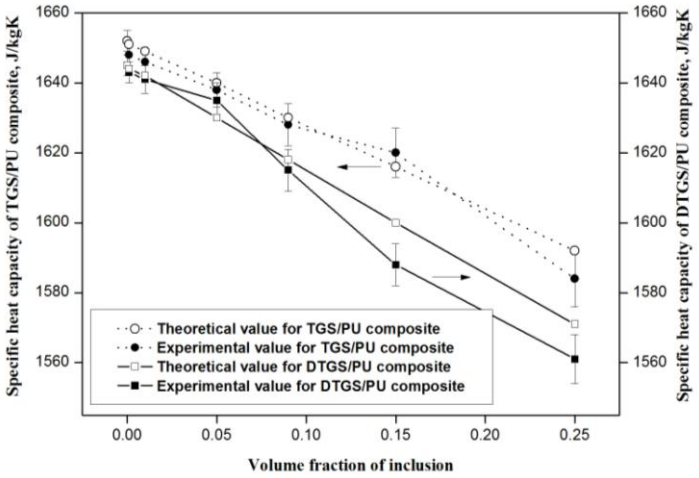

Fig. 6.12 Variations of theoretical and experimental specific heat capacities of TGS/PU and DTGS/PU composites with volume fractions of inclusions

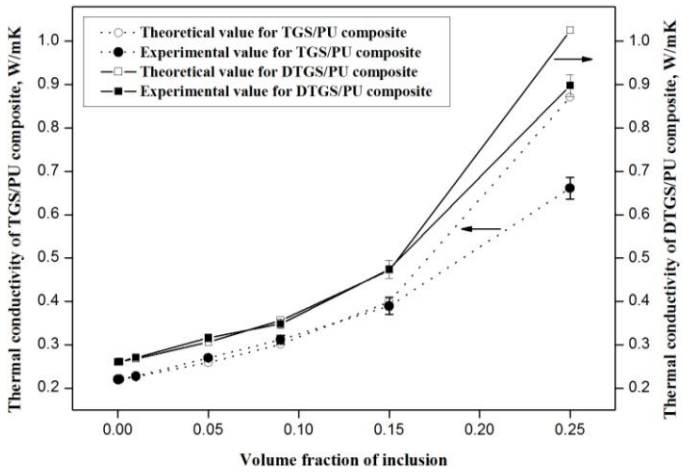

Fig. 6.13 Variations of theoretical and experimental thermal conductivities of TGS/PU and DTGS/PU composites with volume fractions of inclusions

Both these parameters for both sets of composites are in good agreement with theoretical values, except at high filler concentrations. It is

found that, in general, the deviations between theoretical and experimental values of thermal conductivity and heat capacity increase as the filler concentration increases. Moreover, deuteration gives rise to significant decrease in specific heat capacity and increase in thermal conductivity for these composites.

6.3.6 Pyroelectric figures of merit

The most important properties for thermal/infrared sensor materials are their figures of merit. In order to improve the figures-of-merit the sensor materials should possess low dielectric constant and loss, high pyroelectric coefficient, low specific heat capacity and thermal conductivity. The important figures-of-merit for pyroelectric infrared detector materials F_I, F_V and F_D, the figures-of-merit for high current sensitivity, high voltage responsivity, high detectivity respectively have been calculated for both TGS/PU and DTGS/PU composites [34-37]. For TGS/PU composites F_I varies from 48×10^{-3} μCm/J to 200×10^{-3} μCm/J, F_V varies from 7.17×10^{-3} μCm/J to 19.21×10^{-3} μCm/J and F_D varies from 270×10^{-3} μCm/J to 415×10^{-3} μCm/J. The corresponding variations for DTGS/PU composites are 49×10^{-3} μCm/J to 233×10^{-3} μCm/J, 7.43×10^{-3} μCm/J to 24.56×10^{-3} μCm/J and 266×10^{-3} μCm/J to 491×10^{-3} μCm/J for F_I, F_V and F_D respectively. It is found that the figures-of-merit increase with increase of filler concentration. Variations of these figures of merit normalized to the corresponding ones for pure PU, plotted against the volume fractions of TGS and DTGS crystal powders, are shown in Fig. 6.14. It can be seen that the figure of merit increases more or less linearly with filler concentration, which are in tune with mean field approximation [38].

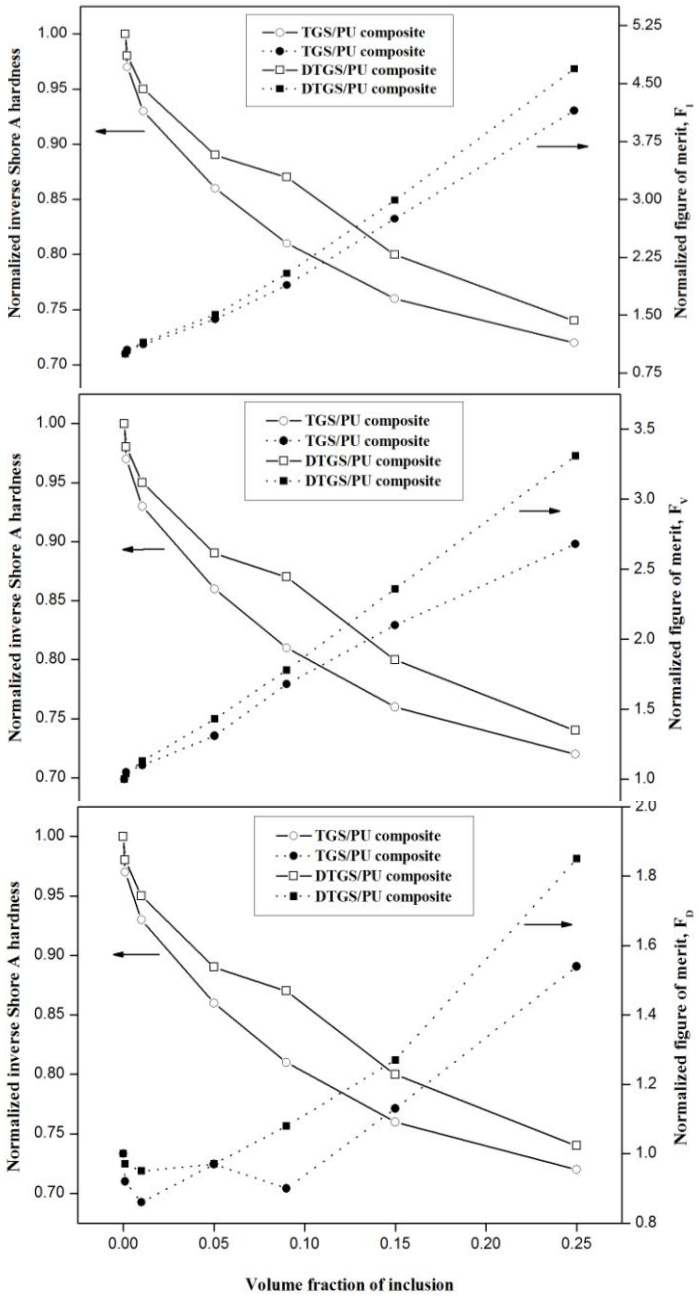

Fig. 6.14 Variations of normalized pyroelectric figures of merit and normalized inverse Shore A hardness for TGS/PU and DTGS/PU composites with volume fractions of inclusion

6.3.7 Hardness studies

For TGS/PU as well as DTGS/PU composite films, Shore A hardness values increase with increasing volume fractions of inclusions (Fig. 6.11). The variation of inverse Shore A hardness with varying volume fractions of TGS and DTGS are also shown in Fig. 6.14 for a direct comparison of figures of merit with hardness. Since Shore hardness scales inversely with flexibility of the polymer, it is clear that the samples get harder (or flexibility decreases) as the inclusion concentration increases.

For TGS/PU composites, the inverse Shore hardness curves meet the figure of merit curves for high current sensitivity (F_I), high voltage responsivity (F_V) and high detectivity (F_D) at volume fractions 0.11, 0.11 and 0.14 respectively. At these points the TGS/PU composite possesses good flexibility as well as high figures of merit. For DTGS/PU the respective volume fractions are 0.13, 0.12 and 0.14. These data provide guidelines for the selection of a suitable composite of this class for sensor applications.

6.3.8 Comparison of pyroelectric properties with other similar detector materials

In order to compare the pyroelectric properties of present TGS/PU and DTGS/PU composites with those of comparable composites reported in literature, we tabulate the relevant properties of a few composites in Table 6.1. It can be seen that the present composites with TGS or DTGS volume fraction 0.25 have higher figures of merit than other similar or comparable composites reported in literature. So these can be considered as good

choice for the design and fabrication of thermal and infrared sensors where the application demands materials that are immune to humidity.

Table 6.1 Comparison of figures of merit for thermal/IR detection for TGS/PU and DTGS/PU composites with those reported on similar or comparable composites

Material	Dielectric constant	Pyroelectric figures of merit			Reference
		F_I ($\mu C/m^2K$)	F_V ($\mu C/m^2K$)	F_D ($\mu C/m^2K$)	
PU (Room temperature)	6.7	49*	7.43*	266*	(Present work)
TGS (Room temperature)	20 - 100	160 - 450	5 – 11.4	40 – 121	5
DTGS (at 25^{o}C)	18 - 22.5	250 – 700	14	-	5
$TGS_{(0.25\ vol.\ fraction)}$/PU (Room temperature)	10.45	318*	30.41*	658*	(Present work)
$DTGS_{(0.25\ vol.\ fraction)}$/PU (Room temperature)	9.52	365*	38.32*	767*	(Present work)
$DTGS_{(40\ wt\%)}$/PVDF (at 36^{o}C)	14.4	499	33.5	409	39
$PT_{(0.54\ vol.\ fraction)}$/$P(VDF\text{-}TrFE)_{70/30}$	55	68.2	1.24	49.4	40
$TGS_{(0.43\ vol.\ fraction)}$/P(VDF-TrFE)	12.27	102	8.31	325	41
$DTGS_{(5\ wt\%)}$/PVDF	15.9	38.3	2.4	32.1	42
PCLT/P(VDF-TrFE)	15	56.5	3.7	113.2	43
$PCaT_{(0.1\ vol.\ fraction)}$ /P(VDF/TrFE)	18	40	2.2	74	44
$PCaT_{(0.50\ vol.\ fraction)}$/PEKK	26	17	**0.68**	31.5	45
$PZT_{(0.20\ vol.\ fraction)}$ /P(VDF-TrFE)	29	92	3.17	498.94	46

* values are calculated using the same equations for figures of merit, but without division by specific heat capacity values for direct comparison with other reported results

6.4 Conclusions

Efforts have been made to prepare composites of TGS and its deuterated analogue in polyurethane matrix and investigate their pyroelectric properties so as to evaluate their use as thermal/infrared detectors. Experimental results on dielectric constant, thermal conductivity and specific heat capacity obtained for various inclusion volume fractions for both TGS/PU and DTGS/PU composites are compared with theoretical predictions and the values are found to be in good agreement. The pyroelectric figures of merit for IR detection for both sets of composites are compared with those of comparable composites reported in literature for the first time. In general, deuteration leads to decrease in dielectric constant and specific heat, but increase in thermal conductivity. The pyroelectric coefficient and figures of merit get enhanced significantly with deuteration as well as inclusion volume fraction. Comparison with similar composites shows that these samples have high values for figures of merit, indicating their potential use as thermal/infrared detectors that are immune to humidity.

References:

1. A. K. Batra, J. R. Currie, S. K. Aggarwal, M. D. Aggarwal and R. B. Lal, *Proc. SPIE* **5209**, 133 (2003)

2. S. N. Begum, U. Sankar, T. C. Thanu and P. Selvarajan, *OPTIK* **125**, 1493 (2004)

3. X. Zhao, X. Wu, L. Liu, H. Luo, N. Neumann and P. Yu, *Phys. Status Solidi A* **208**, 1061 (2011)

4. N. Nakatani, *Ferroelectrics* **413**, 238 (2011)

5. M. D. Aggarwal, A. K. Batra, P. Guggilla, M. E. Edwards, B. G. Penn and J. R. Currie (Jr.), *NASA/TM*, 216373 (2010)

6. R. Jimenez and B. Jimenez, *Springer Series in Materials Science* **140**, 573 (2011)

7. C. S. Fang, M. Wang and H. S. Zhuo, *Ferroelectrics* **91**, 373 (1989)

8. R. Capan, *BAÜ FBE Dergisi* **12**, 75 (2010)

9. N. Sinha, N. Goel, B. K. Singh, M. K. Gupta and B. Kumar, *J. Solid State Chem.* **190**, 180 (2012)

10. C. J. Raj, S. Kundu and K. B. R. Varma, *Appl. Phys. A* **105**, 1025 (2011)

11. C. Rai, K. Sreenivas and S. M. Dharmaprakash, *J. Cryst. Growth* **312**, 273 (2010)

12. J. M. Hudspeth, and D. J. Goossens, *J. Cryst. Growth* **338**, 177 (2012)

13. J. M. Hudspeth, D. J. Goossens, M. J. Gutmann and A. J. Studer, *Cryst. Res. Technol*. **48**, 169 (2013)

14. C. Arago, L. G. Menendez and and J. A. Gonzalo, *Ferroelectrics* **462**, 47 (2014)

15. J. M. Hudspeth, D. J. Goossens, T. R. Welberry and M. J. Gutmann, *J. Mater. Sci*. **48**, 6605 (2013)

16. G. M. Loiacono and G. Kostecky, *Thermochem. Acta* **45**, 133 (1981)

17. M. S. Jayalakshmy and J. Philip, *Sens. Actuators A: Phys.* **206**, 121 (2014)

18. W. K. Sakamoto, S. Kagesawa, D. H. Kanda and D. K. Das-Gupta, *J. Mater. Sci.* **33**, 3325 (1998)

19. P. Frubing, H. Kruger, H. Goering and R. Gerhard-Multhaupt, *Polymer* **43**, 2787 (2002)

20. K. S. Lam, Y. W. Wong, L. S. Tai, Y. M. Poon and F. G. Shin, *J. Appl. Phys.* **96**, 3896 (2004)

21. J. Yun and S. S. Lee, *Sensors* **14**, 8057 (2014)

22. M. Steffanson and I. W. Rangelow, *Opto-Electron. Rev.* 22, 1 (**2014)**

23. J. Xiong, F. Li, N. Zhao and N. Jiang, *Sensors* **14**, 7209 (2014)

24. L. Li, X. Zhao, X. Li, B. Ren, Q. Xu, Z. Liang, W. Di, L. Yang, H. Luo, X. Shao, J. Fang, N. Neumann and J. Jiao, *Adv. Mater.* **26**, 2580 (2014)

25. G. Siebke, P. Holik, S. Schmitz, H. Schmitz, M. Lacher and S. Steltenkamp, *Bioinspir. Biomim.* **9**, 036012 (2014)

26. A. Potnuru and Y. Tadesse, *Integr. Ferroelectr.* **150**, 23 (2014)

27. M. D. Sanchez-Garcia, E. Gimenez and J. M. Lagaron, *Carbohydr. Polym*. **71**, 235 (2008)

28. R. L. Byer and C. B. Roundy, *Ferroelectrics* **3**, 333 (1972)

29. C. P. Menon and J. Philip, *Meas. Sci. Technol.* **11**, 1744 (2000)

30. I. H. Rizvi, A. Jain, S. K. Ghosh and P. S. Mukherjee, *Heat Mass Transfer.* **49**, 595 (2013)

31. Z. Han, "Nanofluids with enhanced thermal transport properties", Ph.D. Thesis, University of Maryland, College Park, Maryland (2008)

32. M. E. Hossain, S. Y. Liu, S. O'Brien and J. Li, *Acta Mech.* **225**, 1197 (2014)

33. A. Nautiyal and T. C. Upadhyay, *Int. J. Chem. Sci. Appl.* **4**, 29 (2013)

34. B. L. Sidney and D. K. Das-Gupta, *Ferroelectr. Rev.* **2**, 217 (2000)

35. R. W. Whatmore and R. Watton, "Pyroelectric Materials and Devices" in "Infrared Detectors and Emitters: Materials and Devices", P. Capper, C. T. Elliott, (*Eds.*) Kluwer Academic Publishers Group, The Netherlands (2001)

36. A. Rogalski, *Prog. Quant. Electron*. **27**, 59 (2003)

37. P. Guggilla, A. K. Batra, J. R. Currie, M. D. Aggarwal, M. A. Alim and R. B. Lal, *Mater. Lett*. **60**, 1937 (2006)

38. P. Barber, S. Balasubramanian, Y. Anguchami, S. Gong, A. Wibowo, H. Gao, H. J. Ploehn and H. C. Z. Loye, *Materials* **2**, 1697 (2009)

39. A. K. Batra, M. Simmons, P. Guggilla, M. D. Aggarwal and R. B. Lal, *Integr. Ferroelectr.* **63**, 161 (2004)

40. H. L. W. Chan, W. K. Chan, Y. Zhang and C. L. Choy, *IEEE T. Dielect. El. In.* **5**, 505 (1998)

41. K. Sreenivas, T. S. Rao, A. Dhar and A. Mansingh, *Bull. Mater. Sci*. **6**, 105 (1984)

42. F. Changshui, W. Qingwu and Z. Hongsheng, *J. Korean Phys. Soc.* **32**, S1843 (1998)

43. Q. Q. Zhang, B. Ploss, H. L. W. Chan and C. L. Choi, *Sens. Actuators A: Phys.* **86**, 216 (2000)

44. Q. Q. Zhang, H. L. W. Chan, B. Ploss, Q. F. Zhou and C. L. Choy, *J. Non-Cryst. Solids* **254**, 118 (1999)

45. A. Pelaiz-Barranco, O. P. Martinez and D. K. Das-Gupta, *J. Appl. Phys.* **92**, 1494 (2002)

46. M. Dietze, J. Krause, C. H. Solterbeck and M. Es-Souni, *J. Appl. Phys.* **101**, 054113 (2007)

Chapter

7

Conclusions and Scope for Future Work

This concluding chapter gives a brief overview of the complete investigations carried out on the materials and their properties relevant for pyroelectric thermal/infrared detection applications, including a summary of the salient features of the research work done. Also the chapter ends with some ideas on the scope for further investigations in this field.

7.1 Conclusions

In all the chapters of the thesis, results are concluded on the basis of a series of laboratory experiments performed for analysing the pyroelectric properties, dielectric properties, Shore hardness, densities and thermal properties such as thermal conductivity and specific heat capacity. This chapter summarizes the conclusions drawn in the entire investigation.

In order to prepare polymer/ceramic composites, the polymers selected were electro-active polymers such as Poly(vinylidene fluoride) (PVDF) and Polyurethane (PU). The nanoparticle ceramic and microcrystalline inclusions chosen were $LiTaO_3$, $LiNbO_3$ and SBN30 in the

form of nanopowders and TGS and DTGS in the form of microcrystalline powders. For our studies all the samples were prepared in the form of flexible free standing films. Nanocomposites of $LiTaO_3$/PVDF, $LiNbO_3$/PVDF and $Sr_{0.30}Ba_{0.70}Nb_2O_6$/PU and microcrystalline composites of TGS/PU and DTGS/PU, with different volume fractions of inclusions were prepared and their properties studied.

Pyroelectric studies of the pre-poled samples were carried out by a quasi static direct method. The results have shown the dependence of PVDF and PU to an applied high DC electric field. Experiments for thermal studies were conducted using a photopyroelectric (PPE) set up. By the addition of ceramic nano/microcrystalline particles, the thermal conductivity indicated an increase and the specific heat capacity a decrease. Dielectric properties were studied using an Impedance analyser. The thermal and dielectric measurements were carried out at room temperature. Experimental values are compared with theoretical predictions and found that they are in good agreement.

All the three figures of merit for pyroelectric thermal/IR detection applications were calculated. The figures of merit for high current sensitivity (F_I), high voltage responsivity (F_V) and high detectivity (F_D) were calculated for getting an idea about their performance in fast-pulse detection, large area detection and to understand their signal-to-noise performance respectively. By measuring the Shore hardness, flexibility/moldability of the prepared polymer composites could be analyzed.

In the first chapter a detailed description of composites, electroactive polymers, polymer composites, pyroelectric IR detectors, figures of merit, etc. are given. The chapter also introduces the work done on the topic of research.

In the second chapter all the experimental techniques adopted for the entire investigation are explained in detail.

In the third chapter the preparation and properties of $LiTaO_3$/PVDF nanocomposites are explained. Experimental results for the average pyroelectric coefficients and the figures of merit for different volume fractions of LT are summarised in table 7.1.

Table 7.1 Pyroelectric property and figures of merit for $LiTaO_3$/PVDF nanocomposites

Volume fraction of LT in PVDF	Pyroelectric coefficient, *p(T)* ($\mu C/m^2K$)	Pyroelectric figure of merit		
		F_I ($\times 10^{-3}$ $\mu Cm/J$)	F_V ($\times 10^{-3}$ $\mu Cm/J$)	F_D ($\times 10^{-3}$ $\mu Cm/J$)
0	36	25.07	2.48	165.3
0.001	41	28.77	2.67	160.8
0.01	54	38.30	3.23	186.8
0.05	106	72.63	5.89	282.7
0.09	150	113.55	7.91	313.7
0.15	208	166.13	10.88	340.5
0.25	318	278.46	16.23	510.9

In the fourth chapter $LiNbO_3$/PVDF nanocomposites with varying volume fractions of the ceramic were selected as the materials for study. Their thermal, electrical and hardness properties were studied and reported.

Table 7.2 given below shows the experimental results for pyroelectric coefficient and the calculated figures of merit for each volume fraction of LN in PVDF polymer matrix.

Table 7.2 Pyroelectric property and figures of merit for $LiNbO_3$/PVDF nanocomposites

Volume fraction of LN in PVDF	Pyroelectric coefficient, *p(T)* ($\mu C/m^2K$)	Pyroelectric figure of merit		
		F_I ($\times 10^{-3}$ $\mu Cm/J$)	F_V ($\times 10^{-3}$ $\mu Cm/J$)	F_D ($\times 10^{-3}$ $\mu Cm/J$)
0	31	21.71	2.13	117.74
0.001	33	23.59	2.29	116.50
0.01	37	26.93	2.55	120.43
0.05	51	38.12	3.40	127.07
0.09	71	53.99	4.45	143.27
0.15	98	76.56	5.76	153.42
0.25	127	104.96	6.76	186.13

Nanocomposites of SBN30/PU with varying volume fractions of SBN30 are the selected composites in chapter 5. Here also the room temperature measurements of thermal and dielectric properties were carried out. In our studies this SBN30/PU nanocomposite showed the highest pyroelectric coefficient for 0.25 volume fraction of inclusion. The highest values for the figures of merit F_I and F_D were also obtained for this nanocomposite for the volume fraction of inclusion 0.25. Table 7.3 gives a summary of the experimental results for pyroelectric coefficients. The three figures of merit calculated for each volume fraction of inclusion are also given in the table.

Table 7.3 Pyroelectric property and figures of merit for SBN30/PU nanocomposites

Volume fraction of SBN30 in PU	Pyroelectric coefficient, *p(T)* ($\mu C/m^2K$)	Pyroelectric figure of merit		
		F_I ($\times 10^{-3}$ $\mu Cm/J$)	F_V ($\times 10^{-3}$ $\mu Cm/J$)	F_D ($\times 10^{-3}$ $\mu Cm/J$)
0	81	48.74	6.83	191.17
0.001	85	51.52	7.20	200.54
0.01	94	57.70	7.91	223.82
0.05	123	77.36	8.83	292.39
0.09	190	122.98	12.77	432.10
0.15	278	187.21	16.86	556.91
0.25	388	283.63	20.99	792.76

A comparative study of the properties of TGS/PU and DTGS/PU microcrystalline composites is given in chapter 6. Here the partial deuteration of TGS shows an increase in pyroelectric coefficient and thermal conductivity but a decrease in specific heat capacity. In the study, values of the pyroelectric coefficients did not show an expected increase because being ferroelectric crystals having pyroelectric property, both TGS and DTGS will show a reduction in polarization during temperature varying experiments. But for the entire samples studied, the highest value for the figure of merit F_V (~25) obtained is for DTGS/PU composite at 0.25 volume fraction. The experimental results for pyroelectric property and the calculated figures of merit for TGS/PU and DTGS/PU microcrystalline composites are given in tables 7.4 and 7.5 respectively.

Table 7.4 Pyroelectric property and figures of merit for TGS/PU microcrystalline composites

Volume fraction of TGS in PU	Pyroelectric coefficient, *p(T)* (μC/m^{2}K)	Pyroelectric figure of merit		
		F_I (×10^{-3} μCm/J)	F_V (×10^{-3} μCm/J)	F_D (×10^{-3} μCm/J)
0	80	48.42	7.17	270.67
0.001	84	50.97	7.53	248.71
0.01	89	54.07	7.92	232.68
0.05	115	70.20	9.38	263.45
0.09	149	91.52	12.05	242.01
0.15	216	133.33	15.06	304.28
0.25	318	200.75	19.21	415.88

Table 7.5 Pyroelectric property and figures of merit for DTGS/PU microcrystalline composites

Volume fraction of DTGS in PU	Pyroelectric coefficient, *p(T)* (μC/m^{2}K)	Pyroelectric figure of merit		
		F_I (×10^{-3} μCm/J)	F_V (×10^{-3} μCm/J)	F_D (×10^{-3} μCm/J)
0	82	49.84	7.43	266.40
0.001	85	51.73	7.73	258.65
0.01	94	57.28	8.42	253.64
0.05	123	75.22	10.60	258.00
0.09	164	101.54	13.20	288.35
0.15	237	149.24	17.51	339.70
0.25	365	233.82	24.56	491.84

Overall, the studies give guidelines for the selection of composite materials for pyroelectric thermal/IR detection applications.

7.2 Salient features of the research work done

Some important factors considered during the material fabrication stages were maximum flexibility and maximum figures of merit for pyroelectric thermal/IR detection applications. In order to achieve these goals, all the samples are synthesized as composites of polymers and nano/microcrystalline particles and are prepared in the form of freestanding films.

The selected polymer matrices and particle inclusions possess good pyroelectric coefficients, low thermal and dielectric properties, so that good pyroelectric figures of merit could be achieved.

The salient features of the work include the particle size of the selected ceramic materials. Since they are in nanometer size it was possible to achieve high flexibility and moldability with high figures of merit for even low volume fractions of inclusions of the prepared nanocrystalline composites. In the case of microcrystalline TGS and DTGS, their composites in PU matrix protect them from fragility and humidity susceptibility and made them for environmental friendly applications.

7.3 Scope for future work

We propose to extend our work for the fabrication of practical IR sensors using one or more of the presently investigated polymer/ceramic nanocomposites having high figures of merit.

Today pure polymer (PVDF) and pure ceramic ($LiTaO_3$) sensors are available for pyroelectric detection applications. But polymer/ceramic composites are yet to emerge as sensors. So, our future investigations will also focus on the fabrication of a highly sensitive pyroelectric sensor using

polymer/ceramic nanocomposites. We have already succeeded in the fabrication of a practical sensor using $LiTaO_3$/PVDF nanocomposite with volume fraction 0.10 of nano LiTaO3 in PVDF polymer. The fabricated sensor having $1cm^2$ area and 210μm thickness, with gold electrodes sputtered on both sides, was tested using a homemade photopyroelectric apparatus fabricated in the laboratory. The results are then compared with a commercially available PVDF film sensor having the same area and 28 μm thickness with Ni/Cr alloy coated on both sides. But the results indicated low amplitude for our sensor compared to the commercially available sensor. Currently, efforts are underway to improve the amplitude (sensitivity) of the newly prepared LT/PVDF sensor for practical sensor applications. More work is necessary to fabricate commercially viable sensors adaptable to practical environment.

Of late, applications that require mouldable sensors and actuators are emerging, particularly for biomedical system applications. We think that composite materials of the kind investigated and reported in this thesis can be used for such applications too.

We do not claim that the samples investigated by us have the best performance for this application. There could be other composites with other ceramic or polymer constituents that may provide better performance in terms of pyroelectric sensitivity and figures of merit. There is scope for further work in this direction as well.

****

Appendix I Papers Published

1. **M. S. Jayalakshmy** and J. Philip "*Enhancement in pyroelectric detection sensitivity for flexible $LiNbO_3$/PVDF nanocomposite films by inclusion content control*", ***J. Polym. Res.*** 22, 42 (**2015**)

2. **M. S. Jayalakshmy** and J. Philip "*Pyroelectricity in strontium barium niobate/ polyurethane nanocomposites for thermal/infrared detection*", ***Comp. Sci. Technol.*** 109, 6 (**2015**)

3. **M. S. Jayalakshmy** and J. Philip "*Triglycine sulphate and its deuterated analogue in polyurethane matrix for thermal/infrared detection: A comparison*", ***J. Appl. Polym. Science*** DOI: 10.1002/APP.42250 (**2015**)

4. **M. S. Jayalakshmy** and J. Philip "*Pyroelectric figures of merit and associated properties of $LiTaO_3$/polyvinylidene difluoride nanocomposites for thermal/infrared sensing*", ***Sens. Actuators: A*** 206, 121 (**2014**)

5. **M. S. Jayalakshmy** and J. Philip "*Thermophysical properties of plant leaves and their influence on the environment temperature*", ***Int. J. Thermophys.*** 31, 2295 (**2010**)

6. M. R. Nisha, **M. S. Jayalakshmy** and J. Philip "*Effective thermal conductivity of condensed polymeric nanofluids (nanosolids) controlled by diffusion and interfacial scattering*", ***Pramana*** 81, 849 (**2013**)

Appendix II Papers Published with External Collaborators

1. K. Thukral, N. Vijayan, B. Rathi, G. Bhagavannarayana, S. Verma, J. Philip, A. Krishna, **M. S. Jayalakshmy** and S. K. Halder "Synthesis and single crystal growth of L-proline cadmium chloride monohydrate and its characterization for higher order harmonic generation applications", ***Cryst. Eng. Comm.*** 16, 2802 (**2014**)

2. N. Vijayan, J. Philip, D. Haranath, B. Rathi, G. Bhavannarayana, S. K. Halder, N. Roy, **M. S. Jayalakshmy** and S. Verma "Bulk growth of ninhydrin single crystals by solvent evaporation method and its characterization for SHG and THG applications", ***Spectrochim. Acta: Part A*** 122, 309 (**2014**)

3. A. Krishna, N. Vijayan, B. Riscob, B. S. Gour, D. Haranath, J. Philip, S. Verma, **M. S. Jayalakshmy**, G. Bhagavannarayana and S. K. Halder "Phase matching, X-Ray topography, optical and thermal analysis of L-alanine cadmium chloride monohydrate: a nonlinear optical material", ***Appl. Phys: A*** (**2013**) (DOI: 10.1007/s00339-013-7902-1).

4. G. Sreekanth, S. Chandralingam, J. Philip, **M. S. Jayalakshmy**, R. Philip, K. Sridharan, R. S. Kumar and G. P. Joseph "Investigations on the electrical, thermal and optical properties of the nonlinear optical allylthiourea mercury chloride single crystals", ***Mater. Res. Bull.*** 47, 4043 (**2012**)

5. R. Mohandoss, S. Dhanuskodi, **M. S. Jayalakshmy**, J. Philip and G. Bhagavannarayana "Structural, electrical, thermal and optical properties of the nonlinear optical crystal L-arginine fluoride", ***Cryst. Res. Technol.*** 47, 620 (**2012**)

6. "Effect of ZnO nanoparticles on the Electrical, Mechanical and Thermal Properties of Ethylene Vinyl Acetate (EVA) Thin Films", ***Comp. Sci. Technol.*** (*communicated*)

Appendix III Conference Papers

1. **M. S. Jayalakshmy** and J. Philip "Pyroelectric properties of Strontium Barium Niobate/Polyurethane nanocomposites for thermal/infrared detection", NANO INDIA 2015, SASTRA University, Thanjavur, India, **2015**.

2. **M. S. Jayalakshmy** and J. Philip "LiNbO3/PVDF nanocomposites for thermal/IR sensing applications", KKTM Govt. College, Kodungalloor, **2014**.

3. **M. S. Jayalakshmy** and J. Philip "LiTaO3/PVDF nanocomposites for thermal/IR detection applications", National Seminar on Biopolymers and Green Composites – Emerging Science and Technology (BPGC 13), Kalamassery, **2013**.

4. **M. S. Jayalakshmy** and J. Philip "$LiNbO_3$/PVDF nanocomposites for thermal/IR sensing applications", NANO INDIA 2013, Thiruvananthapuram, India, **2013**.

5. **M. S. Jayalakshmy** and J. Philip "$LiTaO_3$/PVDF nanocomposites for pyroelectric infrared detection applications", 25^{th} Kerala Science Congress, Technopark, Thiruvananthapuram, **2013**.

6. **M. S. Jayalakshmy** and J. Philip "Influence of thermophysical properties of plant leaves on environment temperature", 23^{rd} Kerala Science Congress, Centre for Earth Science Studies, Thiruvananthapuram, **2011**.